OVERPRESSURE PREDICTION BY MEAN TOTAL STRESS ESTIMATE USING WELL LOGS FOR COMPRESSIONAL ENVIRONMENTS WITH STRIKE-SLIP OR REVERSE FAULTING STRESS STATE

A Thesis

by

ASLIHAN OZKALE

Submitted to the Office of Graduate Studies of
Texas A&M University
in partial fulfillment of the requirements for the degree of

MASTER OF SCIENCE

December 2006

Major Subject: Petroleum Engineering

OVERPRESSURE PREDICTION BY MEAN TOTAL STRESS ESTIMATE USING WELL LOGS FOR COMPRESSIONAL ENVIRONMENTS WITH STRIKE-SLIP OR REVERSE FAULTING STRESS STATE

A Thesis

by

ASLIHAN OZKALE

Submitted to the Office of Graduate Studies of
Texas A&M University
in partial fulfillment of the requirements for the degree of

MASTER OF SCIENCE

Approved by:

Chair of Committee,	Jerome Schubert
Committee Members,	Jerry L. Jensen
	Brann Johnson
Head of Department,	Steve Holditch

December 2006

Major Subject: Petroleum Engineering

ABSTRACT

Overpressure Prediction by Mean Total Stress Estimate Using Well Logs for Compressional Environments with Strike-Slip or Reverse Faulting Stress State.

(December 2006)

Aslihan Ozkale, B.S., Middle East Technical University,Turkey

Chair of Advisory Committee: Dr. Jerome Schubert

Predicting correct pore-pressure is important for drilling applications. Wellbore stability problems, kicks, or even blow-outs can be avoided with a good estimate of pore-pressure. Conventional pore-pressure estimation methods are based on one-dimensional compaction theory and depend on a relationship between porosity and vertical effective stress. Strike-slip or reverse faulting environments especially require a different way to determine pore-pressure, since the overburden is not the maximum stress.

This study proposes a method which better accounts for the three-dimensional nature of the stress field and provides improved estimates of pore-pressure. We apply the mean total stress estimate to estimate pore-pressure. Pore pressure is then obtained by modifying Eaton's pore-pressure equations, which require either resistivity or sonic log data.

The method was tested in the Snorre Field in the Norwegian North Sea, where the field changes from strike-slip to reverse stress state. Eaton's resistivity and sonic equations

were used to predict pore-pressure in this region by replacing the vertical stress by the mean total stress estimate. Results suggest that the modified Eaton method with resistivity log data gives better results for the area than the conventional method. The ratio of maximum horizontal stress to minimum horizontal stress throughout each well should be known for best results.

DEDICATION

To my mother, Sevim, and my father, Ali.

ACKNOWLEDGEMENTS

I would like to express my deepest gratitude and appreciation to my committee chair, Dr. Schubert, and my committee members, Dr. Jensen and Dr Johnson, for their guidance and support throughout the course of this research.

Sincere thanks are extended to Knowledge Systems Inc. for allowing me to use their Drillworks Predict software for this study. I also would like to thank the Knowledge Systems Inc. staff who answered my all questions throughout the project. I also express my sincere appreciation to Steve Hobart an experienced researcher for his interest in my work.

TABLE OF CONTENTS

Page

CHAPTER Page

LIST OF FIGURES

FIGURE Page

FIGURE Page

FIGURE Page

FIGURE Page

LIST OF TABLES

CHAPTER I

INTRODUCTION

Overview

Determining overpressured zones is quite important for the petroleum industry. Drilling success, safety and reservoir depletion history are all affected by the presence of overpressured strata.[1] This research will focus on the drilling part of the problem.

For a successful drilling design it is extremely important to know or estimate the pore pressure for a given area. Casing design and mud weight designs are planned according to the estimated pore pressure. If the mud weight is not adjusted for the correct pore pressure, unwanted events like "kicks" can occur, which may result in lost time, or even blowouts. A good estimate of pore pressure is also essential to avoid wellbore stability problems like borehole breakouts or stuck pipes. Avoiding problems related to pore pressure determination can save lives and money. This research project will investigate the pore pressure determination in tectonic environments where strike slip or reverse faulting is present.[1]

Background

There are many mechanisms for the generation of overpressure. The important ones are:

1. Undercompaction,

This thesis follows the style of *SPE Drilling and Completion.*

2. Fluid volume increase,
3. Fluid movement and buoyancy,
4. Tectonics.[2,3]

For undercompaction and fluid volume increase mechanisms, there are methods to detect overpressure using well log data.[4-7] Present day methods to determine overpressure using well logs are related to undercompaction and fluid volume increase. This thesis reports on the extension of the existing methods to include the influence of tectonics on compaction and resultant fluid pressures.

The industry practice to determine pore pressure or overpressure from well logs depends on important assumptions. One assumption is that the shale pore pressure is the same as pore pressure in sand-rich nearby formation (e.g. sands). Another assumption is the relationship between porosity and effective stress is an indicator for pore pressure. A consequence of the last assumption is that excess porosity is an indicator of overpressure due to undercompaction or fluid volume increase.

Excess pore pressure determination methods that use well logs can be classified as direct methods, vertical methods, horizontal methods and others.[4-8]

Direct methods and some of other methods use porosity indicators such as resistivity and sonic logs. During compaction, porosity decreases with depth as effective stress increases. Deviation is defined by the normal trend observed for hydrostatically

pressured strata above the overpressured zone. When an overpressured lithology is encountered, there is a deviation observed from the normal compaction trend of porosity indicators. The amount of deviation is correlated with the observed pore pressure increase. In this method pore pressure from previously drilled wells from the same field can be related to the previously known porosity indicator deviations.

Regardless of the method used, either horizontal or vertical, porosity trend lines are used for pore pressure prediction. The methods that use a trend line project the value of the porosity indicator for a hydrostatic pressure throughout the well. With the help of shale analysis from the gamma ray log, applied to a porosity indicator log, shale points are obtained for the well. The calculated pore pressure then is obtained by relating the deviation of the shale points from the trend line with an empirical equation.

Other methods eliminate the explicit use of a trend line, however, the existing methods are generally based on either directly or indirectly establishing an effective stress-porosity relationship.[9] Interestingly, the empirical or semi-empirical methods used by the industry for pore pressure prediction were developed for the Gulf of Mexico. The Gulf of Mexico is known to be a tectonically relaxed, normal fault region. Notice that the effective stress defined for these methods is based on the vertical stress so that the effective stress used for these methods is the vertical effective stress. The method proposed in this thesis use mean effective stress instead of vertical effective stress.

Need for Solution

Vertical effective stress for overpressure determination can only be applied to normal-tectonically relaxed environments. Often we see the horizontal stresses affecting the predictions where compressional lateral stresses are present near the target area.[10] In normal faulting or passive environments, the relationship between the observed stress magnitudes is $S_v > S_H > S_h$, where S_v is the vertical or overburden stress, S_H is the maximum horizontal principal stress, and S_h is the minimum principal horizontal stress. The existing techniques of estimating pore pressure are successfully applied in normal faulting environments because the effect of horizontal principal stresses is negligible and porosity changes are mainly related to overburden. Thus, detection methods based on vertical effective stress are successful in where maximum compressive stress is vertical (extensional tectonic regimes) regions.

In tectonic compressional environments, however, the overburden stress may not be the component controlling pore pressure. The observed stress distribution in these environments changes according to the type of the faulting system present. In strike-slip faulting environments, the observed stress state is $S_H > S_v > S_h$; while in reverse faulting environments, $S_H > S_h > S_v$.[11] In strike-slip and reverse faulting environments, the pore pressure arises not only because of overburden stress, but horizontal (lateral) stresses also play an important role in overpressure development. There is evidence that where observed porosity does not result simply from overburden change, overpressured zones can not be adequately estimated by the existing methods of pore pressure prediction.[12]

Since the stress distribution is not the same everywhere, the magnitude of the principal horizontal stresses may vary spatially compared to stress created by the overburden alone. In the areas where we see the effect of large lateral (horizontal) principal stresses, the existing methods for predicting pore pressure tend to incorrectly estimate pore pressure. This error could result in inefficient well designs and unmanageable borehole stability issues.

Description of the Solution

This study proposes to incorporate estimates of maximum and minimum horizontal principal stresses into an overpressure analysis technique. We calculate the mean of all three principal stresses and use this mean total stress in the calculation of pore pressure estimation

$$S_m = (S_H + S_h + S_v)/3 \quad \text{..... (1)}$$

The technique can be applied to three faulting regimes; normal, strike slip, and reverse, for estimation of the pore pressure. Where lateral stresses are higher than vertical stress, such as in strike-slip or reverse faulting systems, the excess pore pressure cannot be explained by use of overburden stress alone. As shown later, incorporation of the mean total stress approach provides better estimates. To evaluate S_m, several quantities have to be measured or estimated.

1. Vertical stress S_v is calculated from density logs. Vertical stress is

$$S_v = \int g(z)\,\rho(z)\,dz \quad \text{..... (2)}$$

Vertical stress is the easiest of the three principal stresses to estimate.

2. The magnitude of the minimum horizontal stress is calculated from leak off and hydraulic fracture test data.[13] Caliper, image logs, and mud weight can be used to obtain the azimuth and magnitude of minimum horizontal stress around the wellbore.[14]
3. It is difficult to calculate the magnitude of maximum principal horizontal stress. But the direction of maximum principal horizontal stress is perpendicular to both S_v and S_h directions. It is also possible to bound the magnitude of S_H by the Anderson's Faulting theory if S_v and S_h are known.[15] Recent techniques used in the petroleum industry suggest that the magnitude of S_H can be calculated using sonic log readings.[16] It is also possible to use World Stress Map Data base to obtain an estimate of the ratio S_H / S_h.

Thus, while some characteristics are directly available from well logs, the direct determination of maximum horizontal stress and minimum horizontal stress by well logs is not possible. Until recently, four or more arm caliper logs have been used to determine the orientation of minimum horizontal stress and to estimate its magnitude. Another petrophysical tool is the use of image logs from which the orientation of the minimum horizontal stress can be interpreted. The Anderson Faulting Theory combined with Mohr-Coulomb failure analysis can provide bounds on a quantitative solution for maximum principal horizontal stress in tectonic environments where pore pressure, vertical stress and minimum horizontal stress are known.[15] The knowledge of these stresses allows us to calculate the mean total stress, which is necessary to more

accurately estimate pore pressure in environments where lateral stress magnitudes are greater than vertical stress.

Objective

The objective of this study is to explore and develop a mean total stress technique for estimation of pore pressure. This study will give a better understanding of the pore pressure distribution over the areas where faults and lateral stresses are present.

The difference between industry practice for pore pressure determination, which uses only overburden stress, and pore pressure determination using mean total stress (or mean effective stress) will be demonstrated. The difference in estimation of pore pressure between the two techniques may significantly affect well drilling design.

To validate this work, pressure test readings, like a Repeat Formation Test (RFT) or Modular Formation Dynamic Test (MDT), from the well in concern will be used to evaluate the improvement in pore pressure estimation using a mean stress approach compared to vertical stress approach.

Data Required

The data required for the analysis can be categorized into three categories. First one is well logging data for shale porosity determination as sonic log, gamma ray log, Resistivity log. Second data category is well test data as MDT, RFT and Leak off Test

(LOT) data. LOT data is used as minimum horizontal stress. MDT and RFT data is used to evaluate the results of pore pressure determination techniques. The final and third category is stress state data for a given field. The stress state data is needed to indicate what kind of stress state the field is in and any information related to horizontal stress ratio boundaries is also needed.

Method

In this research I am going to calculate pore pressure using mean total stress as a replacement for overburden in the existing pore pressure evaluation techniques. Data from the Snorre Field from North Sea will be used to validate the Mean Total Stress Pore Pressure Prediction Method. This field is known to be in a strike slip to reverse faulting stress regime.[17] Three wells from this region will be evaluated. The result of the two methods will be compared to actual pore pressure readings from the RFT data. Results will presented as percent changes between pore pressure calculated from mean total stresses and overburden stress normalized to measured RFT data.

CHAPTER II

LITERATURE SURVEY

Overpressure estimation methods generally use the compaction theory. In order to be able to understand the methods the following concepts should be understood.

What Is Overpressure?

Overpressure is often also called abnormally high pore pressure. It is known as the excess pore pressure observed for the area. In this context it will be defined as any pore pressure which is higher than the hydrostatic water column pressure extending from surface to the drilling target. Figure 1 shows the definition of overpressure.

The Main Overpressure Generating Mechanisms

In the literature, there are many mechanisms proposed to explain the development of overpressure. In this text, four main categories will be mentioned. It is important to differentiate the porosity changes with respect to these different mechanisms. Every mechanism has its own method to relate porosity change to pore pressure change. Recent surveys of overpressure mechanisms have been published by Swarbrick et al.[18] and Bowers[4]. Swarbrick classified three mechanisms, and Bowers classified four.

Bowers[4]classified the mechanisms as; undercompaction, fluid expansion, lateral transfer, and tectonic loading. However, Swarbrick et al.[18] classified the mechanisms as: stress related, fluid volume increase, and fluid movement including buoyancy.

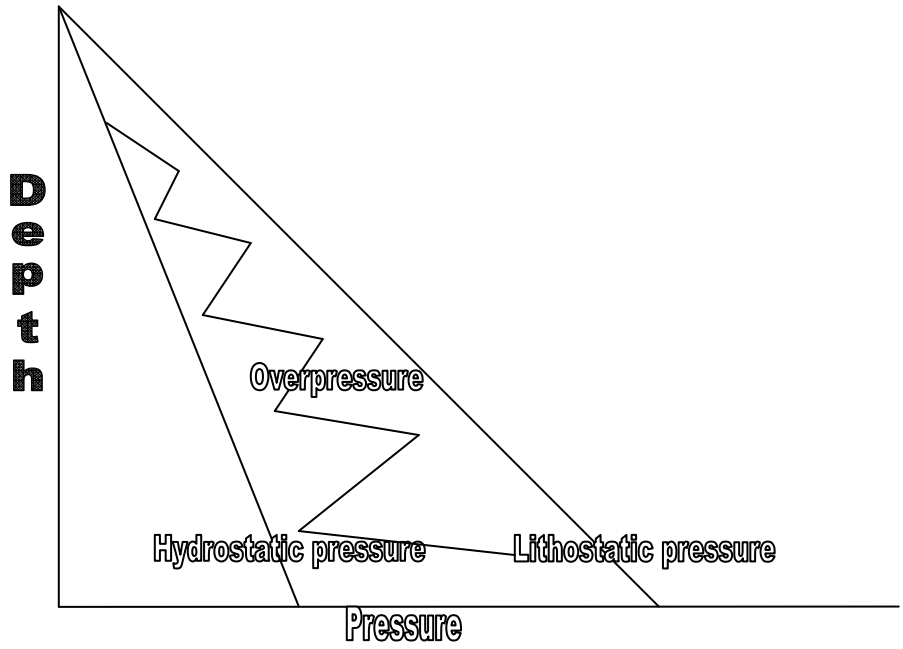

Figure 1 Definition of overpressure.

For this study, it is critical to differentiate the tectonic mechanisms in a separate heading since Mean Total Stress Pore Pressure Prediction Method proposed is mainly interested in porosity change due to tectonics.

So this text will explain mechanisms under four categories; undercompaction, fluid volume increase, fluid movement and buoyancy, and tectonics.

Undercompaction

Undercompaction is also known as disequilibrium compaction. In this type of mechanism vertical loading stress (overburden stress) is the main agent on shaping the pore space and pore throat systems. Hydrostatically pressured (normally pressured) areas usually have a characteristic rate of compaction. The reflection of this characteristic rate of compaction on well logs is a trend. Figure 2 shows the compaction process. During compaction the fluid in the systems will flow into upper sediments under the influence of vertical stress (overburden) if there is sufficient permeability. As the fluid escapes grains continue to support the applied vertical stress.

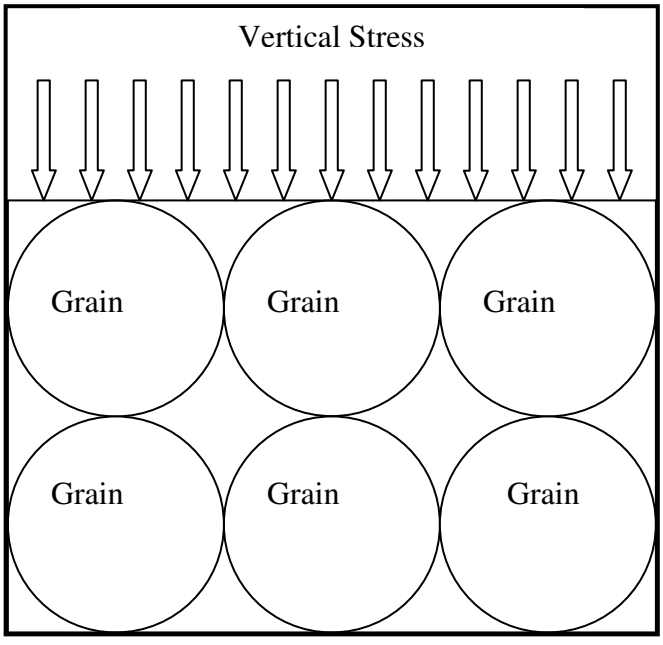

Figure 2 Representation of compaction process.

In hydrostatically pressured areas, with increasing depth, a porosity decrease is observed. Porosity is related to depth vs. vertical stress, therefore porosity is also related to increasing vertical stress. Figure 3 illustrates porosity vs. depth and porosity vs. effective stress relationships for normally pressured-shales.

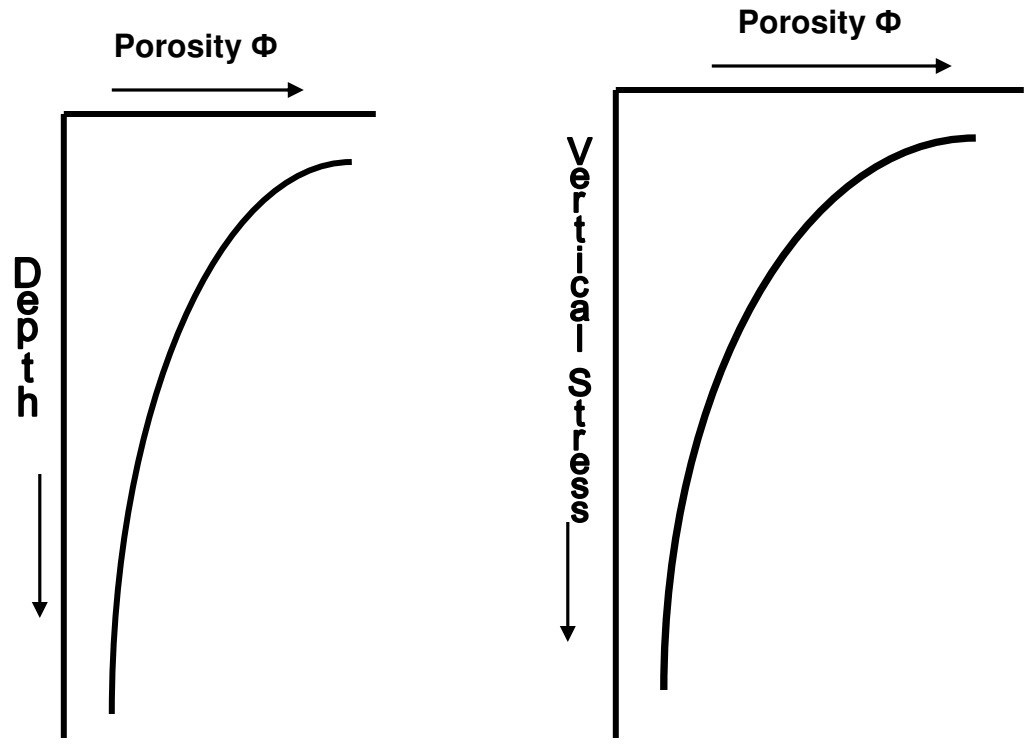

Figure 3 Porosity vs. depth and porosity vs. vertical stress relationships. Arrows indicate porosity increase.

However, in some cases where the sedimentation rate is fast and low permeability is observed, fluid is trapped and supports a part of the increased vertical load. Overpressure results where this kind of phenomenon is observed in the target area. This mechanism is known as undercompaction or disequilibrium compaction.

Understanding compaction mechanism is critical for overpressure detection. Compaction can be defined as porosity reduction as pore water escapes under loading. Loading causes the formation to get squeezed and expel water as much as the vertical permeability will allow in establishing a stress equilibrium.

Terzaghi & Peck [19] conducted some experiments in 1948 to show the effect of permeability which is directly related to the ability of the pore fluid to escape. They showed this using a closed system where they control the ability of the water to escape by taps while they applied vertical stress. They used springs to model the resistance of pore grains in reaction to the load applied. When the tap was open, fluid was free to escape. Fluid escaped leaving the pore grains supporting the vertical load. When the tap was closed or nearly closed fluid could not escape and pore fluid and grains together were supporting the vertical load. This is a very good demonstration of what is happening when a rock rich with water and high in porosity is deposited on earth. It loses its free water during compaction leaving the grains supporting the load. This is also the explanation of porosity reduction due to loading. Sediments are compacted by reducing the space between the grains.

Drilling below a very low permeability zone, one can come across the trapped fluid supporting the loading above. It is the transition zone. Figure 4 illustrates how overpressure occurs when there is low permeability and good sealing.

Terzaghi did not perform those experiments just to show the effect of loading alone. The main aim was to demonstrate the effective stress concept.

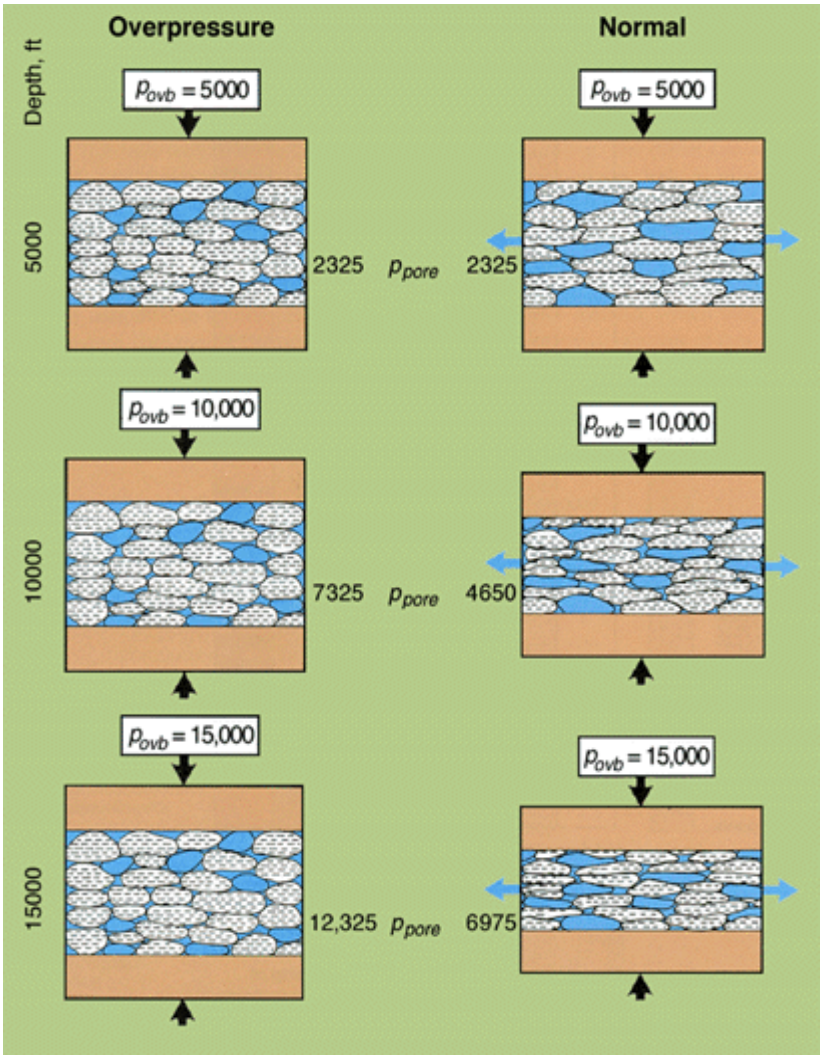

Figure 4 Example of Terzaghi's example on actual formations. P_{ovb} is overburden pressure inserted on sediment. Notice that in each case, same overburden is applied. But in the case where overpressure is observed, the permeability was low. In normal pressured case, the permeability was higher, fluid escapes freely under increasing overburden.[20]

$$S_v = \sigma_e + P \quad (3)$$

where S_v is vertical load, vertical stress or overburden stress, σ_e is effective stress and P is pore pressure.

Biot studied the effect of compressibility of the pore space and its effect on the pore fluid ability to sustain vertical stress.

$S_v = \sigma_e + \alpha P$ ..... (4)

where α is the Biot poroelasticity constant. It changes between 0 and 1. Terzaghi's effective stress equation uses α = 1. However, researchers around the world use Biot poroelasticity constant to relate observed pore pressure to observed effective stress. Where observed pore pressure and overburden stress can not explain the effective stress, Biot constant is used to formulate these quantities.[12]

Fluid Volume Increase

There are three main mechanisms associated with in pore fluid volume increase: Aquathermal expansion due to temperature increase, Mineral Transformation, hydrocarbon generation and oil to gas transformation.

Aquathermal Expansion

Water has the tendency to expand more than the mineral framework as temperature increases. Where the pore fluid is sealed and the temperature increase observed after the compaction is completed, this type of mechanism results in high overpressure. But Swarbrick[16] and Mouchet &Michell[3] argue against a long duration for this pressure

mechanism. Water will have reduced viscosity under the influence of temperature and could be expelled easily. The integrity of the seal supporting the overpressure mechanism is also in question because the seal can be breached under the pressure increase. This type of mechanism is discounted relative to the importance of overpressure generated by other overpressure generating mechanisms. [22]

Mineral Transformation

Bound water is released when minerals are transformed in sediments. Smectite Dehydration, Gypsum to Anhydrite Dehydration, Smectite –Illite Transformation are the main examples of this type of transformation. All these water releasing mechanisms may result in pore pressure increase when the reservoir is sealed and transformation occurs after the sedimentation.

Hydrocarbon Generation and Oil to Gas Transformation

Kerogen transforms to coal, oil and gas depending on the depth, pressure and temperature it is subjected to. Kerogen maturating into oil and gas, results in excess fluid and oil cracking into gas, again resulting in excess fluid. Under good sealing and low permeability conditions this phenomena can cause overpressure.[21]

Fluid Movement and Buoyancy

Osmosis

Natural salinity variation in the sediments creates an osmotic pressure from low salinity concentrated sediments to highly concentrated sediments through the semi-permeable membranes such as shales.

Hydraulic fluid pressure transfers the pressure to a shallower formation, resulting in overpressure. Bowers[4] suggests this transfer can happen through fractures of breached faults or seals.

Hydraulic Head

Elevation differences between the targeted drilling zone and outcropping aquifer can result in this type of mechanism. The observed pressure will be much higher than the expected one since the target drilling strata is connected to a higher elevated structure.[18] Figure 5 represents this phenomenon.

Density –Buoyancy

Drilling is financially successful when there are hydrocarbons in the target zone. Oil and gas have lower densities than the formation water. By definition, overpressure is pressure higher than the hydraulic head encountered for a given depth. So due to their lower densities, gas or oil columns above an aquifer will have overpressure.[18]

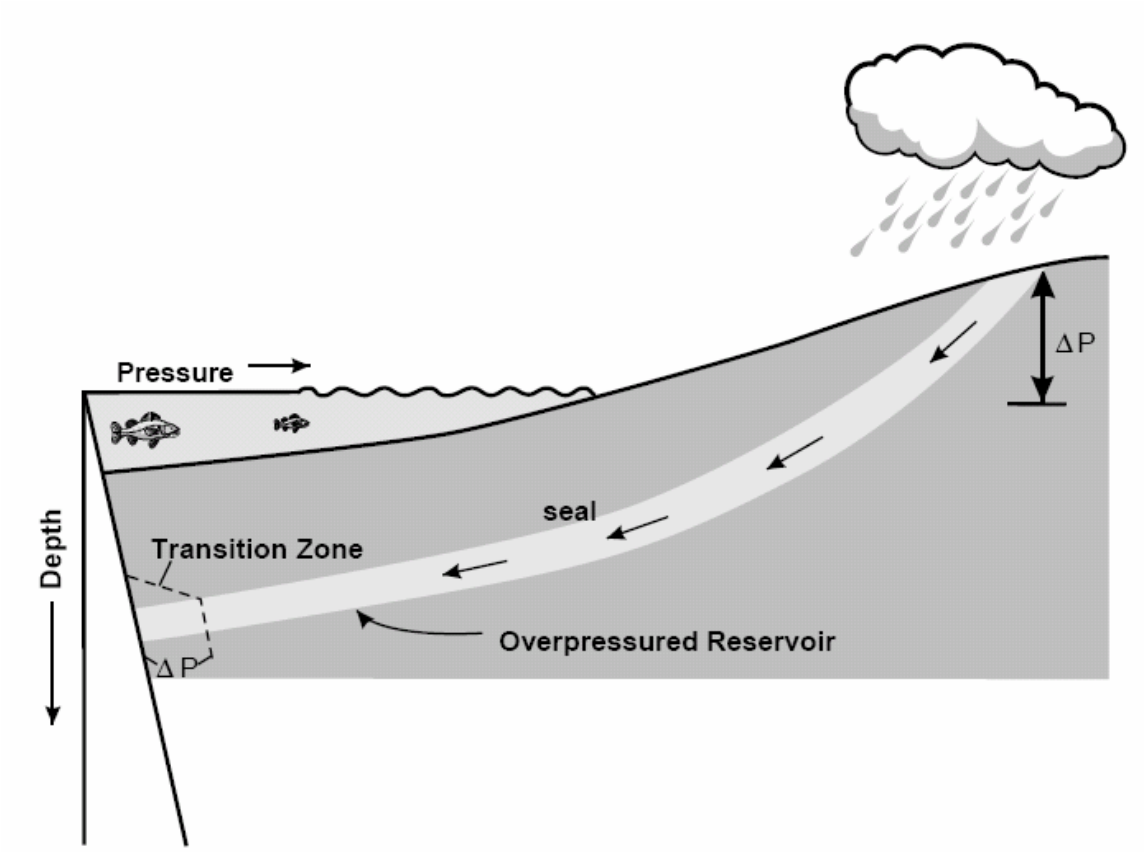

Figure 5 Overpressure due to hydraulic head mechanism. If the reservoir is interconnected to a higher level fluid head, overpressure will be observed. [18]

Tectonics

Tectonic activity may result in lateral compression. This type of overpressure mechanism can be divided into three categories; Tectonic loading, Tectonic Shear-imposed overpressure, and Fluid Flow supported faults.[6]

Tectonic Loading

At this point it is important to state that all recent studies about pore pressure and compaction assume one dimensional loading, where vertical stress is the main stress

inducing agent. This is only true for tectonically relaxed environments (extension regimes), which are normal faulting environments. Anderson[11], in his study about faults, states there are three kinds of stress systems on earth: normal faulting where vertical stress is the main stress inducer, strike-slip faulting where the magnitude of vertical stress is the intermediate stress inducer and the reverse fault case where the vertical stress is the smallest of all. Figure 6 illustrates these stress regimes. $S_1, S_2,$ S_3 are maximum, intermediate, minimum principal stress respectively in magnitude. For each stress regime shown in Figure 6, the maximum principal stress is represented by S_1 independent of stress regime. S_1 is S_v for normal faulting environments. However S_v is intermediate principal stress, S_2 for strike-slip environments, and minimum principal stress, S_3 for reverse faulting environments.

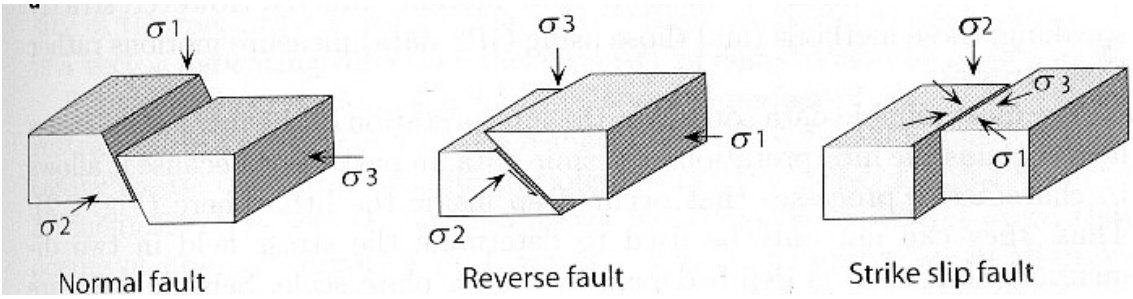

Figure 6 Stress regimes.

1D The compaction theory can be expanded to include the horizontal stresses present during compaction. There is still the reduction of porosity but porosity reduction is not controlled by only the vertical stress change. The 1D compaction theory is valid for the

Gulf of Mexico since the horizontal stresses are similar in magnitude. However, this is not the case for other parts of the world. Even though porosity can be quite successfully related to vertical stress in the GOM, there are many reported cases in Norway, Nigeria, Caspian Sea, etc. that vertical stress compaction model is not valid.[6] Figure 7 shows the distribution of tectonically-influenced overpressure around the world. There is a wide distribution of tectonically induced, pore pressure around the world.

Figure 7 Tectonically influenced overpressure distribution on earth. Shaded regions represent where tectonically induced pore pressure is observed, lines represent where Cenozoic folding occurred, and triangles represent where mud volcanoes are observed. [6]

Schutjens et.al[22] include horizontal stresses in their work to quantify compaction due to all stresses. Even though they assume that horizontal stresses are equal, it is clearly a

start in recognizing the effect of horizontal stresses on compaction. In their work they have shown an elastic zone where the pore structure can handle stresses in three dimensions and also a "shear-enhanced, pore collapse region'. This states that in elastic theory according, to the Mohr –Coulomb Failure envelope, it is possible for pores to sustain horizontal stresses up to a point and after that pore collapse due to shear takes place.

In the elastic theory point of view, if we do not observe shear failure, there will be an equilibrium where all three principal stresses are supported by the grain framework. This means the porosity change will be related to all of the stresses imposed on the pores. So this type of mechanism is simply the extended version of compaction disequilibrium in three dimensions.

Tectonic Shear Imposed Overpressure

As mentioned above during compaction, as elastic limits are exceeded there is shear resulting from the horizontal stresses around the pore space. This shear results in deformation. Shear failure results in stress being imposed on the remaining strong pore space and the fluid in it. This will result in a pore pressure increase with decreasing or significantly changing pore structure: porosity. This phenomenon generally can not be observed as porosity change with well logs. Therefore it is possible that where porosity is not changed, there can be overpressure. [6]

Fluid Flow Supported Faults

Reverse Faults tend to have a lot of shear resulting from rupture of the faults. This shear may cause fractures throughout the faulted zone. If there is already undercompaction present, overpressure will be observed. Overpressure will occur because of both undercompaction and pore structure shear deformation from faulting. Fluid flow will be observed throughout the reverse fault decollement. This is observed in the Barbados diapirism in an ODP study.[23]

Undercompaction is the most encountered overpressure mechanism around the world while drilling. Observed overpressure magnitude in this mechanism is smaller than other mechanisms. Fluid expansion and fluid movement and buoyancy are encountered less often than undercompaction. The magnitudes of overpressure in these types of mechanisms are considered to smaller than undercompaction mechanism for some researchers. For others however it is considered to be larger in magnitude. Tectonics is the rarest encountered mechanism around the world; however the magnitude of overpressure due to tectonics is higher than any mechanism generating overpressure. Independent of generating mechanisms, any overpressure encountered during drilling is important.

State of Art for Pore Pressure Determination

Today overpressure techniques are performed before drilling, while drilling and after drilling. Pre-drill pore pressure analysis is done by using data from offset wells, seismic

data and regional geology. While drilling pore pressure analysis is done by updating the pre-drill findings. Bit penetration rate, cutting characteristics, hole conditions, gas-cut mud, change in drilling fluid properties, Measurement While Drilling (MWD), Logging While Drilling (LWD) data are used to update the pre-drill analysis.

After drilling analysis we use Drill Stem Test (DST), Leak-Off Test (LOT), hydraulic fracturing test and well test data to update the analysis and for future reference, well completion or reservoir performance analysis applications. Data collected are used to model pore pressure. This work will discuss the methods which use well logging data to perform prediction and quantification of overpressure.

Shale is the lithology which compacts the most under stress by changes in its pore structure, reducing its porosity.[24]

The following well logging based, pore pressure prediction methods will use this fact with the assumption that sediments interbedded with shale will have the same pore pressure.

Traugott[8] divides pore pressure determination techniques into two categories: vertical and horizontal methods. Vertical methods assume that for a given porosity, there will be a unique effective stress. This is the basis for the equivalent depth method. Horizontal methods, however, use the assumption of empirical relationship between pore pressure

gradient and the ratio of porosity indicators like well logs. Eaton's equation is an example of this category. Bowers added two classifications to Traugott's pore pressure determination methods: direct and other methods. [9]

Direct Methods

Overpressure determination using well logs started with Hottmann & Johnson.[25] They used sonic and resisitivity log readings as indicators of the porosity and fluid property change throughout the well. They used the idea that fluid pressure is related to the state of compaction and depth. They determined a "normal compaction trend" for the clean shale observed throughout the well, knowing that shale is the most compaction-sensitive lithology and determined the trend of well log measurements in hydrostatically pressured shales. Deviation from this trend shows excess fluid porosity, meaning overpressure. This method is summarized below:

- Sonic log readings from depths which are thought to contain hydrostatically pressured clean shale are plotted against depth showing the compaction trend for the area of interest as normal trend.
- Sonic log readings, for the zones which are of concern are also plotted with respect to depth.
- Trends are compared and the deviations from the normal trend are marked. The difference between log readings are plotted against the known pore pressures for the well. After obtaining the trend of excess pore pressure, at any depth the required pore pressure can be obtained.

This method is a direct method for pore pressure estimation since the difference in the log reading is related to known pore pressures. A limitation of this method mentioned by the authors is that, this method can only be used in the areas where overburden stress is the main stress component for compaction.

Wallace[26] proposed a similar graphical method for conductivity or resistivity logs. He gave a lot attention to the limitation of well logging applications and readings.

Pennbaker[27] proposed using crossplots for a given area. They basically show the normal compaction trends for the area of concern. The crossplots used the Hottmann and Johnson method. The Pennbaker method also uses seismic data to predict pore pressure pre-drill.

Vertical Methods

Ham[28] tried to solve the problem of estimating pore pressure without direct measurements. In his method he used resistivity and sonic log data trends and the points where the deviation start from these trend lines. He developed this method for the Gulf of Mexico using known reservoir pressure measurements and a hydrostatic gradient of 0. 465 psi/ft. His method is known as the "Equivalent Depth Method". This method can be summarized as:

$$P = 0.465\ Z_N + 1.0(Z_A - Z_N) \quad (5)$$

$$P = Z_A - 0.535\ (Z_N) \quad (6)$$

where, P is pore pressure, Z_N is normal pressure depth, Z_A is abnormal pressure depth. An assumption of the overburden gradient being 1.0 psi/ft is used in this method as well. The idea behind these formulas is that in overpressured formations, the overburden below a pressure seal will also be supported by fluid present in the formation, which is trapped by a good seal. So the pore pressure calculated for a depth where it is known that there is overpressure is the sum of hydrostatic fluid column pressure to the observed top of overpressure and the difference of depths between total depth and top of overpressure depth multiplied by overburden gradient of 1.0.

This method can give an estimate for pore pressure, but the degree to which the fluid carries of the entire overburden load is unknown. So the assumption of 1.0 is not necessarily a good assumption.

Foster and Whalen[29] actually relate the porosity- vertical effective stress to well logs by using F, the formation factor and combining Archie's equation. F_{sh} is the formation factor, for shale formations. They used resistivity and electrical logging data to determine the log-linear relationship between porosity and effective stress. They also showed any deviation from the linear trend is an indicator for overpressure. Figures 8-10 give examples from this study.

Pore pressure is quantified by the equivalent-depth method. If effective stresses are the same for both normal and overpressured zones for a point in a given region, then abnormal pressure can be quantified by using the equivalent depth method.

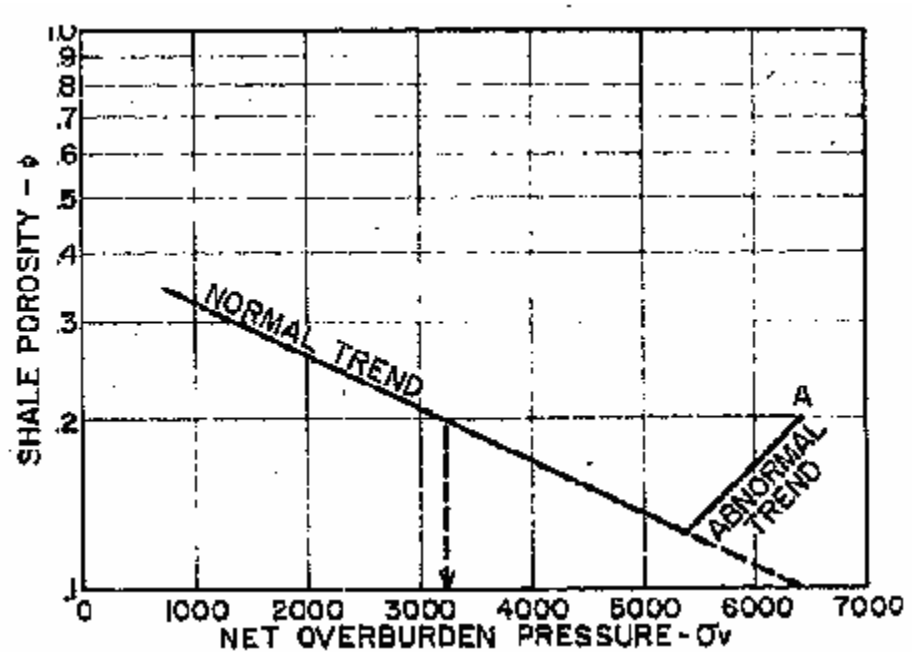

Figure 8 Example of Foster and Whalen study to determine overpressure from net overburden which is vertical effective stress.[29]

Ransom[30] suggested " two similar samples of compressed clay or shale having equal porosities must support the same net- overburden pressure regardless of depth." He used the equivalent depth method but he used the vertical effective stress assuming one-dimensional compaction. His suggestion was that if we know the pore pressure and overburden for a given depth before the overpressure observed form the trend line we obtained from rich in clay / poor in other minerals; clean shales using well logs, like resistivity and sonic, we can obtain the pore pressure for the desired depth by knowing the overburden at that depth.

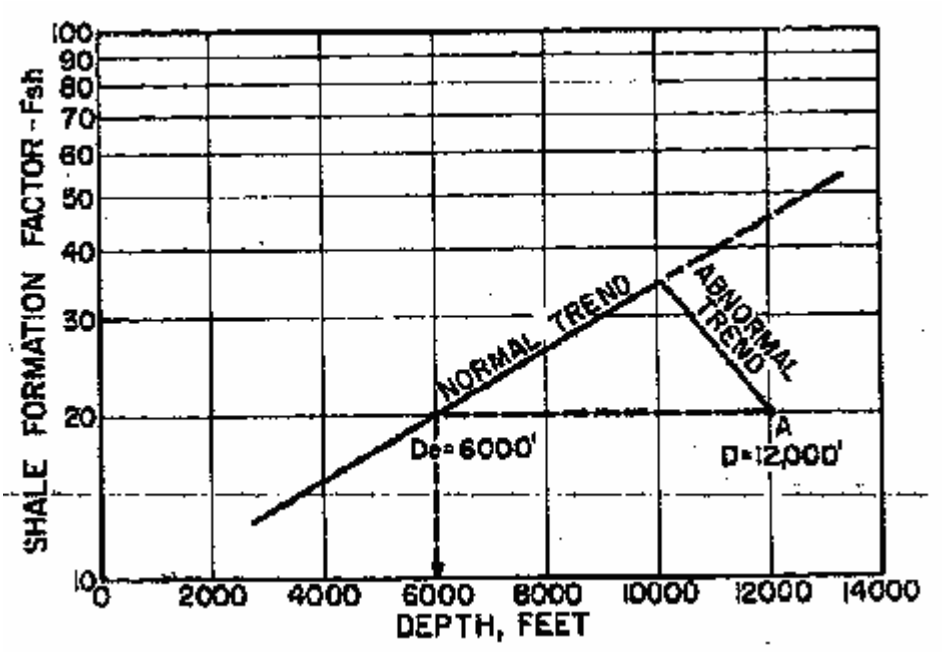

Figure 9 Determination of pore pressure from equivalent depth method of Foster and Whalen. F_{sh} is the formation factor of clay rich shale formations.[29]

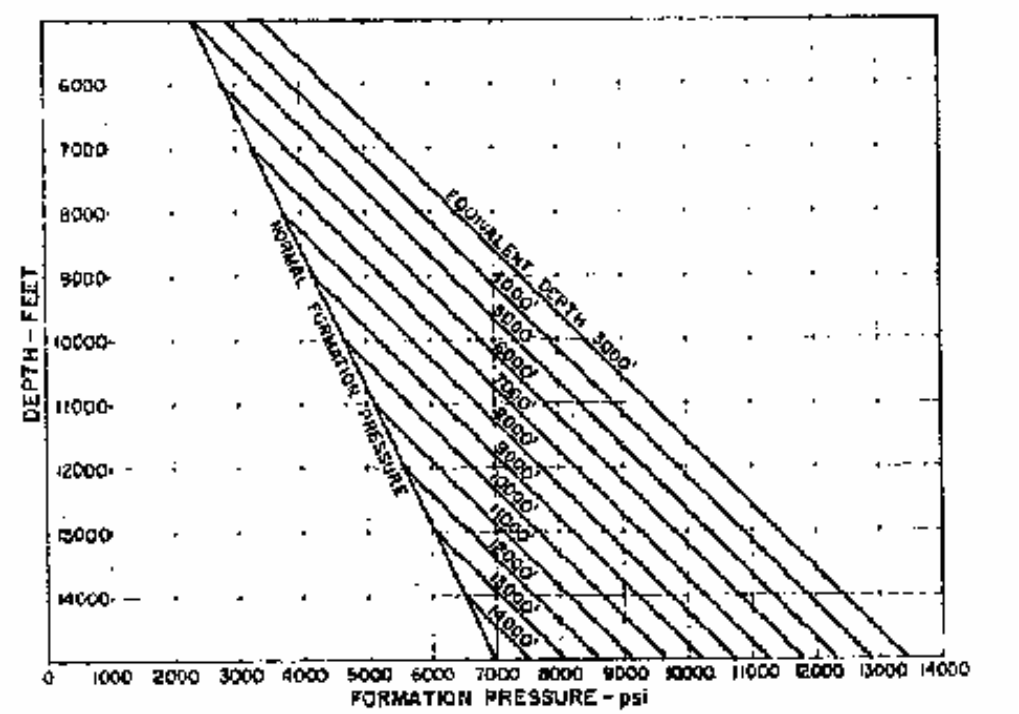

Figure 10 Pore pressure estimation nomograph example for equivalent depth method used by Foster and Whalen.[29]

$$\sigma_1 = \sigma_2$$

$$(S_1\text{-}P_1) = (S_2\text{-}P_2)$$

where σ is the effective vertical stress, S overburden stress, P is the pore pressure. At two different depths represented by 1 and 2, effective stresses are equal. If vertical stresses and one of pore pressures are known, the unknown pore pressure can be calculated.

Bryant[31] developed a method called "Dual Shale Pore Pressure Detection Technique". He claimed that the technique can predict pore pressure without too many inputs required as compared to previous techniques. For this technique to be used, the only inputs which are needed are local air gap, local water depth, normal pore pressure density, minimum and maximum gamma ray value, resistivity of water in shale. The technique is as follows: The overburden gradient is calculated from Bell's equation for the Gulf of Mexico;

$$S/Z = OB + (2.64E-05*Z) - (1.97E-09*Z^2) + (6.6E-14*Z^3) - (5.97E-19*Z^4) \quad (7)$$

where *S* is the overburden stress, *OB* is the overburden gradient at the mud line which is usually taken as 0.850 psi/ft, Z is the true vertical depth (TVD) with air gap and water gap subtracted. Normal pore fluid pressure is used to calculate normal matrix pressure, σ_N by using Terzaghi's effective stress principle.

$\sigma_N = S - P_N$ ..... (8)

The minimum and maximum gamma ray value indicate the shale points on resistivity data to calculate the pure shale zones for calculating the shale porosity from Archie's

equation using formation resistivity factor. Bryant[32] used Archie's equation for shale even though the equation is designed for clean sand formations.

$$\phi = \exp(\ (\ln R_w - \ln R_{sh})/m) \quad \text{..... (9)}$$

where R_w is resistivity of water in shale and R_{sh} is shale resistivity from well logs. Porosity exponent m is taken as 2.0 for this technique. Then he used the Baldwin and Butler relationship for clay compaction:

$$Z = Z_{\max} * e^{6.35} \quad \text{..... (10)}$$

where e is (1-ϕ), solidity, Z_{max} is the depth where S is 1, meaning porosity is 0 .Using the Rubey and Hubbert equation for effective stress relationship, the equation becomes;

$$\sigma_{act} = \sigma_{\max} * (1-\phi)^{7.35} \quad \text{..... (11)}$$

Inserting the porosity relationship computed before;

$$\sigma_{act} = \sigma_{\max} * (1 - \exp((\ln R_w - \ln R_{sh}\ )/m))^{7.47} \quad \text{..... (12)}$$

With this equation σ_{act} is calculated for each depth for the analysis. For abnormally pressured formations and normally pressured formations; the overburden stress will be the same, if the formations are buried at the same depth.

$$Z_O = Z_N$$

$$\sigma_o + P_o = \sigma_N + P_N \quad \text{..... (13)}$$

Keeping in mind that under the same overburden, if the formation is experiencing higher pore pressure, effective stress will be reduced.

$$\Delta P = \sigma_N - \sigma_{act} \quad \text{..... (14)}$$

For a 1D application of pore-pressure prediction, which means the method uses only vertical stress, it is a relatively easy method for non-expert users. However, it should not be applied anywhere except the Gulf of Mexico, since the overburden computation and depth- solidity relationship are only applicable to Gulf of Mexico.

Alixant and Desbrandes[32] implement a two module method as similar to Bryant[31] for pore-pressure determination. The reason they come up with this new technique is the two shortcomings of previous methods. These shortcomings are; establish a regional trend line and empirical relationship between petrophysical measurements, which are well logs, and pore-pressure gradient. The method they propose has the same two modules as previously used by Holbrook and Bryant: a petrophysical module and a mechanical module.

The petrophysical module computes the shale porosity, which is an indicator of pore pressure and the mechanical module computes pore pressure using Terzaghi's effective stress principle and a porosity-effective stress relation. The methods differ in the way the equations and assumptions used in petrophysical module and mechanical module. Alixant and Desbrandes[32] used Perez-Rosales equation to obtain porosity;

$$R_o / R_w = 1 + G\left[(1-\phi)/(\phi - \phi_r)\right] \quad (15)$$

where G is the geometrical factor which compensates for the shape change of particles from a spherical shape, ϕ_r is residual porosity which does not affect the electrical conductivity. These parameters change as the lithology changes.

They also used the assumption of shale-water resistivity being constant over depth like Bryant[31]. However, Alixant and Desbrandes[32] include a temperature correction in their model. To find the true bound-water resistivity value they used the formula below;

$$R_{wb} = 297.6\, T^{-1.76} \quad \text{..... (16)}$$

T is measured in ^{o}F. Using the Perez- Rosales formula they calculate the porosity necessary for their mechanical module. They used 1D compaction as the mechanism for the deformation, using the Perloff- Baron relationship for vertical effective stress:

$$\sigma_{eV} = 10^{(r - r_i)1 - I} \quad \text{..... (17)}$$

where r is the void ratio, defined as;

$$r = \phi/(1-\phi) \quad \text{..... (18)}$$

I_c is compression index. I_c and r_i (initial void ratio) can be obtained from core analysis in the laboratory for a given area. After obtaining $\sigma_{eV,}$ they used the Biot poroelasticity, effective stress law to obtain pore pressure;

$$\sigma_{eV} = S_v - \alpha P_p \quad \text{..... (19)}$$

where α taken as 1 in this study. This method requires G, ϕ_r, I_c, r_i as calibration coefficients. Having so many variables can be a problem since obtaining these constants for a new area is usually not possible at the beginning.

Table 1 summarizes the vertical methods.

Horizontal Methods

Eaton[33] discusses the relationship between overburden and pore pressure and came up with empirical equations for the Gulf of Mexico. His equations are based on Terzaghi's effective stress concept. He used resistivity logs and sonic logs. Initially he computed was the change of overburden with depth. He showed there is a linear relationship between log (overburden pressure) and depth for Gulf of Mexico.

Table-1 Summary of the vertical methods.

Vertical Methods		
Ham[28]	Pioneered "Equivalent Depth Method". The Depth of top of overpressure is used to calculate pore pressure. Vertical Effective Stresses are same for the same porosity different depths.	Method was designed for Gulf of the Mexico. Overburden gradient of 1 psi/ft is used.
Foster & Whalen[29]	Formation Resistivity Factor of shale formations, F_{sh}, is used as porosity indicator. Fsh vs. depth plot is used for same porosity at two different depths.	Graphical method. Trend line should be obtained for the area so that the method can be applicable.
Ransom[30]	Using clean shale well logs, resistivity, sonic logs, can be used to predict pore pressure.	Another example of equivalent depth method application. This time resistivity and sonic logs are directly used as porosity indicators.
Bryant[31]	Two module method example. ϕ is obtained in the first module. ϕ is used to calculate vertical effective stress in the second module.	Archie's equation is used to obtain Fsh. Archie designed his equation for clean sandy formations.
Alixant & Desbrandes [32]	Another example of two module methods. Perez-Rosales equation is used to calculate porosity from resistivity logs	Many variables are needed to be known for a new area to apply and calibrate the method. (G, ϕ_r , Ic, ri)

He stated the equation of overburden of a specific layer as,

$S = \rho.g.Z$ ..... (20)

where ρ as density of the strata, g gravitational gravity, Z depth.

He also showed that pore pressure observed is a function of resistiviy and sonic readings since they are representative of petrophysical properties of formation.

$$P = F\ (\text{Normal Rsh}/\ \text{Observed Rsh})$$

$$P = F\ (\text{Observed } \Delta\text{tsh} - \text{Normal } \Delta\text{tsh})$$

He finally related overburden to pore pressure using Terzaghi's equation.

$$\frac{P}{Z} = \frac{S}{Z} - 0.535\left(\frac{Observed\ Rsh}{Normal\ Rsh}\right)^{1.5} \quad \text{..... (21)}$$

In this formula, 0.465 psi/ft is the hydrostatic fluid column gradient of the water in Gulf of Mexico. Any deviation from the trend line of observed clean shale data indicates of excess pore pressure. The exponent 1.5 is known as the compaction exponent. In the following published papers, Eaton used 1.2 for this component.

By its nature this is an empirical equation to relate log (resistivity) and pore pressure gradient. This equation could be used in the environments where sediment compacted rapidly. Undercompaction is usually observed in these kinds of environments. So Eaton's equation is very useful to quantify pore pressure where sediments show undercompaction. Figure 11 shows the empirical relation between pore pressure and resisitivity ratio.

Fertl and Chilingarian used the same method to establish charts for a given area when dielectric (electromagnetic wave propagation) logs are used.[34]

Weakley[35], claimed to have another method. The method is to construct overlays for the data from offset wells and uses these to predict pore pressure for the target well. The method uses Eaton's equation for resistivity and sonic logs. The difference is that the exponent of Eaton's equation is calibrated using a known pore pressure at a given depth. The exponent is re-calculated for that area to fit the data. Weakley claims that only one pore-pressure calibration point is needed for the trend line to be established.

First draw the trend of normally pressured zone, extrapolate this trend line through the abnormal zone as well. Then, for a given depth, indicate the pore pressure as increments by 1 ppg on the same plot and then estimate the pore pressure. This method is a graphical method.

All the methods presented to this point were interested in 1D compaction model and assume compaction disequilibrium as the overpressure generating mechanism. Table 2 summarizes the horizontal methods.

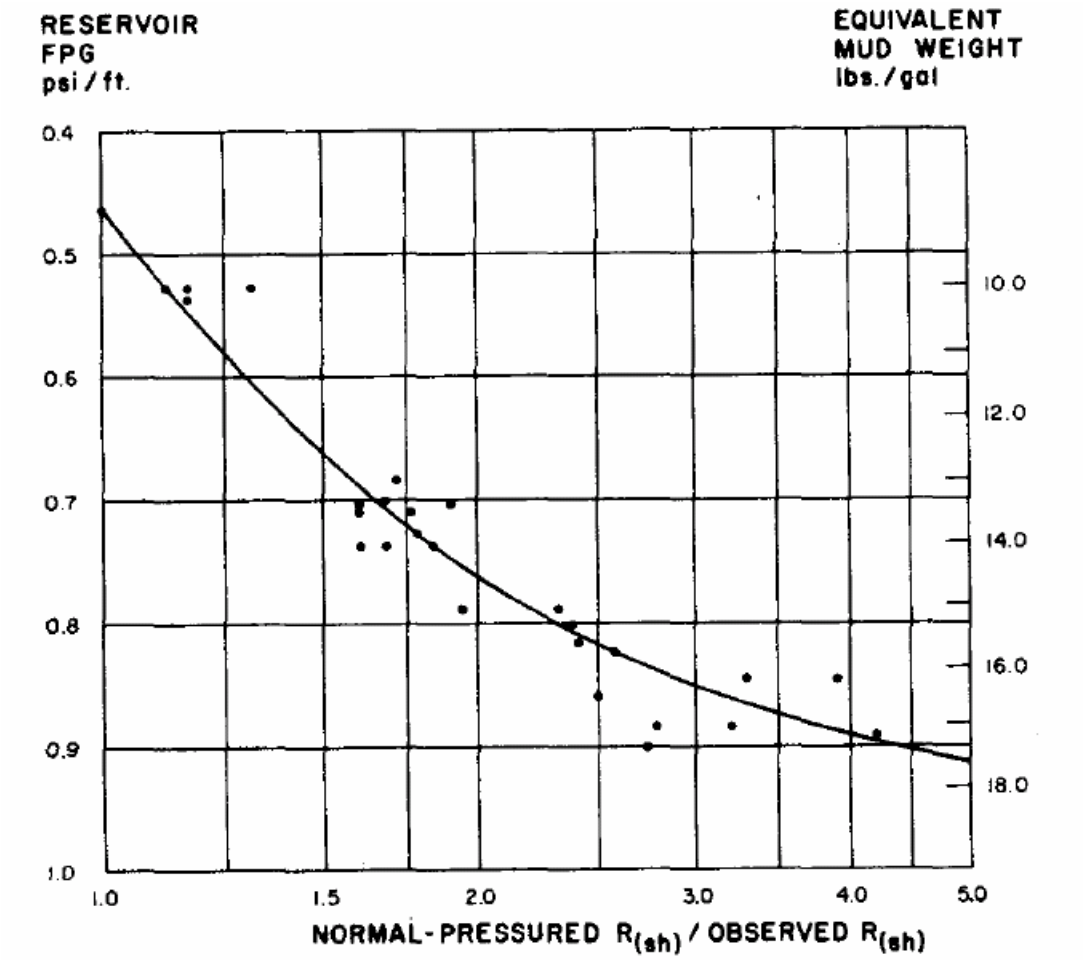

Figure 11 Resistivity ratio trend for Eaton's equation.[33]

Table 2 Summary of the horizontal methods.

Horizontal Methods		
Eaton[33]	Pioneered an empirical equation where pore pressure is a function of observed and normal well log data.	It is an empirical method designed for Gulf Of Mexico. An empirical mathematical relationship is obtained by using well logs.
Fertl & Chilingarian[34]	Eaton method is used. Electromagnetic wave propagations logs are used.	Charts are established for different areas. A library of charts is necessary.
Weakley[35]	Eaton method is used. The exponents are adjusted after obtaining measured pore pressure.	Graphical Method. Compaction trend should be known.

Other Methods

Bowers[36] showed the effect of fluid expansion on overpressure. Fluid expansion occurs where formation fluid volume is increased by either hydrocarbon generation, temperature increase on clay diagenesis. This phenomenon can be observed in sonic logs. A plot of effective stress vs. velocity readings from a sonic log plot shows the compaction trend for a given area. The trend observed shows the normal compaction for that area. The trend is called the "virgin curve" by Bowers. A key point made by Bowers is that undercompaction can not cause effective stress reductions as fluid expansion does. The effect of undercompaction on sonic logs would at most be a "freeze" in porosity as Bowers states. When one observes a reversal in sonic log velocity readings, it is due to a reduction in the effective stress as well. If a trend other than this virgin curve is observed in the effective stress vs. velocity plot, as in Figure 12, this trend is called the "unloading" curve.

Bowers[36] claims that some of the overpressure observed in the Gulf of Mexico is due to fluid expansion. According to Bowers, Hottmann and Johnson[25] estimated pore pressure correctly in their study without knowing that the mechanism generating that pore pressure was fluid expansion.

If the virgin curve is used to estimate pore pressure due to fluid expansion instead of the unloading curve, the pore pressure will be underestimated. Figure 13 gives an example of Fluid expansion in Indonesia. He also notes that not all velocity reversals are an indicator of fluid expansion. Sonic velocity decreases can occur when the lithology changes from shale to another lithology.

He proposed two equations: one to be used in undercompacted zones and the other one to be used inside the velocity reversals. The first method used for an undercompacted zone is the same as Weakley's overlay method. In this method, the exponent of sonic velocity ratio is adjusted for the geographic region with calibration pore-pressure values.

The second method is used where velocity reversals are observed and where other evidence indicates there is fluid expansion. The method is as follows; the virgin curve is represented with the formula below;

$$V = 5000 + A\sigma^{B} \quad \text{..... (22)}$$

V is the velocity ft/s; σ is effective stress (psi), A and B are the parameters to fit the curve for a given area. A and B are usually determined from offset wells for that area.

The unloading curve is represented by an empirical equation;

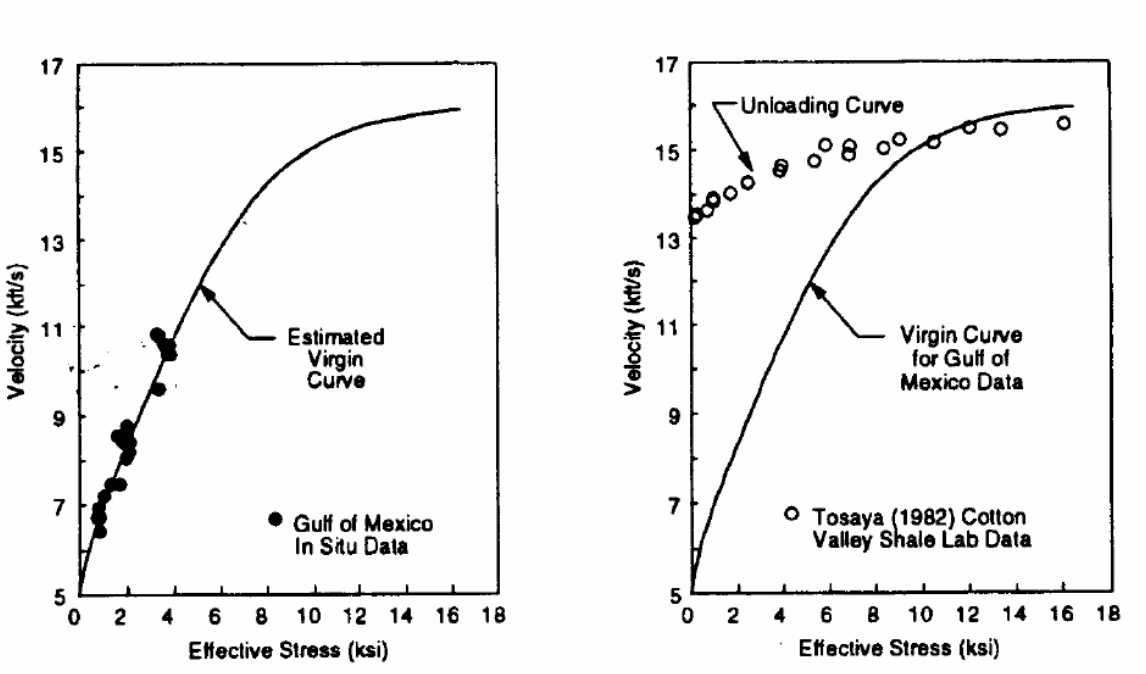

Figure 12 Virgin compaction curve and unloading curve example, Bowers' study. [36]

$$V = 5000 + A\left[\sigma_{\max}\left(\sigma/\sigma_{\max}\right)^{1/U}\right]^{B} \quad \text{..... (23)}$$

A and B are the parameters as found for a given area from the virgin curve. U is an unloading parameter. It reflects the plastic deformation of the sediment. Bowers states that U varies between 3 and 8 practically. U equal to 1 means there is no permanent deformation and where $U = \infty$ means the sediment is at its maximum deformation. σ_{max} is calculated using the maximum velocity observed, V_{max}, where unloading started.

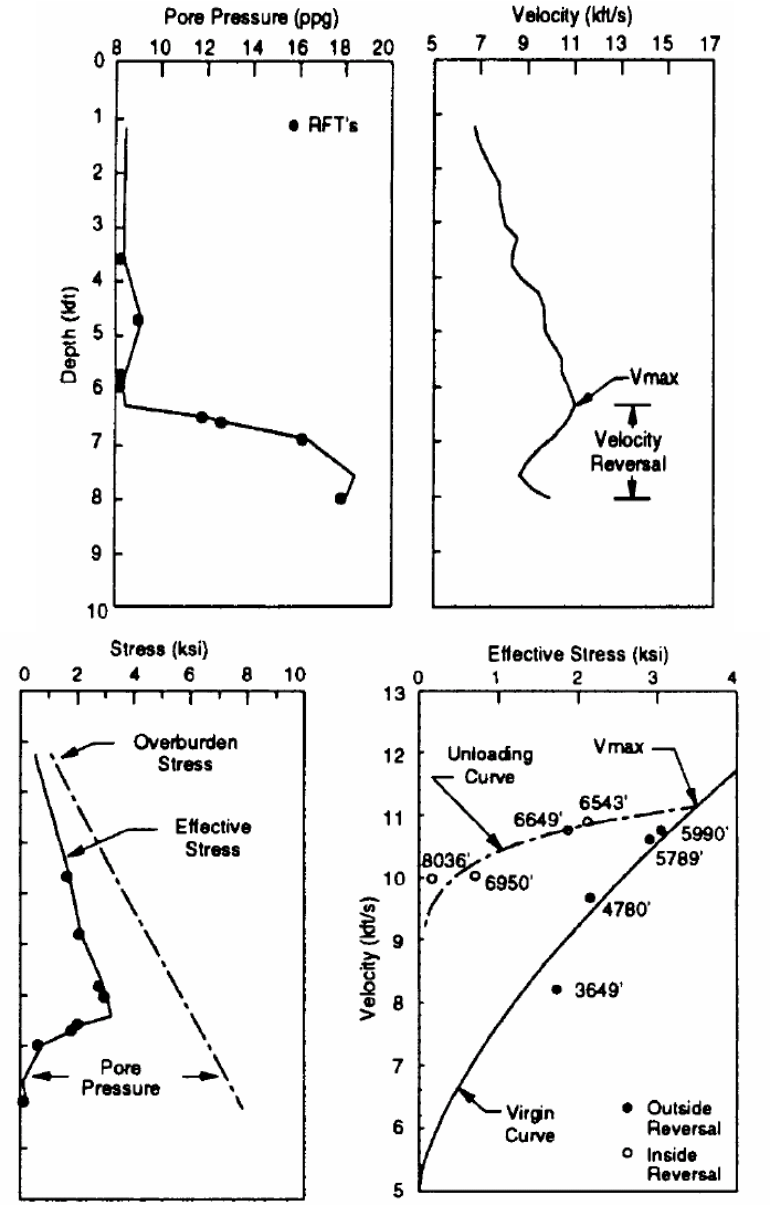

Figure 13 Example of fluid expansion from Indonesia, Bowers' study. [36]

$$\sigma_{\max} = \left(\frac{V_{\max} - 5000}{A} \right)^{1/B} \quad \text{..... (24)}$$

U needs to be determined. This parameter can be obtained by defining a stress for a given velocity to intersect the virgin curve, $\sigma_{vc.}$

$$\sigma_{vc} = \left(\frac{V - 5000}{A} \right)^{1/B} \quad \text{..... (25)}$$

Then *U* can be determined from the following equality:

$$(\sigma / \sigma_{\max}) = (\sigma_{vc} / \sigma_{\max})^{U} \quad \text{..... (26)}$$

An estimate of pore pressure would be calculated for a proposed well by using Eaton's modified equation and Bowers' unloading curve. These two sets of pore-pressure data could give the boundaries of a pore pressure window for a pre-drill analysis.

Bowers tried to clarify where the unloading method should be used in his 2001 paper.[37] He showed that not every reversal in the sonic log trend means unloading. He mentions the unloading method as a high pressure technique. If this technique is applied in all the velocity reversals seen in an overpressured zone, there is a high possibility of overestimating the pore pressure in this zone. When a centroid is expected or observed it is also important to know that pore pressure techniques will under estimate overpressure. He introduced a decision-making process to determine the appropriate pore pressure prediction technique.

1- Use the data from clean shale points from well logs.
2- Filter them
3- Plot velocity vs. depth, and velocity vs. density. If the data from the overpressured zone is following another trend than the virgin curve, a high pressure technique will be needed. However if the data follow the virgin compaction curve, then the equivalent-depth method would be sufficient. Figure

14 illustrates unloading detection by a velocity vs. density plot, as in Bowers' study.

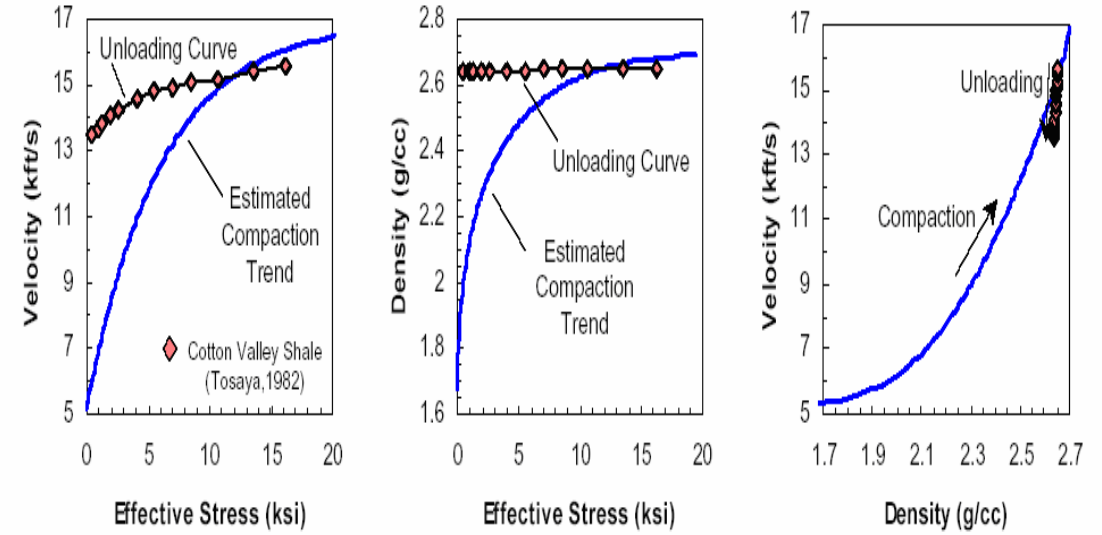

Figure 14 Representation of unloading by velocity vs. density plot, Bowers' study. If unloading is present as an overpressure generating mechanism, pore pressure calculated by existing methods will underestimate the pore pressure. Effective stress vs. velocity plot should be checked for unloading before any computation. [37]

The rule of thumb Bowers gives is, observe the trends for all resistivity, density and sonic logs. If Resistivity and sonic logs show a reversal but the density log does not, this might be an indicator of unloading. This can be explained because the resistivity and sonic logs reflect transport properties whereas a density log shows bulk properties. Bowers also revised his method using density and effective stress data. He related sonic velocity and density data by:

$$V = V_o + C(\rho - \rho_o)^D \quad \text{..... (27)}$$

V_o, ρ_o, C and D are the parameters obtained from a log velocity vs. density plot. Density used in this equation is;

$$\rho - \rho_o = (\rho_{\max} - \rho_o)\left(\frac{\rho_v - \rho_o}{\rho_{\max} - \rho_o}\right)^{\mu} \quad \text{..... (28)}$$

ρ is current density, ρ_o found from the equation 27, ρ_{max} is the density where the unloading curve intersects the loading curve, μ is elastic rebound parameter, $\mu = 1/U$. ρ_v is the density obtained by inserting V in the equation 27.

$$\rho_{\max} = \rho_o + \left(\frac{\rho - \rho_o}{(\rho_v - \rho_o)^{\mu}}\right)^{1/(1-\mu)} \quad \text{..... (29)}$$

V_{max} can be calculated where ρ_{max} is substituted in the equation 27.

Ward et al.[38] question which porosity indicator is the best to calculate porosity for pore pressure analysis in high pressure and high temperature (HPHT) wells in Norway. Accurate pore-pressure determination is especially important in these wells since the drilling window, difference between pore pressure and fracture gradient are especially narrow relative to non- HPHT wells.

Previous methods determined porosity from resistivity logs by Archie or Waxman and Smits equations. They claim bulk density readings and resistivity to be better porosity indicators for Norway HPHT wells. Difficulties they face when they use resistivity data are: difficulty in knowing water salinity for C_w, shale surface charge effect BQ_v, presence

of hydrocarbons affecting conductivity and salt formations. Bulk density data are used to calculate porosity with the equation below:

$$\phi=(\rho_{matrix}-\rho_{bulk})/(\rho_{matrix}-\rho_{fluid}) \quad \text{..... (30)}$$

There are some complications when using the bulk density data to obtain porosity. First, shale percentage in the matrix is unknown. Second, if there are hydrocarbons present in the formation fluid, ρ_{fluid} is hard to estimate from water conductivity, $C_{w.}$ Thirdly, there is a problem with the quality of the bulk density readings due to loss of hole structure and shale swelling. These drilling problems affect the bulk density readings by creating low bulk density readings. Porosity also can be obtained from sonic data with the following equation from well logs:

$$\phi=(\Delta t_{matrix}-\Delta t_{bulk})/(\Delta t_{matrix}-\Delta t_{fluid}) \quad \text{..... (31)}$$

Challenges they had when sonic data are used to estimate porosity is explained as lack of knowledge for Δt_{matrix} and Δt_{fluid}. However, they also stated that no LWD sonic tool is used. The challenge for Δt_{matrix} was data variability due to fabric anisotropy of the formation and the fractures observed. Fluid salinity, hydrocarbon presence, and temperature profile are given as the parameters affecting Δt_{fluid}. According to Ward et al.[38], the sonic log is the best log, because it shows less effect from those factors. Sonic log readings are widely used as a trustworthy pore-pressure tool in the industry. It is chosen over resistivity and bulk density tools to show porosity changes,

Traugott[8] introduced the centroid concept in 1997. In his paper he gave attention to the importance of overburden stress used in pore-pressure analysis. He defined a “pressure

cell", where all six sides of an isolated compartment is surrounded by impermeable shales. According to Traugott, the centroid is the depth where the pore pressure in the hydraulically connected formations and in the shale is in equilibrium. This is shown in Figure 15. Observed pore pressure at the top of the centroid structure will be higher than in the middle of the centroid. Meaning that within a water-filled pressure compartment there will be higher pore pressure above the centoid depth, but the pressure gradient will show the same trend as hydrostatic. However the shale pore pressure above the centroid depth indicated as in the Figure 15 will show a lower pore pressure than in the permeable bed. Figure 15 shows the pressure vs. depth plot from Traugott's study to demonstrate the centroid effect.

Holbrook and Hauck[39] developed a" petrophysical and mechanical model" in 1987. In their paper they claim they are the only ones until that day who use Terzaghi's effective stress relation. But the previous studies were using this relationship at some point in their empirical analysis. Their method can be divided into two parts. The first part determines porosity and shale volume, V_{shale}. Using Waxman and Smits equation they calculate F, the formation factor:

$$F = \frac{C_w + BQ_v}{Ct} \quad \text{..... (32)}$$

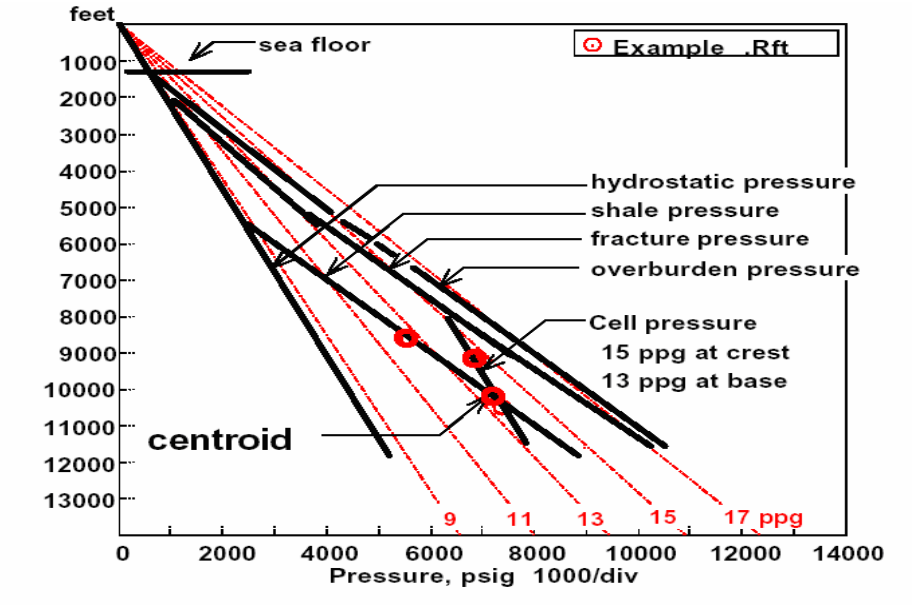

Figure 15 Pressure vs. depth plot to demonstrate centroid effect, Traugott's study.[8]

where C_t is rock conductivity, C_w is the conductivity of the water which is saturated with water, Q_v is the cation exchange capacity in milliequivalents per unit volume of pore fluid, B is specific counterion conductivity in mho/m per meq/cc. Given examples in this study assume that water conductivity and cation exchange capacity are known and used for a given area. Use of this equation should be limited to rock 100% saturated with water. After this they use Archie's equation to calculate porosity, solve equation 33 for ϕ,

$$F = \frac{a}{\phi^m} \quad \text{..... (33)}$$

They used the value of 1 for a, and 1.8-2.3 for m the cementation exponent. It is also necessary to calculate shale volume, V_{shale} for the second part of the method.

$$V_{shale} = \frac{\gamma_{obs} - \gamma_{\min\ sand}}{\gamma_{\max\ shale} - \gamma_{\min\ sand}} \quad \text{..... (34)}$$

where γ_{obs} is the observed gamma ray log reading, $\gamma_{\min\ sand}$ is the minimum sand gamma ray reading, and $\gamma_{\max\ shale}$ is the maximum shale gamma ray reading. After calculating *Vshale* and porosity, the method uses these values for the mechanical part of the model. This part is based on Terzaghi's effective stress relationship.

$P = S_v - \sigma_v$ ..... (35)

To calculate overburden, S_v, the average density for each depth is added up. This constitutes vertical total stress. σ_v, vertical effective stress is calculated from the Rubey and Hubert equation.

$$\sigma_v = \sigma_{\max} (1-\phi)^{\alpha+1} \quad \text{..... (36)}$$

σ_{max} is the stress required for a formation where it has zero porosity. σ_{max} is calculated using V_{shale} volume for each depth required. According to Holbrook and Hauck, the value of σ_{max} varies between 6000 psi and 50,000 psi for shale and quartz sandstone respectively. Figure 16 shows the values of σ_{max} and α for different types of rock. After first calculating S_v and σ_{max}, one can calculate the pore pressure required.

Mineral (or rock)	σ_{max} (kPa)	Log (σ_{max})	α	Hardness (mohs)	Solubility (ppm)
Quartz Sand	896 318	5.952	13.219	7.0	6.0
Average Shale	127 215	5.104	8.728	3.0	20.0
Limestone	82 737	4.917	13.000	3.0	140.0
Anhydrite	10 928	4.038	20.000	2.5	3000.0
Halite Sand	586	2.769	31.909	2.0	350000.0

Figure 16 Halbrook study results for effective stress constants for different lithologies.[40]

Drauo et al.[7] proposed two methods in 2001. The methods are called the Compaction Concept Method and the Power law Relationship Method. The Compaction Concept Method uses the relationship between vertical stresses. Acoustic logs are used for this method. For normally pressured shales, the relationship between porosity and vertical stress is;

$$\phi_n = \phi_i \exp(-K\sigma_v) \quad \text{..... (37)}$$

$$\phi_n = \phi_i \exp(-K(\sigma_{ob} - Pp)) \quad \text{..... (38)}$$

where σ_v is vertical effective stress, σ_{ob} is overburden stress, P_p is pore pressure, Φ_N is normally pressured shale porosity and Φ_i is porosity of shale at the surface. K is constant. Wyllie's equation is used to relate sonic readings to porosity:

$$\Delta t = m\phi + b \quad \text{..... (39)}$$

where m is Δt_{fluid}-Δt_{matrix} and b is Δt_{matrix}. Where abnormal pressure is observed, sonic readings can be related by:

$$\Delta t_a = m\phi_i \exp(-K(\sigma_{ob} - Pp)) \quad \text{..... (40)}$$

They solve for abnormal pore pressure gradient:

$$Gp = 1 + 1/(KZ) \ln\left[((\Delta_{ta} - \Delta_{tn})/m\phi_i) + \exp(-K\alpha Z)\right] \quad \text{..... (41)}$$

where α is vertical stress gradient. In this solution, they assumed Δt_{matrix} is constant. When they apply this formula to actual field data they observed 3% to 6% difference between computed and actual pore pressure. In the power law relationship method, they used the relationship between the logarithm of sonic transit time vs. depth.

$$\Delta t = a * b^{Z} \quad \text{..... (42)}$$

where *a* is the intercept of the plot and *b* is the slope of the trend line of the sonic transit time. Using this power law relationship they obtained a pore-pressure equation;

$$Pp = 1.0 * Z - \frac{\alpha}{\log b} * \left(\frac{\Delta_{ta} - \Delta_{tn}}{a} - b^{Z} \right) \quad \text{..... (43)}$$

This method gave 1% to 3 % difference between computed and actual pore pressure. This method is also another method which uses the vertical effective stress. Table 3 summarizes the other methods.

Conclusions

Pore pressure detection methods have changed over time due to the improvements in technology. When there were only electrical wireline logs, empirical correlations were used to create an estimate before drilling. These empirical relations were obtained from offset well data. Some of these methods provided general pore pressure trend curves such as Pennbaker[27]. However, every area requires its own curve for analysis, which leads to the necessity of having a library of these curves. With the inventions of LWD and MWD measurements, real time well site computations of pore pressure became available.

Nearly all the methods in the literature relate shale excess porosity with excess pore pressure. This is explained by the shale compaction behavior. Since shale is compacted to a greater extent as compared to the other lithologies, any excess porosity is interpreted as indicating undercompaction resulting in overpressure.

The methods which use seismic data for pore pressure interpretation generally parallel the methods which use sonic log data. They have not been included in this review.

Table 3 Summary of the other methods.

Other Methods		
Bowers [36]	Method detects unloading due to fluid expansion. Effective stress vs. Sonic velocity cross plot can be used. Effective stress vs. Density cross plot is used.	Method is able to detect a part of yielding. Best method for pore pressure prediction using sonic data where there is unloading.
Traugott[8]	He introduced the centroid concept. He suggested that a mean effective stress based pore pressure prediction method should be used universally.	Centroid concept is important to notice that RFT values may not help to calibrate the pore pressure prediction methods. Center of centroid should be known.
Holbrook and Hauck[38]	They have a petrophysical – mechanical model. ϕ is calculated from Waxman and Simits equation combined with Archie equation. σ_v is calculated using parameters of the formation.	This method can be extended to use mean total stress for compressional environments. For a specific stress regime, specific formations mean total stress can be represented by a function as in Holbrook and Hauck method.
Drau et al.[7]	They have two mathematical proposed models for pore pressure prediction.	Vertical effective stress vs. depth relationship extended with mathematical models to be used in the pore pressure model. Nothing different from previous applications, though it is the newest methods.

CHAPTER III

MEAN TOTAL STRESS METHOD

Introduction

Previous methods mentioned in the state of art part of this study, were all based on the 1D compaction theory. In that theory, sediment is compacted under only vertical stress and lateral stresses are not considered directly. The 1D compaction theory also states that porosity is reduced as a function of only vertical stress with depth. [24]

When overpressure due to undercompaction was studied, researchers used Terzaghi's effective stress theory as their basic theory to quantify pore pressure. Most of the research done in the Gulf of Mexico show very impressive results when vertical effective stress-based methods are used. However, this is not the case for other parts of the world.

Hottmann et al.[41] published drilling problems they had faced in the Gulf of Alaska in 1979. Borehole stability problems occurred due to high pore pressures. When they examined the region they realized that the wells were drilled near an active plate subduction boundary. The area was not tectonically relaxed and strike slip faults were present. They brought attention to the fact that pore pressure estimation methods which work for the Gulf of Mexico were not working for the Gulf of Alaska.

Hermanrud et al.[42] question the porosity estimates from well logs for the offshore Mid-Norway, Haltenbanken field. For some wells they were observing high porosities for normally pressured zones, whereas in overpressured zones they were not observing high porosities as expected. In their review of the geology of the area, they mentioned the occurrence of strike-slip faults in the middle of the field. However, their pore pressure estimate just took vertical stress, (overburden), into account. So the pore pressure techniques which assume vertical stress is the main stress inducing agent and compaction is due to only vertical stress, were not working well for this area.

Swarbrick[43] questioned where to use porosity based methods. He concluded that porosity-based method fail where centroids are observed, where top of overpressure start at the mudline, where clean shale formations were not observed, where unloading occurred, where cementation and dissolution is observed in the lithology and where lateral stresses are higher than overburden. He stated that the Eaton and the equivalent-depth methods will fail under these circumstances.

From a rock mechanics point of view, 1D compaction assumes that there is only one normal strain. This assumption is valid in normal, tectonically relaxed areas like the Gulf of Mexico.

Infinitesimal normal strain is represented by:

$$\varepsilon = \frac{\Delta l}{l_i}$$

where ε is normal strain, Δl is the change in length and l_i is original length. After 1D compaction there is no lateral change in size which means no (zero) lateral normal strain.

$$\begin{pmatrix} \varepsilon_v & 0 & 0 \\ 0 & 0 & 0 \\ 0 & 0 & 0 \end{pmatrix} \text{vs.} \begin{pmatrix} S_v & 0 & 0 \\ 0 & S_h & 0 \\ 0 & 0 & S_h \end{pmatrix}$$

The first tensor represents 1D strain tensor. The second tensor represents the Cauchy stress tensor of the stress state for the 1D compaction theory. Even though there are lateral horizontal stresses which are equal, the strain tensor has only one normal strain for compaction in 1D compaction. Notice that compression is positive and the stress magnitudes are; $S_v > S_h = S_h$.

However, Anderson[11] pointed out in his study that in strike-slip environments and reverse faulting environments vertical stress is not the maximum principal stress. Figure 17 shows the stress states defined by Anderson as associated with the three types of faults. Vertical stress is the intermediate principal stress in strike-slip environments and vertical stress is the minimum principal stress in reverse faulting environments.

The general stress state for a given area where 3 principal stresses are observed can be represented by;

$$\begin{pmatrix} S_1 & 0 & 0 \\ 0 & S_2 & 0 \\ 0 & 0 & S_3 \end{pmatrix}$$

If the well is drilled vertically, vertical stress as one of the three principal stresses will be parallel to the well bore and the other two principal stresses will be mutually perpendicular to the vertical stress. This is one of the assumptions that the following pore pressure prediction method is based on.

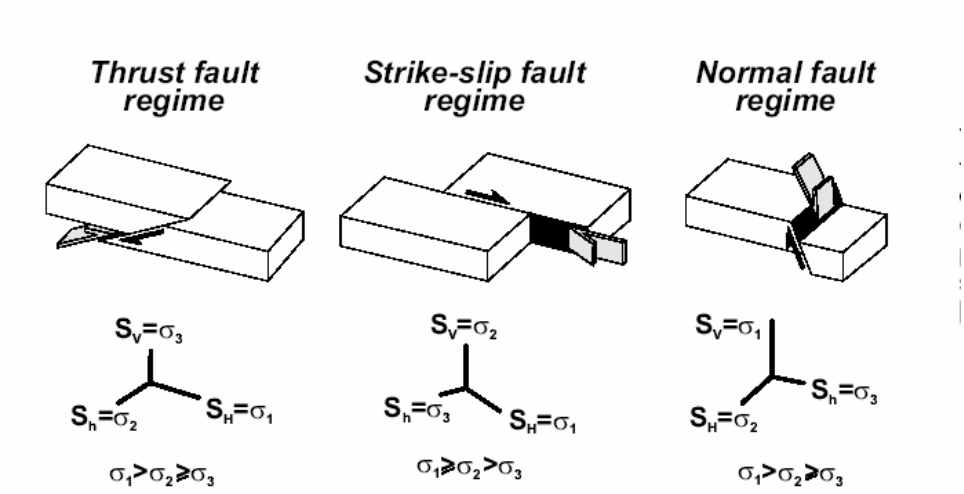

Figure 17 Representation of Anderson Faulting Theory.

At this point the question which may arise is “why use the mean of the principal stresses instead of just one, vertical stress”.

Goulty answers this question in his paper in 1998[12]. He gives the Mahakam Delta Field as an example where mean stress is the main compaction controller. Overpressure

observed in the Mahakam Delta is explained by undercompaction without unloading. When the analyst relates pore pressure to overburden stress, they used Biot constant.

$$\sigma_v = S_v - \alpha P \quad \text{..... (44)}$$

The Biot constant value was 0.67 for Mahakam Delta. Goulty used the theory of poroelasticity to explain the Biot coefficient relationship to dilatancy of a rock. He uses the word dilatation for the phenomenon where there is a change in the volume of the rock. He expressed the change in volume when the mean stress increased during compaction by infinitesimal volumetric strain;

$$\frac{\Delta V}{V} = -\frac{1}{k_s}\Delta p - \frac{1}{k_{nc}}(\Delta s_m - \Delta p) \quad \text{..... (45)}$$

where Δs_m is the change of mean total stress, Δp is change in pore pressure, k_{nc} is matrix bulk modulus and k_s is the bulk modulus of the solid grains. When $\Delta p = 0$, k_{nc} is the parameter which relates change in mean total stress to the change in volume. For this reason it is also called the drained bulk modulus. First set the change of pressure Δs_m and Δp equal so that

$$\Delta s_m - \Delta p = 0$$

At this point equation 45 becomes;

$$\frac{\Delta V}{V} = -\frac{1}{k_s}\Delta p \quad \text{..... (46)}$$

meaning the change in volume related to the pore pressure change is related to volume change of the grains, which will decrease as the pore pressure increases.

Now an additional increase in mean stress by $\Delta\sigma_m = \Delta s_m - \Delta p$, but with no change in the pore pressure is applied to the formation. The equation becomes:

$$\frac{\Delta V}{V} = -\frac{1}{k_{nc}}\Delta\sigma_m \quad \text{..... (47)}$$

If the Biot coefficient during normal compaction is α_{nc} and it is defined by,

$$\alpha_{nc} = 1 - \frac{k_{nc}}{k_s} \quad \text{..... (48)}$$

then equation 45 becomes

$$\frac{\Delta V}{V} = -\frac{1}{k_{nc}}(\Delta s_m - \alpha_{nc}\Delta p) \quad \text{..... (49)}$$

He introduces the porosity in equation 45 by using the stress concept. By definition, stress is the force applied to the unit area. The force applied at this case is $\Delta\sigma_m = \Delta s_m - \Delta p$, and unit area is $1-\Phi$. Stress becomes

$$\frac{\Delta\sigma_m}{1-\phi} = \frac{\Delta s_m - \Delta p}{1-\phi}$$

Volume reduction due to this stress is expressed by

$$\frac{\Delta\sigma_m}{k_s(1-\phi)}$$

Now equation 45 becomes

$$\frac{\Delta V_s}{V_s} = -\frac{1}{k_s}\Delta p - \frac{1}{k_s}\left(\frac{\Delta s_m - \Delta p}{1-\phi}\right) \quad \text{..... (50)}$$

where V_s represents the change of volume of solid material. Porosity is expressed in the form,

$$\phi = 1 - \frac{V_s}{V} \quad \text{..... (51)}$$

When this expression is differentiated, the change in porosity becomes

$$\Delta\phi = \frac{V_s \Delta V}{V^2} - \frac{\Delta V_s}{V} \quad \text{..... (52)}$$

$$\Delta\phi = (1-\phi)\left(\frac{\Delta V}{V} - \frac{\Delta V_s}{V_s}\right) \quad \text{..... (53)}$$

When he substituted equation 45 and equation 50 into the change in porosity expression, he obtained

$$\Delta\phi = -\left(\frac{1-\phi}{k_{nc}} - \frac{1}{k_s}\right)\Delta\sigma_m \quad \text{..... (54)}$$

He did not include the effect of temperature in the analysis, however since the terms subtracted from each other and the temperature term will cancel.

The conclusion he arrived as after this computation is that porosity change is directly related to mean effective stress rather than vertical stress. He refuses to use the Biot constant to relate effective stress to pore pressure. Instead he advocates using equation 54.

He indirectly uses the assumption that S_v is the normal stress acting on the plane which is parallel to the formation where the formation is not tilted. S_v, S_H, S_h are orthogonal normal stresses and they are also principal stresses acting on the rock matrix.

For equation 54 to be useful for determining pore pressure, k_{nc}, frame bulk modulus and $k_{s,}$ the bulk modulus of the solid grains must be known. It is not easy to know these parameters, so he uses empirical equations from soil mechanics to relate porosity to effective stress. The Rubey and Hubbert equation is given as one alternative for this relation,

$$\phi=\phi_o \exp(-\varsigma \sigma_v) \quad \text{..... (55)}$$

where ς is the slope of log σ_v vs. porosity plot and ϕ_o is the porosity at the surface. He also mentions Burland's equation for the effective stress- porosity relationship.

$$\sigma_v = \sigma_1 \exp\left(\frac{r_1 - r}{\beta}\right) \quad \text{..... (56)}$$

where, $r = \frac{\phi}{1-\phi}$, is the void ratio. If we use these empirical relationships for vertical effective stress and porosity, then it is possible to relate the mean effective stress to porosity as well.

Where lateral stresses are higher than normal, such as in strike-slip faulting environments, it is possible that at one point in time the compaction was controlled by mean effective stress rather than vertical stress.

Unloading occurs where the effective stress is reduced at some point in the compaction history. Porosity decrease is primarily elastic when effective stress is reduced. When

effective stress is increased to its normal pattern, this elastic porosity could be reduced again to its normal pattern as effective stress. This is illustrated in Figure 18.

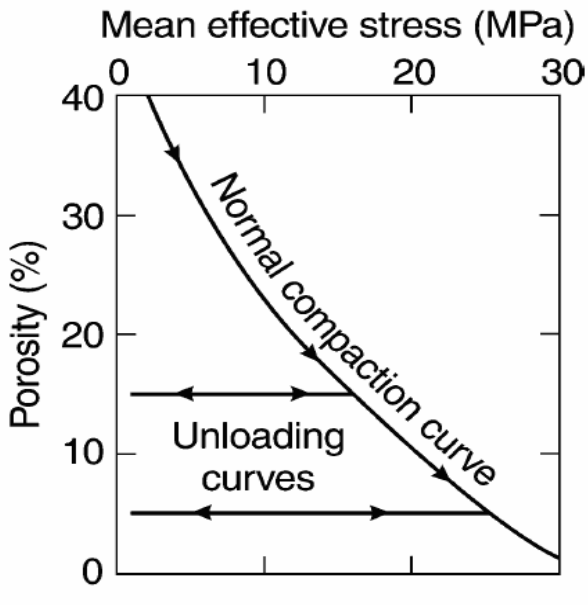

Figure 18 Goulty's representation for relationship between unloading and normal compaction curves.[12]

The method used for this study is time independent, which means the stress applied on the formation during compaction or after compaction is not important for this study. But the present stress distribution in the area will be used to determine the pore pressure.

If the stress applied can help unloading porosity to return to the normal porosity reduction trend, any overpressured zone where unloading occurred once can come back to the normal compaction trend by later applied stresses, therefore the assumption that the present stresses observed in an area is controlling the porosity reduction may not be far from the truth.

Harrold et al.[44] applied Goulty's theory in tertiary basins in Southeast Asia. They studied mudrocks, using Issler's equation to relate porosity to sonic log velocity.

$$\phi = 1 - \left(\frac{\Delta t_{ma}}{\Delta t} \right)^{1/2.19} \quad \text{..... (57)}$$

where Δt is the measured slowness and Δt_{ma} is matrix travel time slowness, which was selected as 220 μs/m. They used this default value in their study. They did not compute the matrix slowness for the three distinct areas they studied. They assumed lateral stresses are equal to each other and they used the empirical relationship of Breckels and van Eekelen to relate minimum horizontal stresses to depth.

$$s_h = 16.6 D^{1.145} + 0.49 (p_f - p_{hyd}) \quad \text{..... (58)}$$

In this computation, they calculated lateral stresses assuming hydrostatic pressure. When they calculated the mean effective stress, the equation reduced to

$$\sigma_m = \frac{1}{3} (s_v + 33.2 D^{1.145}) - p_{hyd} \quad \text{..... (59)}$$

The pore pressure equation they used was

$$p_f = 16.6 D^{1.145} + 0.5 s_v - 0.5 p_{hyd} - 1.5 \sigma_m \quad \text{..... (60)}$$

They compared the pore-pressure estimate using the mean stress method to that of vertical stress method. They claimed that for Southeast Asia fields, the mean stress approach estimated results closer to the real pore pressure values, and the vertical stress approach underestimated pore pressure. They did not specify the empirical relationship they used to calculate pore pressure.

What they did not say was whether the field of study was in strike-slip or not. In areas like the Gulf of Mexico where lateral stresses are smaller than the overburden, the mean stress method will underestimate the pore pressure.

Van Ruth et al.[45] applied the mean effective stress method to explain high overpressure observed in the Cooper Basin. The reason they applied the mean effective stress method to this basin was to explain the effects of lateral stresses due to tectonic loading on pore pressure. They used the assumption that minimum and maximum horizontal stresses are equal. They were able to explain that the excess pore pressure observed in the area was a consequence of lateral stresses. The significance of this was that the mean effective stress method was able to explain the pore pressure in old sediments other than tertiary basins. The claim was that the mean effective stress could be used to explain high pore pressure even though the sediments were not subjected to rapid burial.

Conclusions

It must be noted that the stress distribution for a given area is extremely important. Anderson's faulting theory clearly states that there are three stress regimes and orientation of maximum principal stress is different for each case. Where normal faulting is observed the maximum principal stress is the overburden and is vertical and, the two horizontal stresses will be less in the magnitude. Furthermore, when you add three normal stresses and divide the sum by three, you will obtain mean stress smaller than overburden alone. If mean stress obtained from a normal faulting area is used to

calculate pore pressure the result may be an underestimate of pore pressure. But where the vertical stress is either the intermediate or minimum principal stress for the area, as strike slip and reverse faulting environments respectively, the mean total stress based pore-pressure estimate is likely to be the more accurate pore-pressure estimate due to it is accounting for 3D compaction. Goulty relates mean effective stress to porosity change. When porosity changes with mean effective stress, the pore pressure does as well.

CHAPTER IV

MINIMUM AND MAXIMUM HORIZONTAL STRESS DETERMINATION

The mean effective stress method requires knowing the minimum and maximum in situ horizontal stress for the analysis. in situ stress analysis gives information about the stress state of the rock which is of concern. The Cauchy stress tensor represents the stress state at a point in the subsurface.

$\begin{pmatrix} \sigma_{11} & \sigma_{12} & \sigma_{13} \\ \sigma_{21} & \sigma_{22} & \sigma_{23} \\ \sigma_{31} & \sigma_{32} & \sigma_{33} \end{pmatrix}$ Tied to the reference frame which has directions represented by 1, 2, 3;

Where, $\sigma_{11}, \sigma_{22}, \sigma_{33}$ are normal stresses and $\sigma_{12}, \sigma_{13}, \sigma_{21}, \sigma_{23}, \sigma_{31}, \sigma_{32}$ are shear stresses. Direction and magnitude of stresses must be known to define a complete stress tensor.

However, it is difficult to know the direction and magnitudes of the stresses in the subsurface. There are ways to estimate in situ stresses, and all of them have limitations. Bloch et al.[46] have summarized the techniques on in-situ stress determination as:

- Anelastic strain recovery test (ASRT).
- Borehole breakout analysis.
- Borehole imaging
- Circumferential velocity anisotropy (CVA)
- Differential strain curve analysis (DSCA).
- Direct observation of overcored open-hole microfractures.

- Directional gamma ray logging
- Drilling-induced fractures in cores.
- Earth tilt curves
- Leak-off inversion technique
- Micro- and Mini-Frac Tests
- Petrographic examination of microcracks
- Earthquake focal plane mechanism
- Microfracture pressure analysis
- World stress mapping

All these techniques give some information on components of stress tensor, but not all aspect. Combination of two or more techniques may help to obtain the stress tensor. A complete stress tensor is needed for wellbore stability analysis and reservoir studies.

The mean total stress method, which is going to be used for pore-pressure analysis does not need the azimuth of the horizontal stresses but only their magnitudes. The vertical stress is assumed to be one of the principal stresses and other principal stresses are mutually perpendicular to it. This study will cover the technique which provides magnitudes of horizontal stresses as a result of the analysis.

The analysis will use the results from leak-off test (LOT) inversion, wellbore breakout analysis and data in the world stress map.

Leak-Off Test Inversion

During drilling, after every casing string is set, a pressure integrity test is done. The kind of pressure integrity test done depends on the required knowledge for the well. A simple version of pressure integrity test is to test the strength of formation to a previously targeted value. After setting the casing and performing the cement job, cement should be tested for channels in the cement. For this purpose, the annulus is shut in and mud is pumped to pressurize the formation to the desired pressure where the flow return is restricted. Formation is pressurized to this certain desired pressure. If the pressure is constant for some time and there is no rapid pressure decline after pumping is stopped, the cementing job is considered to be successful. There will be a pressure decline when the pumping is stopped due to formation permeability and mudcake filtration, but it is not as significant as the pressure decline due to a leak in the casing cementing. A pressure integrity test is called a formation integrity test if it is done to test the strength of the formation to a specific pressure.[47]

Leak-Off Test, LOT, is also a pressure integrity test, but this time the pressurization is continuous until there is a pressure decline in the rate of pressure build-up.[48] The pumps are stopped when a decline in the pressure build up is seen. The pressure where the first decline of the pressurization rate is seen is called leak-off pressure. Figure 19 shows a typical example for a LOT, leak-off pressure and associated minimum stress is illustrated on the graph.

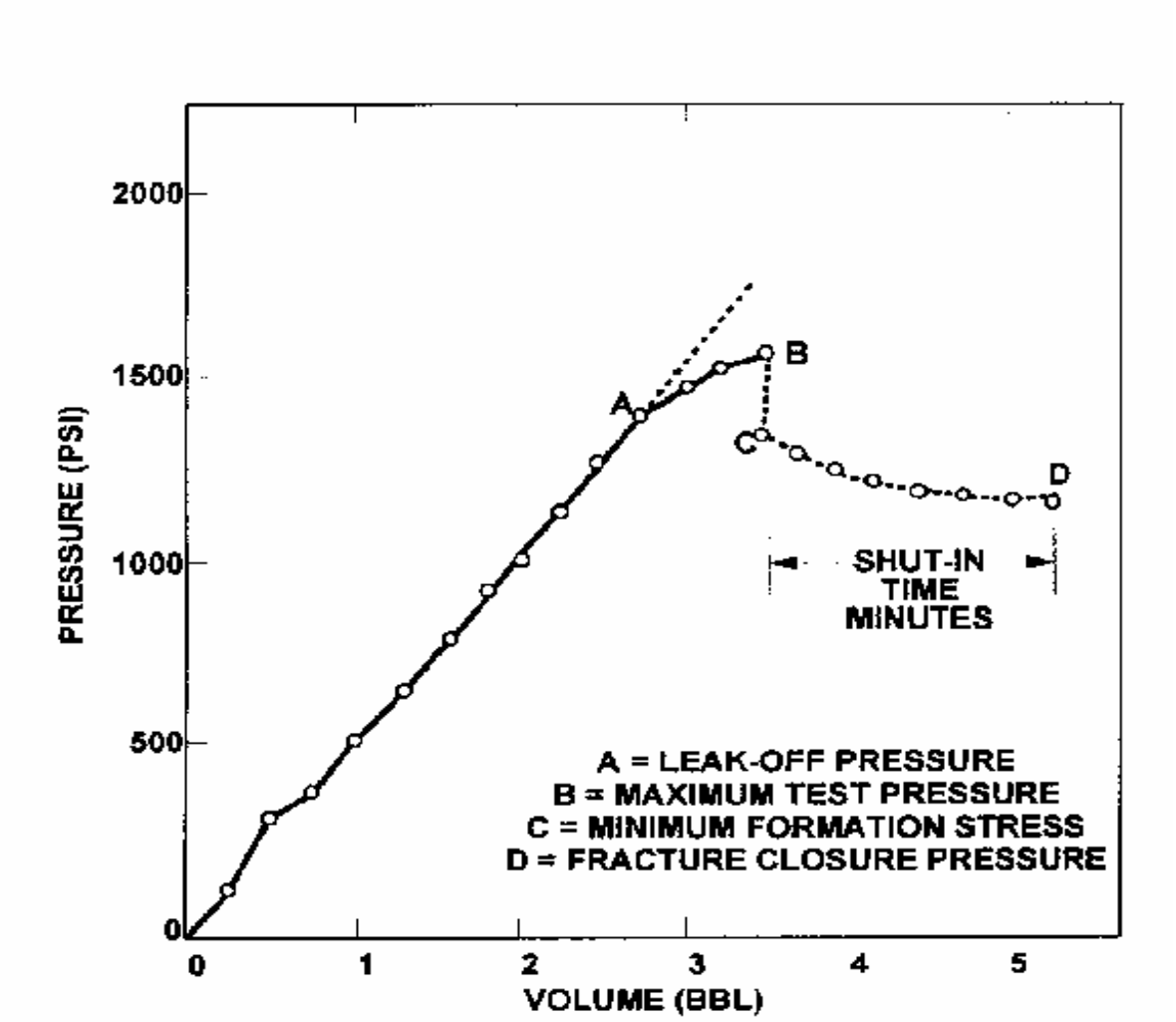

Figure 19 Typical example for LOT. Leak off pressure and minimum stress is illustrated.[47]

Estimation of this leak-off pressure is quite important for drilling industry. Drilling designs for mud weight, casing setting depth, wellbore stability plans are in need of good fracture gradient and minimum horizontal stress estimation.

Addis et al.[49] give a good summary of the pressure integrity test types and limitations on each test. The also compare LOT and extended LOT (ELOT or XLOT) in their study. An ELOT is done by applying more than one pressurization cycle during the test. This is to account for the possibility of the tensile strength of the rock being included in the magnitude of the breakdown pressure. A second cycle of pressurization will show the closure pressure of the initiated fracture since at the first pressurization run the fracture opened should have overcome the tensile strength of the rock. But when the fracture is ok and it is opened again in another pressurization run, the estimate of the closure pressure will be a better estimate. Figure 20 shows the stages required by ELOT.

Raaen et al.[50] states that multiple pressurization of borehole may cause lower estimates of minimum horizontal pressure.

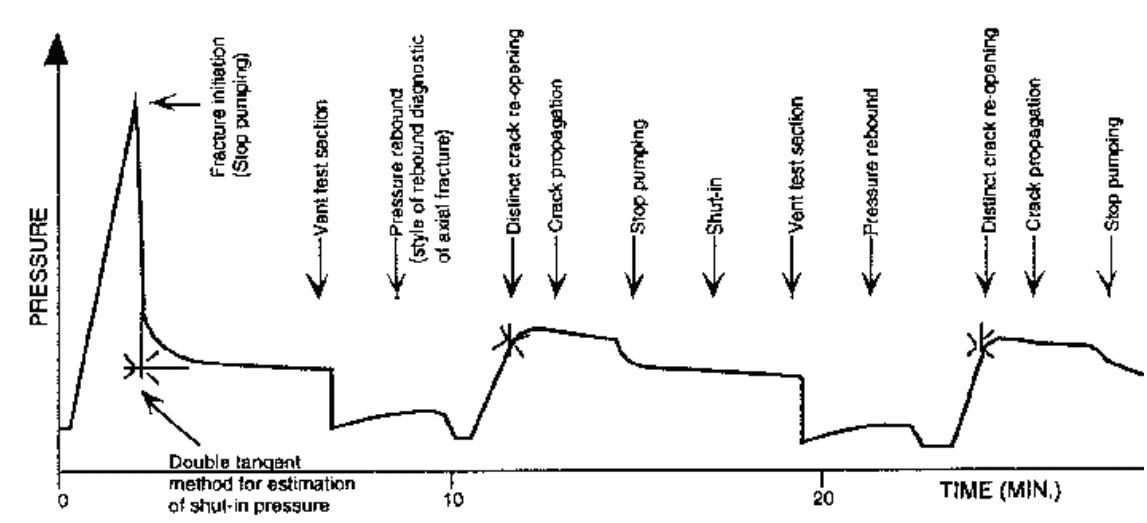

Figure 20 Example for a hydraulic fracturing test. Same test stages are required by ELOT.[48]

The Pressure vs. time graph after pumps are stopped is used to estimate formation stresses. The method used is called the tangential method. The minimum horizontal stress is estimated from this test. After overcoming the tensile strength of the rock, one can conclude that the required fracture opening pressure is the minimum horizontal stress for that formation.

Like every test done in high uncertainty conditions due to the compressibility of the mud, casing expansion or leakage of casing cement, the LOT also has some limitations. the Tangential method predicts closure pressure, which is considered to be minimum horizontal stress for that formation. The square root of time vs. pressure is plotted for the data after the breakdown is observed and the pumps turned off. There will a quarter circle trend for the data. One tangent is drawn from the upper portion of circle and another one will be drawn from the down part of the circle. The intersection of these two lines is interpreted to be the estimation of minimum horizontal stress. According Addis et al.[49], there are some established methods for predicting minimum horizontal stress using LOT or XLOT data. They state them as follows,

1- Using the Hubbert and Willis formula,

$$P_{lo} = 3S_h - S_H + T_o - P_p \quad \text{..... (62)}$$

for impermeable rocks, where P_{lo} is leak off pressure, T_o is the tensile strength of the rock.

2- Solve equation 63 by assuming a relationship between horizontal stresses.

3- Use the assumption of P_{lo} being equal to minimum horizontal stress σ_h.

4- Use instantaneous shut-in pressure ISIP as an indicator of σ_h.

For this study the assumption of leak-off pressure being equal to minimum horizontal stress will be used.

Addis et al.[49] also published horizontal stress magnitude equations for the Snorre field, which is the concern of this thesis. They state that these equations were calculated using XLOT and LOT data. Use of the published equations gave results that deviated from the original values by 3%. The equations are;

$$\begin{aligned} S_H &= 0.023D + 1.8 \qquad for\ D \le 3{,}600\ m \\ S_h &= 0.020D + 0.5 \qquad for\ D \le 3{,}600\ m \end{aligned} \quad \text{..... (63)}$$

where D is depth in meters and σ_H and σ_h maximum and minimum horizontal stresses respectively, in MPa.

Wellbore Break-out Analysis

Wellbore breakouts can help to identify the stress state of a region where the well is drilled. The borehole is affected by stress concentration due to removal of the rock material. Borehole stability is more sensitive to the stress around it. Stress orientations can be found if borehole breakouts occur due to this stress concentration. Borehole breakouts occur in the directions of minimum horizontal stress with the maximum horizontal stress orientation being perpendicular to the breakout direction. Figure 21 illustrates this relationship. The pore-pressure magnitude in combination with the stress distribution created by the presence of the borehole should overcome the tensile strength

of the rock for breakout to occur. The magnitude of maximum horizontal stress can not be estimated by using only borehole breakouts. In addition, even though it may not be possible to measure the exact pore pressure, an estimate can be found. Caliper and image logs are used today to find and analyze borehole breakouts. Four or more armed caliper logs using tools with four or more arms tend to rotate during the logging of a normal borehole, but they stop rotating when they encounter a breakout. An image log also can show the breakouts. The detailed explanation of how they image will not be covered here, however they rely on tool response to the geometry of the borehole. It is very important to notice that hole geometry alterations due to washouts and key seats are not due to the stress state of the formation.[52] Figure 22 shows four-arm caliper responses to borehole anomalies like breakouts, washouts and key seats.

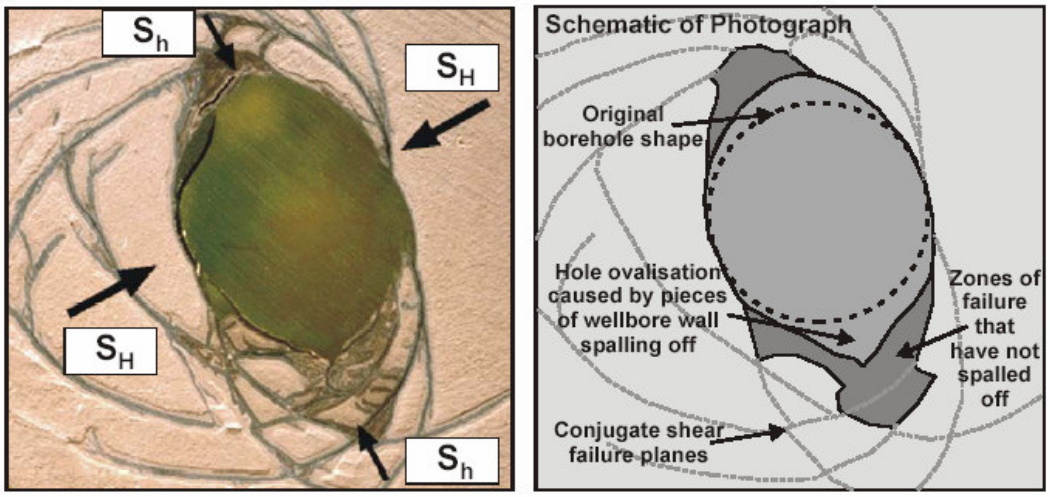

Figure 21 Borehole breakouts and horizontal stress generating them.[51]

World Stress Map

The World stress map is an ongoing project where tectonic stress data are stored in a database. It is a database open to everybody. It is claimed that there are 16,000 stress data sets in the project. Stress maps for specific regions can be obtained from this data base.[52] The stress state indicators used in this project are earthquake focal mechanisms, wellbore breakouts, drilling-induced fractures, in-situ stress measurements, and young geologic data: fault-slip analysis and volcanic vent alignments.[53] The world stress map provides data for, Europe, America, Africa, Asia and Australia.[54] Also regional specific stress data can be obtained from this database. Figure 23 illustrates the North Sea stress map.

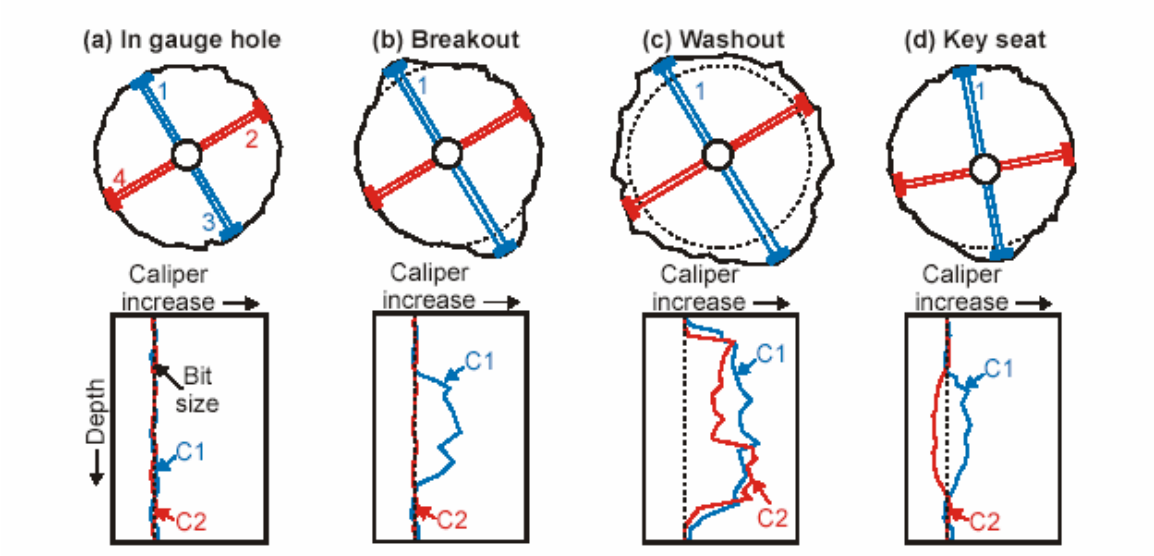

Figure 22 Illustration for four-arm caliper responses to borehole anomalies like breakout, washout and key seat. [51]

Conclusions

Wellbore break-out analysis, World Stress Map Project and Leak-off Test inversion are the most readily available source of earth stresses. Not only one of them will be sufficient to estimate mean stress. Stress distribution studies for a given area use all of these mentioned sources to estimate and relate horizontal stresses.

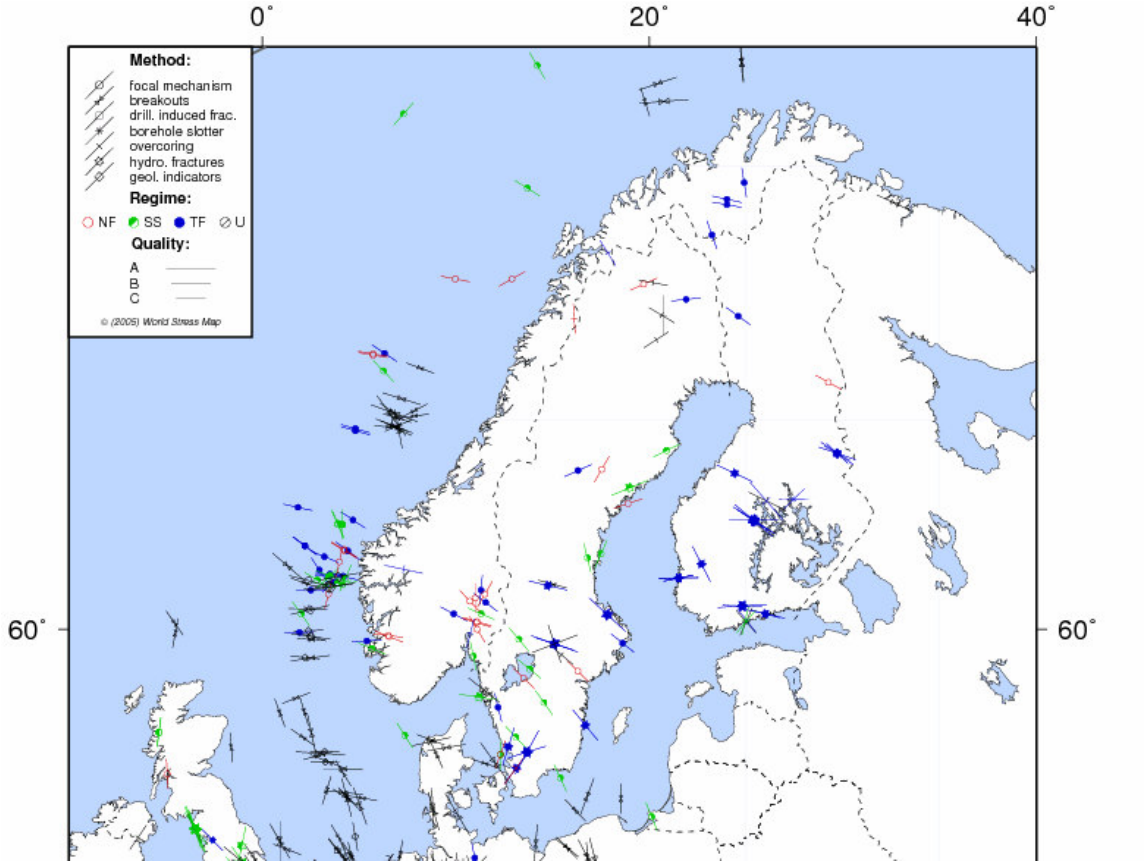

Figure 23 North Sea stress map from the world stress map project.[54]

CHAPTER V

APPLICATION OF MEAN TOTAL STRESS METHOD

Like Harrold et al.[55] and Van Ruth et al.[45] the following application will use mean total stress to predict pore pressure. But unlike Harrold et al. and Van Ruth et al., the horizontal stresses are not assumed to be equal. The stress anisotropy in the horizontal plane is used with changing horizontal stress magnitudes such that the two principal horizontal stresses are not equal The chosen field for the application is Snorre Field from North Sea, which is known to be in a strike-slip to reverse faulting environment.

Geology of the Snorre Field

The geologic description of the Snorre Field is based on the study done by Aadnoy et al.[56] The study was done for stress estimation purposes. The included geological information for the Snorre field is relevant to a stress- related study.

The Snorre field is located in southern part of the Tampen Spur which is a part of Northern Viking Graben. Location on the map is between 61^{o}N and 62^{o}N. (see Figure 25) The main structural features are tilted blocks that dip in the westerly direction. Major faults in the area running from east to west and include the Inner Snorre fault, the Southern Snorre fault, the Outer Snorre fault and the Murchinson fault. There are local strike-slip fault systems in at the area which decrease in importance towards north.

There are two major sea floor-spreading sequences in the area. The earliest involved rifting and subsidence from Permian to Triassic time resulting in the accumulation of the sediments in the Teist, Lomvi, Lunden Statfjord, Dunlin and lower Brent Groups. A later rifting episode during Jurassic and Cretaceous times produced a sequence of tectonic activity in the region resulting in faulting, lateral, vertical and rotational block movements, and subsidence. As a result of these following sequences, the Snorre Block became a "structural high in the area" .[56] Figure 24 gives West-East tectonics and topography profile of Snorre Field.

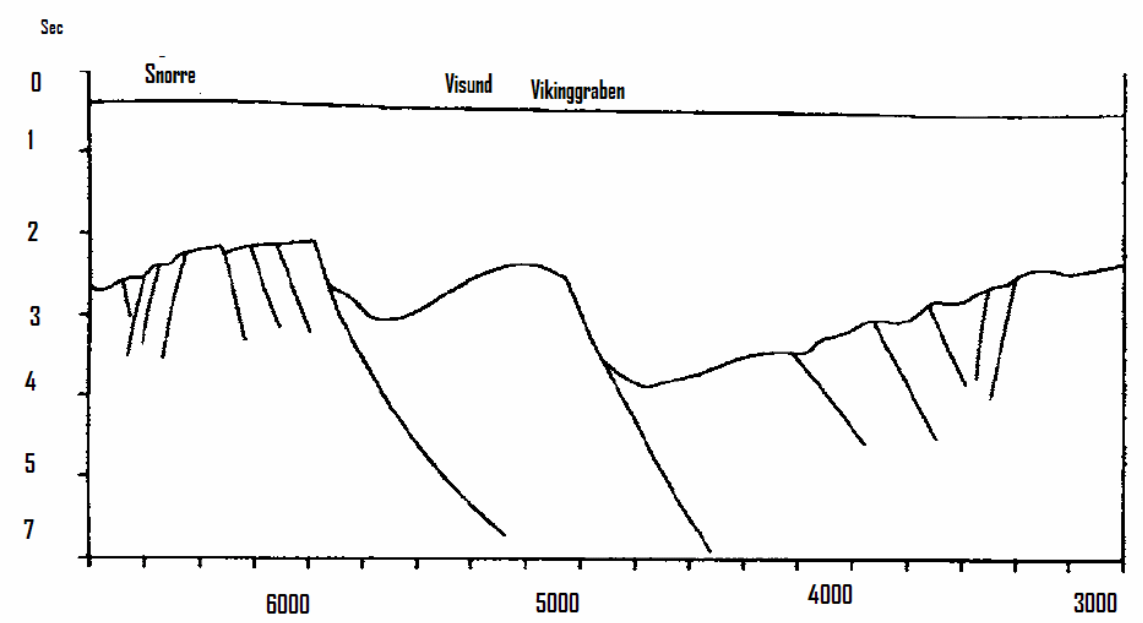

Figure 24 West-East tectonics and topography profile of Snorre Field. Seismic data are used to identify fault.[56]

The stresses caused by ancient and ongoing tectonic activity influence the stress distribution at subsurface. The description given in the study of Aadnoy et al[56] suggests

that the stress distribution in the area is not isotropic but anisotropic. Combined with the study done by Wibrut and Zoback[57], it is concluded that the Snorre Field stress environments includes reverse fault stress states and strike-slip faulting stress states based on the orientation of the fault system in area. These stress states also suggest that the compaction of sediment will have been affected by anisotropic horizontal stresses. This area is a good candidate for mean stress pore pressure determination. There is data available for horizontal stresses and pore pressure.

Horizontal Stress Boundaries for Snorre Field

The Snorre Field and the Visund Field are two fields in the Tamper Spur. Wibrut and Zoback[57] tried to determine the upper and lower bounds for the horizontal stresses in the Visund field. Their aim was to predict the full stress tensor for the Visund field, and use these data to promote successful drilling. In their study, they used drilling- induced tensile wellbore failures, leak-off tests, pore pressure and density readings to obtain their result. They applied the Mohr-Coulomb failure criterion and the Anderson faulting theory solution with the knowledge of pore pressure to determine maximum horizontal stress. As one of the results in their study they found that the orientation of the maximum horizontal stress is the same through the Visund field. Wiprut and Zoback also state that the stress state for the North Norwegian Sea is in compression from east-west to northwest-southeast. They found that at a 2.8 km the stress values are: S_v= 55 Mpa, S_{hmin}= 53 Mpa, S_{hmax}= 71,5 Mpa. This study shows that Visund field stress regime, according to Anderson faulting theory, is strike-slip since $S_{hmax}>S_v>S_{hmin}$.

Grollimund et al.[17] determined the pore pressure and minimum horizontal stress for Norwegian sector of North Sea. They also concluded that maximum horizontal stress direction is the same throughout the area.

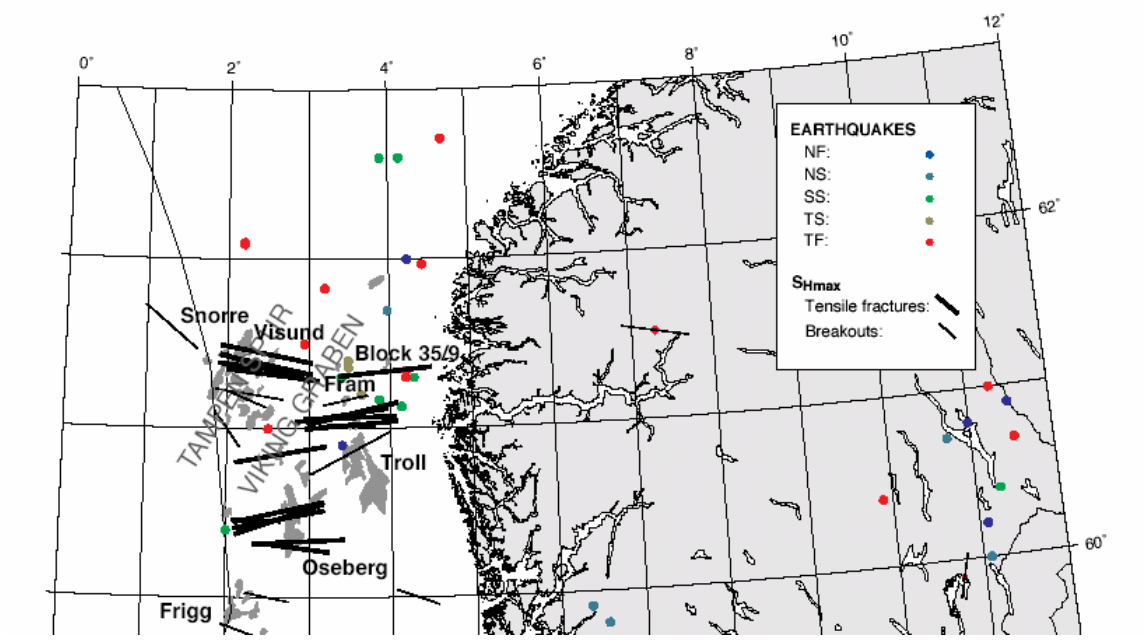

Figure 25 Norwegian North Sea stress map. Snorre Field stress data set is indicated.[17]

Grollimund et al.[58] published a study on the effects of lithospheric flexure on the compression of sediments in the North Norwegian Sea. In this study they concluded that the minimum horizontal stress magnitude in the Tampen Spur is decreasing towards coast of Norway.

They observed strike-slip to normal faulting stress states in Visund field, but reverse to strike-slip stress states for Snorre Field. Going from east to west, normal faults in the

Eastern part of the Visund field are found, then strike slip faults and finally reverse faults in the Western part of the Snorre Field. To illustrate the minimum horizontal stress distribution, they normalized minimum stress values with vertical stress values and plotted this distribution throughout the cross section they studied. Their conclusion about the stress state was summarized in Figure 26.

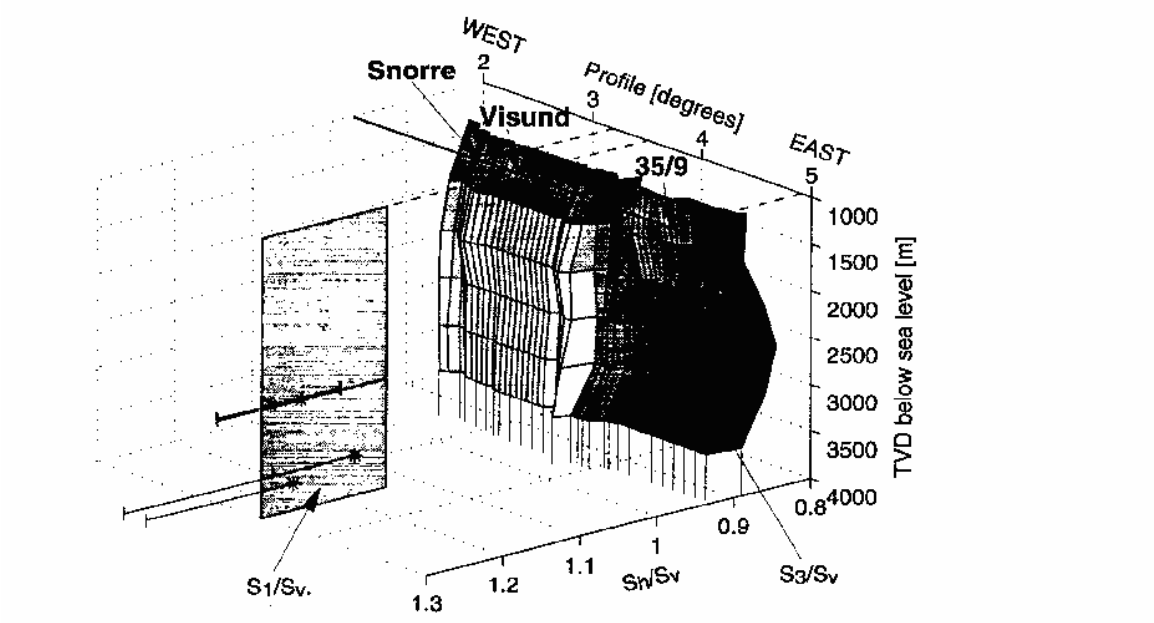

Figure 26 East-west minimum stress profiles of Snorre and Visund Fields over depth. Leak off test results are illustrated by Grollimund et al.[58]

The reported S_H/S_v values for Visund field were 1.2 at the depth of 2500 m and 1.3 at the depth of 3500 m. This means that since the Visund area shows a stress state from normal faulting to strike-slip faulting, one can conclude, due to the presence of reverse faults in the Snorre field, that the stress ratio for S_H/S_v for the Snorre field will be higher.

Grollimund et al.[58] also gave the pore-pressure distribution for Tamper Spur area as a function of depth and orientation in their study. It can be clearly seen that pore-pressure is increasing from Visund and Snorre Field as you go from east to west. (See Figure 27) The observed change in stress distribution seen going from east to west is consistent with their conclusion for normal to strike-slip stress state for Visund field and Strike-slip to reverse faulting stress state for Snorre Field.

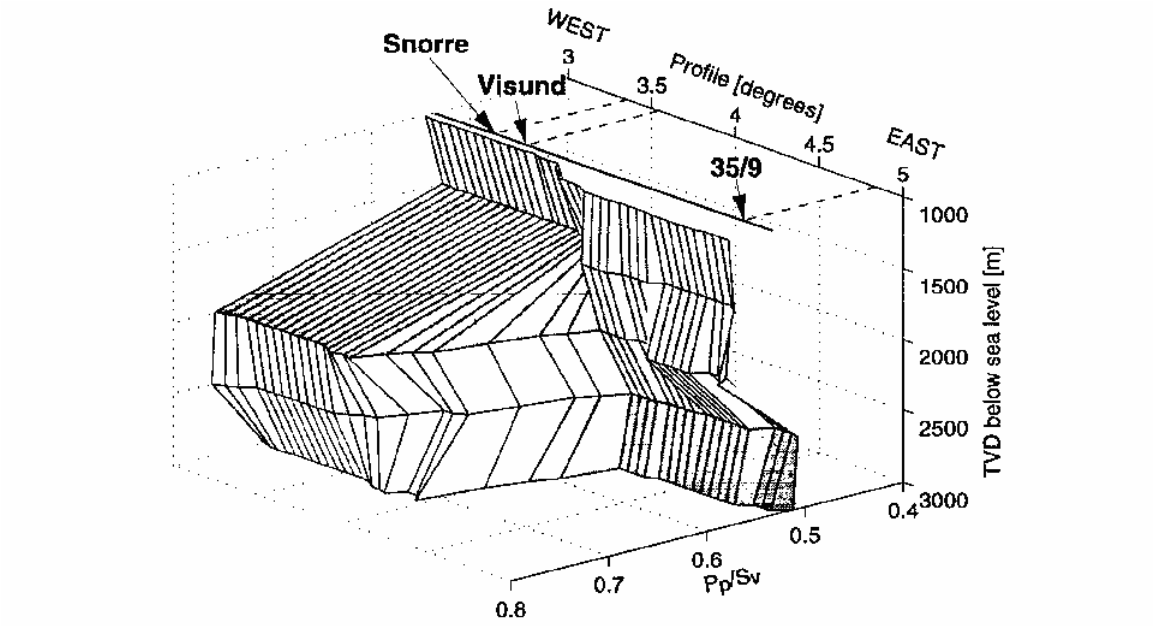

Figure 27 West-East pore pressure profile of Snorre and Visund Fields normalized by vertical stress.[58]

A comparison of Figure 26 and Figure 27 demonstrates a clear correlation between the minimum horizontal stress and observed pore pressure. Going from east to west the pore pressure increases in parallel with the increase in horizontal stress. Therefore, a pore

pressure estimation technique that takes horizontal stresses into account may be expected to provide better results than a purely vertical-stress technique.

Aadnoy et al.[56] also made a study on stress limits for the Snorre Field using earthquake focal mechanism analysis and Leak-off Test inversion. In their study, they found that below 1500 m, the horizontal stress distribution in the area is anisotropic and below 1500 m, the maximum horizontal stress increases over vertical stress. This conclusion is consistent with Grollimund et al.[58] study. However, the stress ratios given in the Aadnoy et al.[56] study show a normal faulting stress-state for the area. Grollimund et. al.[58] explain the difference between the ratios of the Aadnoy et al. study and theirs by commenting that the earthquake focal mechanism analysis gives wide ranges for the boundary values for the horizontal stresses. For this study, the minimum horizontal stress trend will be obtained from Aadnoy et. al.[56] study for shallower depths. Figure 28 shows their suggested trend for Snorre Field.

When we plot minimum horizontal stress and vertical stress vs. depth, we observe that for the Snorre area the $K_o = S_h/S_v$ ratio is not constant through out the depth. Since there is no other published study for complete in-situ stress state of the Snorre Field, the Wiprut and Zoback is bounding values of minimum horizontal stress to maximum horizontal stress ratio will be implemented in this study in order to obtain the range of values for the maximum horizontal stress. From Figure 29, from the Wiprut and Zoback et al.[57] study, at a depth of 2900 we observe, maximum horizontal stress to minimum

horizontal stress ratio is 1.3. For the sake of the analysis, a range for this ratio will be used. The range is 1.2 and 1.4. It has computed from Figure 29. Even though the computed results are for Visund field, the wide range of the ratio should compensate the any errors in the value used.

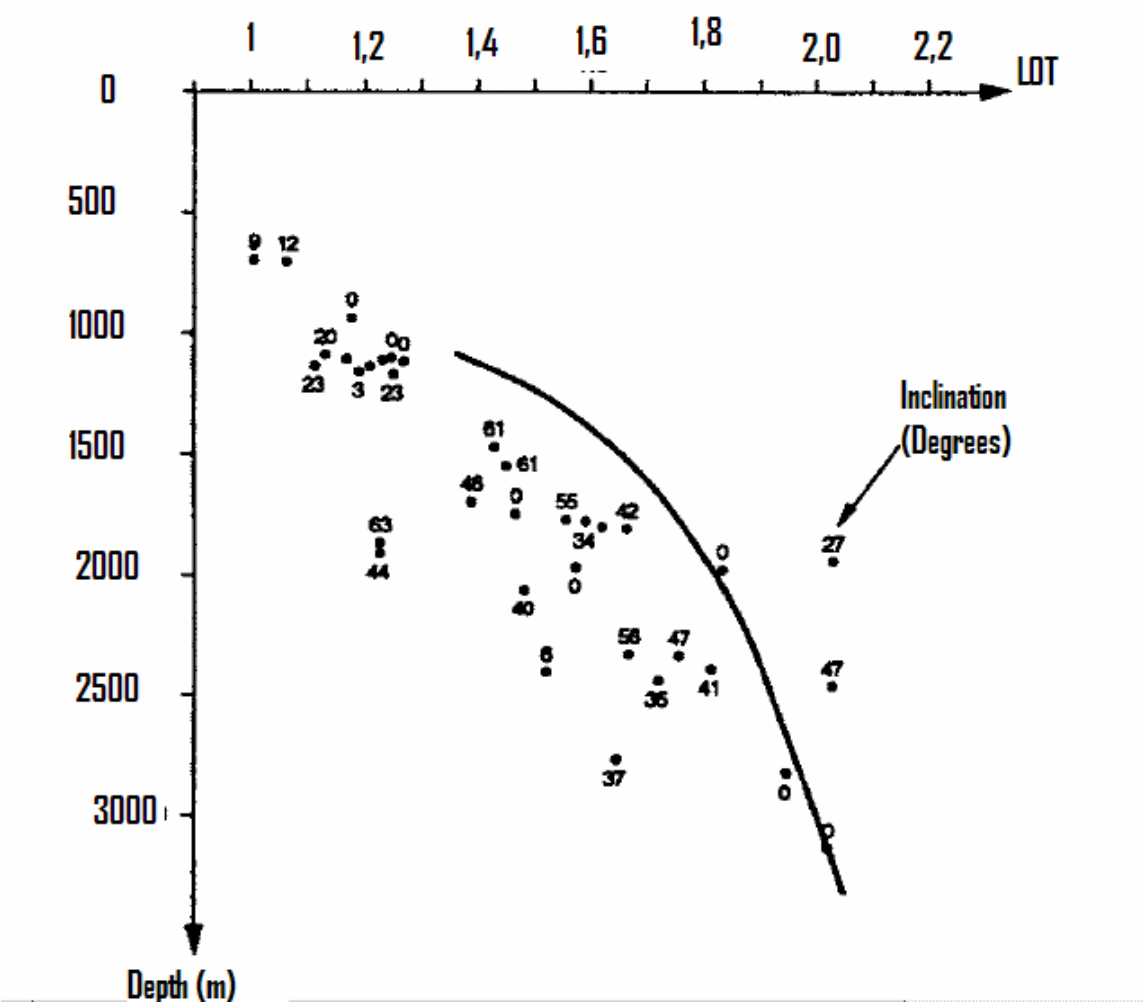

Figure 28 Leak-off test data results for Snorre Field over depth. Inclination is the borehole inclination.[55]

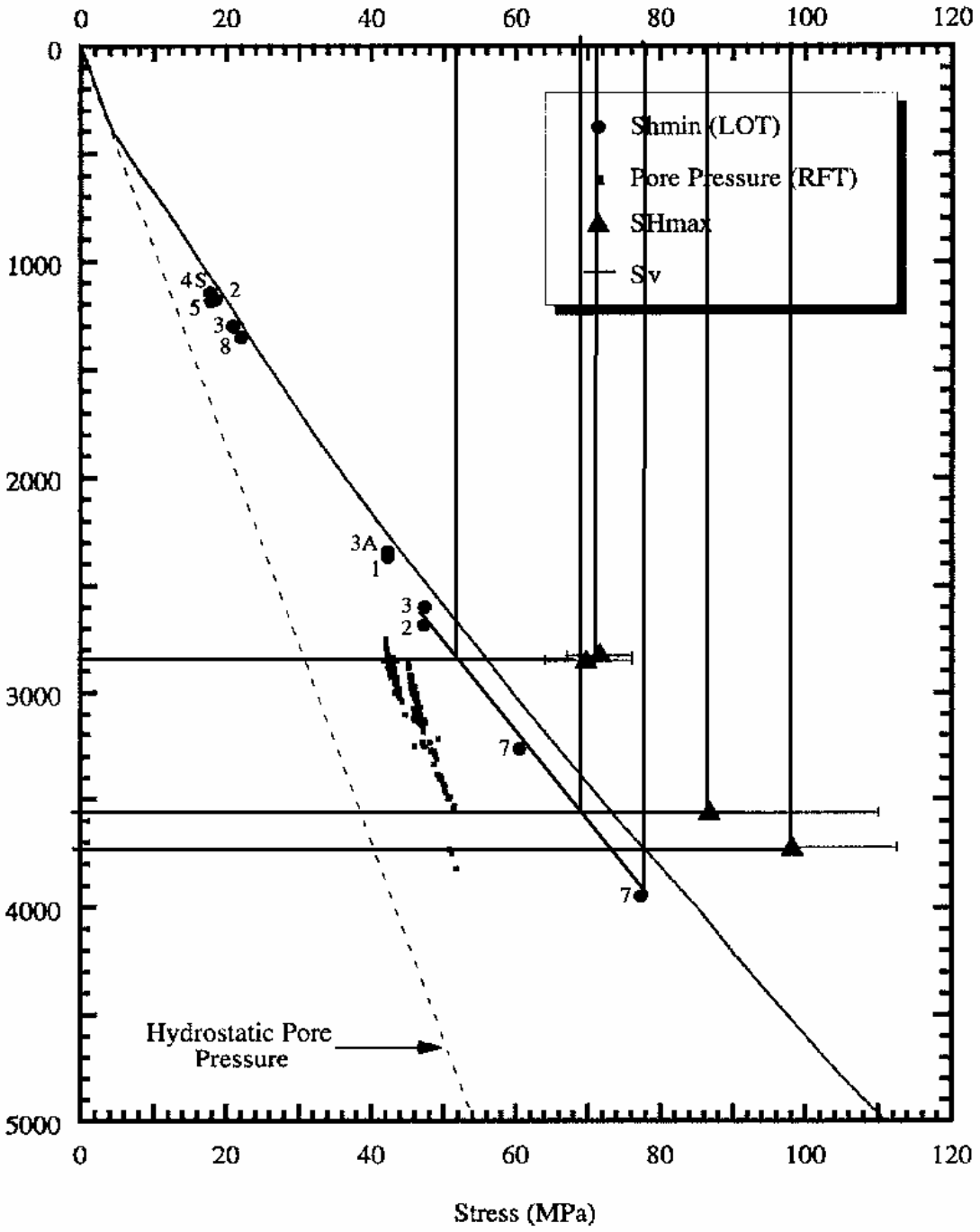

Figure 29 Minimum horizontal and maximum horizontals stress magnitudes for Visund Field. The data are used to set boundaries on mean total stress for the Snorre Field.[57] Horizontal stress ratio for Visund Field is obtained from this figure. The minimum horizontal stress and the maximum horizontal stresses are indicated on the figure by Wiprut and Zoback. At 2900 m the maximum horizontal stress is 70MPa and the minimum horizontal stress 54 MPa. The ratio of max horizontal stress to minimum horizontal stress is 1.3. There is a wide range of error bars for maximum horizontal stress. When these error boundaries include in the analysis, horizontal stress ratio changes between 1.2 and 1.4 for deeper sections.

Three wells are analyzed for this study. The results of the three wells are shown below. Figure 30 shows Leak-off Test data plotted against depth. A trend was extracted from the data. The leak-off test data from Aadnoy et al. study did not have LOT data for deeper depth as the LOT data from the wells used for this study. Leak-off test data from these three wells are used as well and the graph of Figure 30 was obtained. The trend equation from Excel "add trend line" option is

$$LOT = 0.3950 * \ln(Depth) - 1.17265 \quad \text{..... (64)}$$

where, LOT is specific gravity (s.g.) and depth is meters. Vertical stress magnitude is never expressed with a linear trend over depth. Eaton expressed the vertical stress magnitude change as an asymptotic over depth.[2] This is the main reason why LOT trend is expressed with a nonlinear equation with depth in this study.

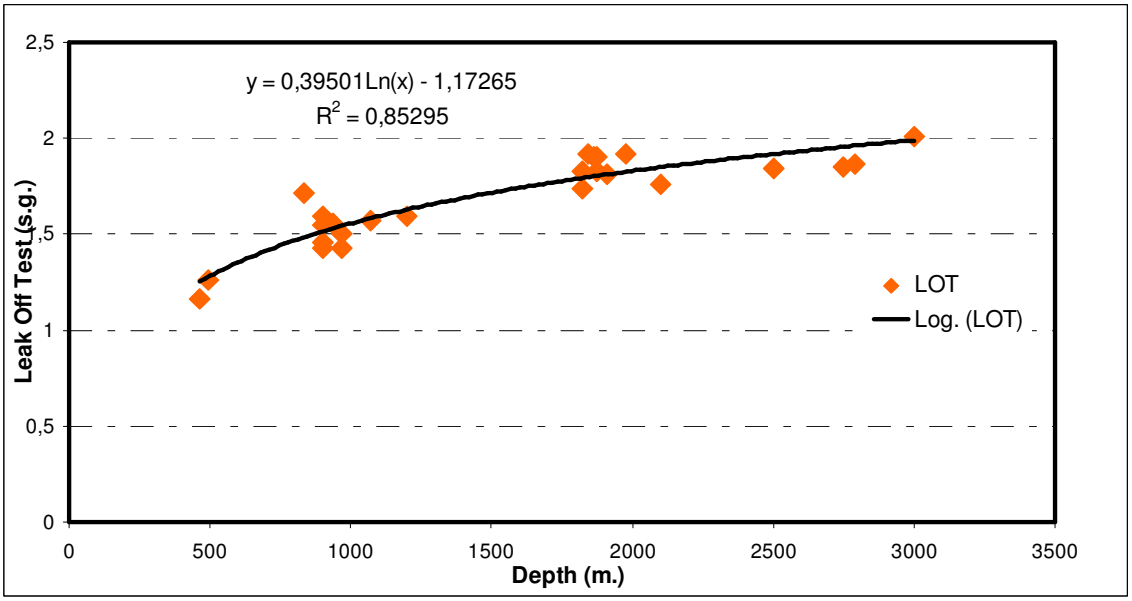

Figure 30 Leak off test stress data in specific gravity plotted against depth. The equation of the trend is also indicated.

This LOT trend equation was used to provide the minimum horizontal stress magnitude for all three wells, the mean stress value for each well is obtained assuming a particular S_H/S_h value. As stated before, a relationship between minimum horizontal stress and maximum horizontal stress is used throughout the area. Value of S_H/S_h were selected to lie between 1.2 and 1.4. This relationship assumed is expressed with following expression:

$$1.2 \leq \frac{S_H}{S_h} \leq 1.4$$

where σ_H is maximum horizontal stress and σ_h is minimum horizontal stress. Using these relationships, the components of the mean total stress are obtained. For each well, mean total stress values are computed from the relationship below;

$$S_m = \frac{1}{3}\left[S_v + S_h + \frac{S_H}{S_h} * S_h \right] \quad \text{..... (65)}$$

where S_m is the mean total stress, S_v is the vertical, overburden stress, S_h is minimum horizontal stress, S_H/S_h is the horizontal stress ratio and S_H is the maximum horizontal stress. Notice that all the stresses are total stresses, not effective stresses.

For this study in the Snorre Field, the S_H/S_h ratios investigated were constrained to the values of 1.2, 1.3, and 1.4. After computing mean stress values, the Eaton sonic pore pressure method and the Eaton resistivity pore pressure methods are used for each of the three mean stress values for each well.

The equations are, for resistivity analysis,

$$\frac{P}{Z}=\frac{S_m}{Z}-\frac{(S_m-P_{hyd})}{Z}*\left(\frac{Observed\ Rsh}{Normal\ Rsh}\right)^{1.2} \quad \text{..... (66)}$$

For sonic data analysis;

$$\frac{P}{Z}=\frac{S_m}{Z}-\frac{(S_m-P_{hyd})}{Z}*\left(\frac{Normal\ \Delta t_{sh}}{Observed\Delta t_{sh}}\right)^{3} \quad \text{..... (67)}$$

Notice that mean total stress is used instead of overburden stress. This is the basic idea of the new method to be used; the pore volume change is not only due to vertical stress applied but rather to the mean of the sum of all three stress components of stress tensor. The normal trends used for this study for each well are given in Figure 31 and Figure 32, Resistivity log compaction trends give better estimates for pore pressure for this area. Resistivity data showed three different compaction trends for depth above 1000 m, between 1000m and 1500 m and deeper 1500m. The top of overpressure observed is 1500m for the three wells. Sonic data showed two different compaction trends.

Pore pressure is calculated by using the same normal compaction trend line for each well. For each well there are four pore pressure calculations for each pore pressure method (Resistivity and Sonic). In total, there are eight pore pressure predictions. These pore pressure predictions are,

- pore-pressure prediction using overburden stress which is represented by PP OBG,
- pore-pressure prediction using mean stress and S_H/S_h = 1.2, represented by PP 1.2 M,

- pore pressure prediction using mean stress and S_H/S_h = 1.3, represented by PP 1.3 M,
- and pore pressure prediction using mean stress and S_H/S_h = 1.4, represented by PP 1.4 M.

The pore-pressure predictions, PP OBG, PP 1.2 M, PP 1.3 M, PP 1.4 M are calculated using Eaton's sonic and resistivity methods. The reason there are 3 pore-pressure calculations for each method using different horizontal stresses ratio is to have a bound on changing stress magnitudes through out the area. Drillworks Predict software of Knowledge Systems Inc. is used for this study to make the computation easier. The verification of the software is in Appendix A.

Results

Pore-pressure analyses and estimates for well number 1, using both vertical stress and mean total stress techniques are given in Figures 33 (for sonic) and 34 (for resistivity). The trend line shifts at 2490m are required due to the apparent presence of a fault. The differences between pore pressures computed from the vertical stress and mean stress are given in Figures 35 and 36.

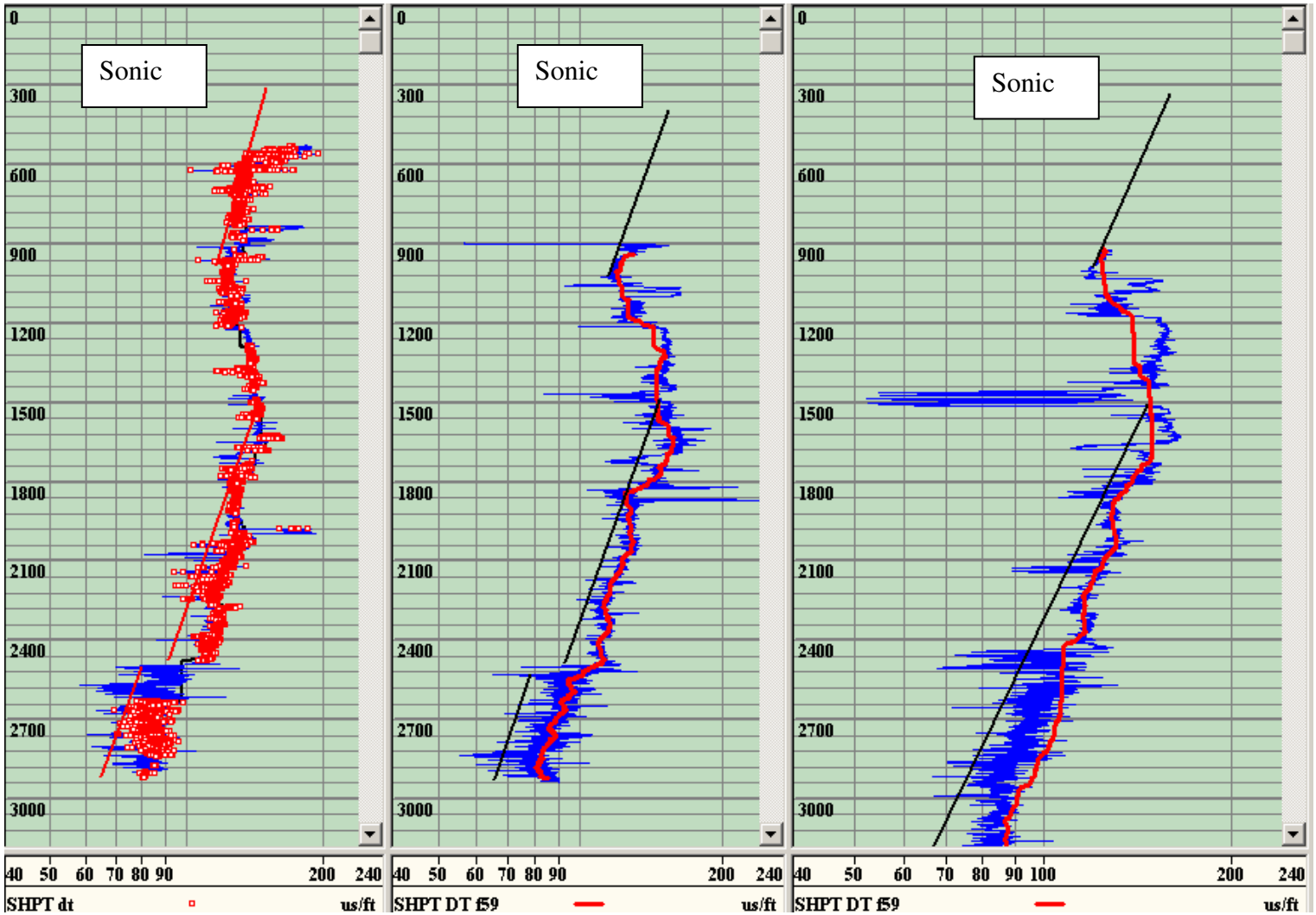

Figure 31 Sonic log compaction trends used for pore pressure prediction for well 1, well 2, well 3, respectively.

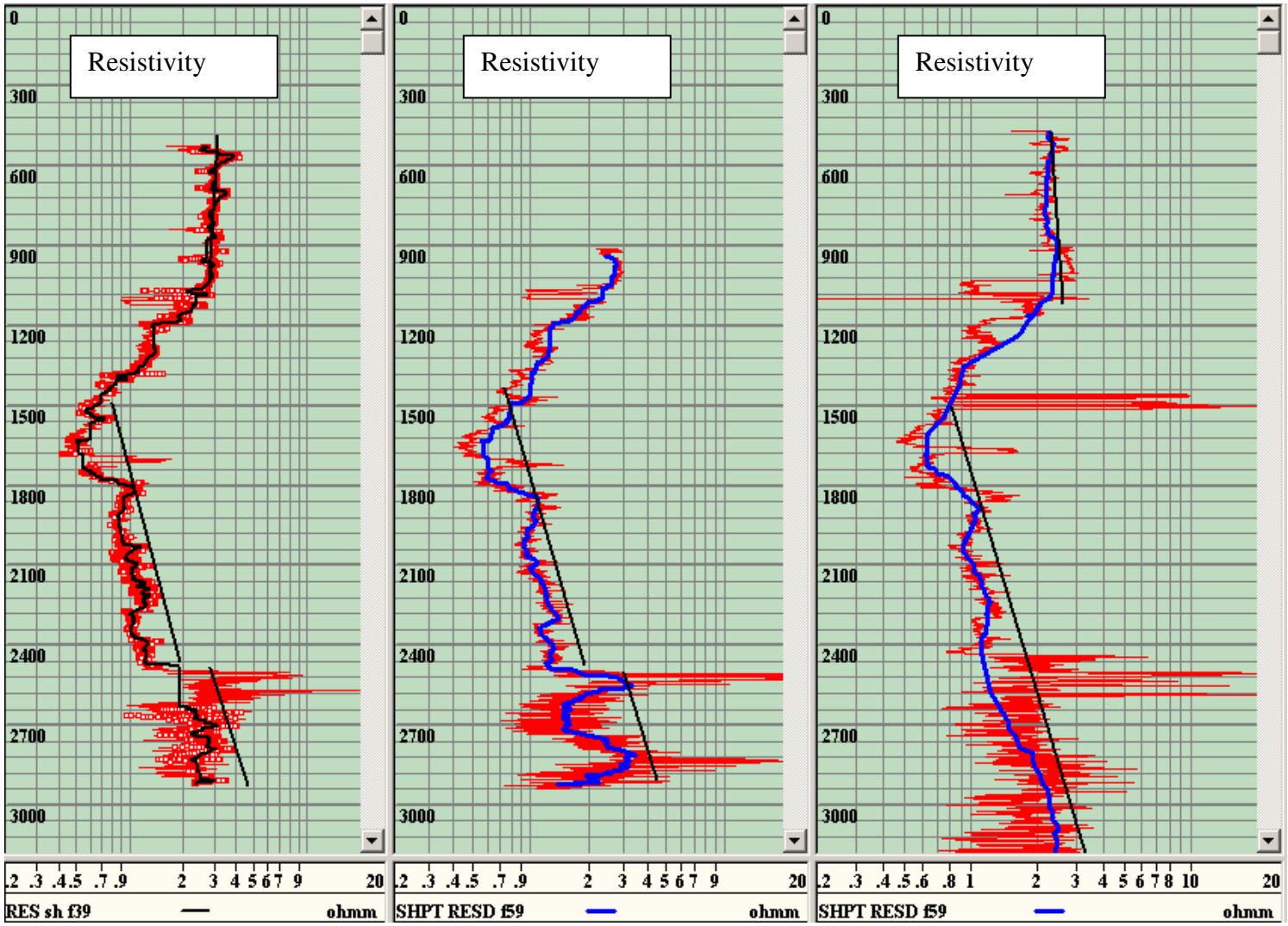

Figure 32 Resisitivity compaction trends used for pore pressure prediction for well 1, well 2, well 3, respectively

In Figure 33, for analysis of Sonic data in well 1, the left track contains the Gamma Ray data in blue and the shale discrimination lines in red. The middle track contains the Sonic data in blue, the individual sonic shale points in red and the filtered shale points in black. The red straight line segments in the middle track are the normal compaction trend that was applied to the Eaton method described earlier.

The results shown in the right track of Figure 33 are scaled from 1.0 to 3.0 specific gravity from left to right. The respective gently curving lines are the vertical stress (overburden) in purple, the mean stress using a S_H/S_h ratio of 1.2 in green, the mean stress using a S_H/S_h ratio of 1.3 in brown and the mean stress using a S_H/S_h ratio of 1.4 in blue. The corresponding pore pressures using the same color scheme are the roughly parallel jagged lines furthest to the left. In Figure 34, the parallel analysis and results using Resistivity data from well 1 are presented.

As can be seen in both plots, the vertical stress technique results in lower pore pressures compared to the mean stress technique for this well.

For each well RFT values are plotted against depth and an equation is found for the RFT trend. Then the Mean Square Error (MSE) value and Mean Absolute Error (MAE) value between RFT values and pore pressure estimates are calculated. The results are given in

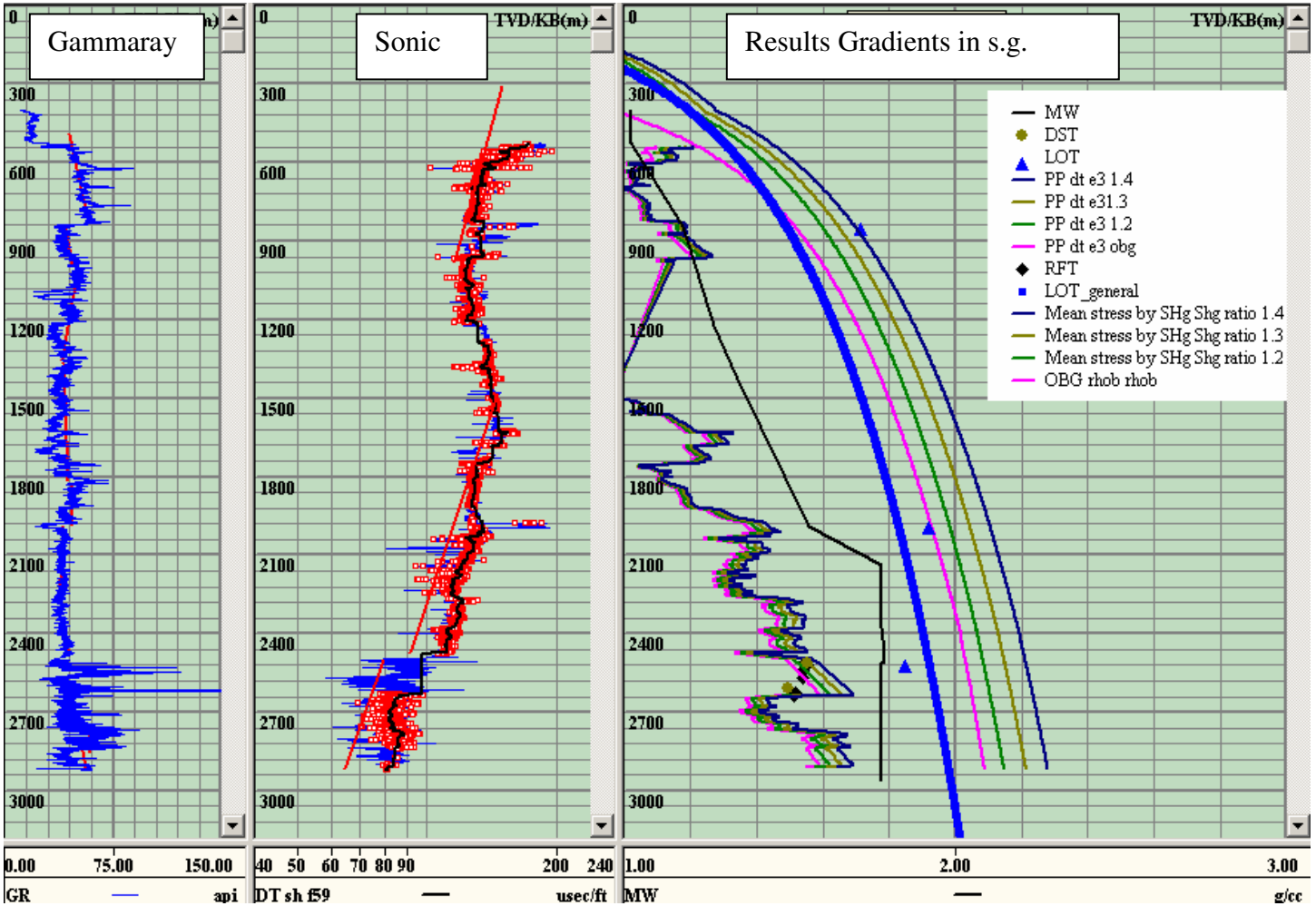

Figure 33 Eaton sonic method results for well 1, results are plotted in result gradient part.

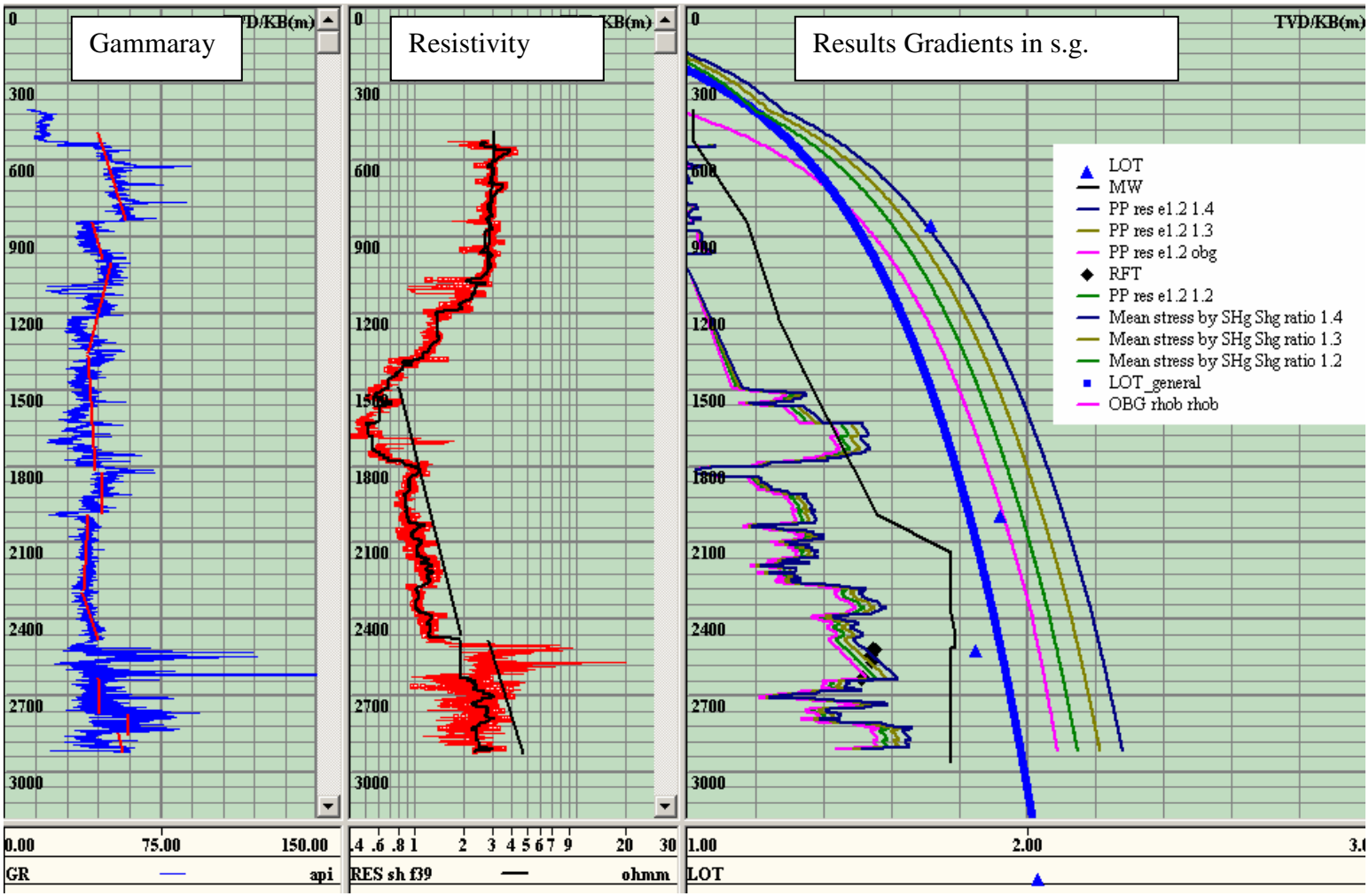

Figure 34 Eaton resistivity method results for well 1, results are plotted in result gradient part.

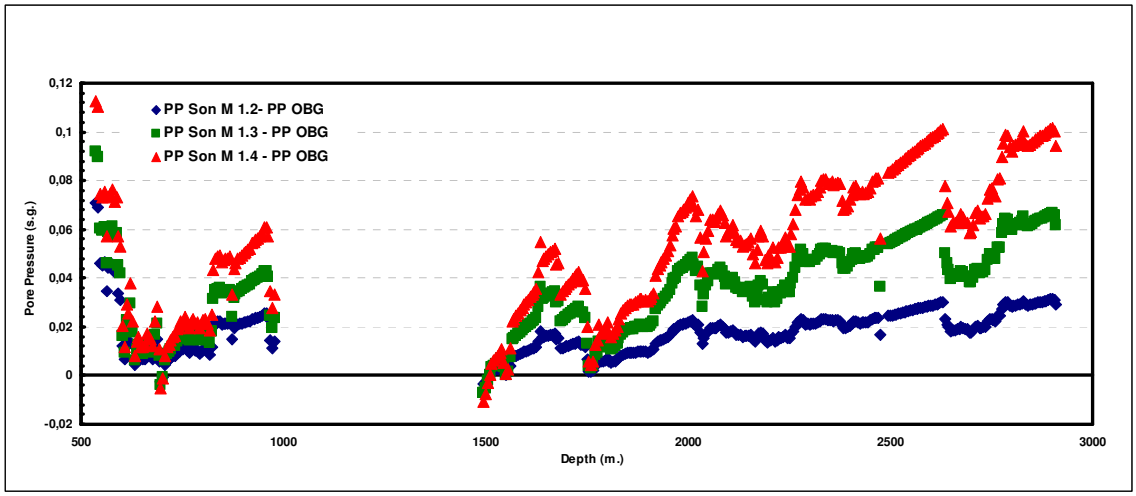

Figure 35 Pore pressure difference between mean total stress used pore pressure prediction and overburden based pore pressure prediction using sonic log data for Well 1.

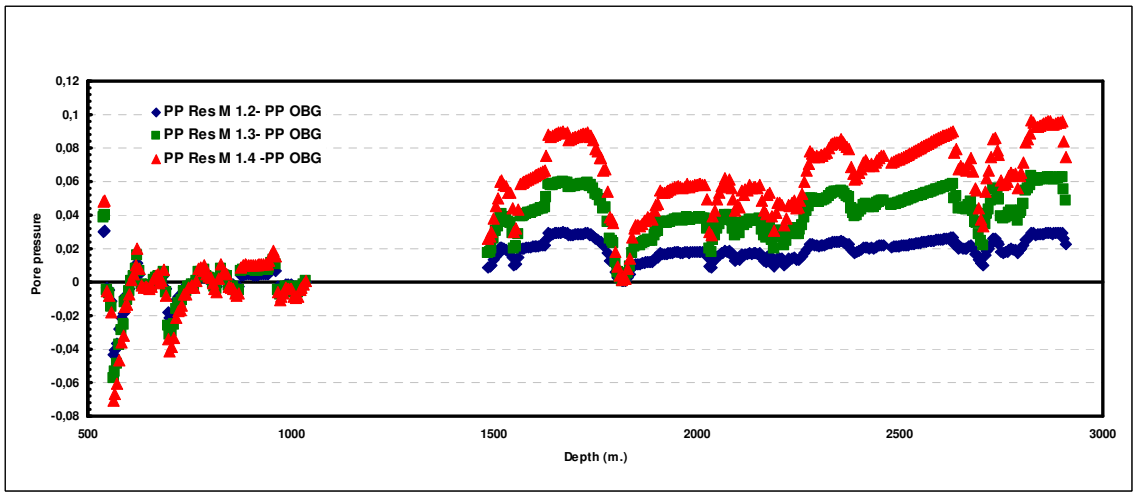

Figure 36 Pore pressure difference between mean total stress used pore pressure prediction and overburden based pore pressure prediction using resistivity log data for Well 1.

Tables 4-8. Table 4 shows the MSE analysis for pore pressure estimate using sonic log data. Table 4 shows that for Well 1 pore pressure estimate using OBG gives smaller error. For Well 2, 1.2 horizontal stress ratio using pore pressure calculations have the

smallest error. For Well 3, 1,4 horizontal stress ratio using pore pressure calculation has the smallest error.

Table 4 Mean Square Error Analysis for the pore pressure estimation methods using sonic log data is compared. For Well 1 PP OBG has the smallest error.

Sonic MSE Analysis				
	RFT-PP OBG	**RFT- PP M1.2**	**RFT-PP M1.3**	**RFT- PP M1.4**
Well 1	*0,001983139*	0,003148614	0,006633313	0,012403
Well 2	0,00125	*0,001231*	0,003411	0,007529
Well 3	0,016433	0,010721	0,008459	*0,007749*

Table 5 Mean Square Error Analysis for the pore pressure estimation methods using resistivity log data is compared. For Well 1 PP M 1,3 has the smallest error.

Resistivity MSE Analysis				
	RFT-PP OBG	**RFT- PP M1.2**	**RFT-PP M1.3**	**RFT- PP M1.4**
Well 1	0,004093	0,002172	*0,001538*	0,002731
Well 2	*0,0489*	0,0516	0,0559	0,0620
Well 3	0,012908	0,005872	0,00258	*0,000756*

Table 6 Mean Absolute Error Analysis for the pore pressure estimation methods using sonic log data is compared. For Well 1 PP OBG has the smallest error.

Sonic MAE Analysis				
	RFT-PP OBG	**RFT- PP M1.2**	**RFT-PP M1.3**	**RFT- PP M1.4**
Well 1	*0,039134*	0,048035	0,07228	0,104651
Well 2	*0,026249*	0,02955	0,053567	0,083291
Well 3	0,104677	0,083076	0,076406	*0,075862*

Table 7 Mean Absolute Error Analysis for the pore pressure estimation methods using resistivity log data is compared. For Well 1 PP M 1.3 has the smallest error.

Resistivity MAE Analysis				
	RFT-PP OBG	**RFT- PP M1.2**	**RFT-PP M1.3**	**RFT- PP M1.4**
Well 1	0,056089	0,040354	*0,034537*	0,044286
Well 2	*0,1684*	0,1762	0,1872	0,2014
Well 3	0,112337	0,074585	0,047512	*0,021898*

The number of RFT normalization points is given in Table 8.

Table 8 Number of RFT calibration point used for normalization to evaluate accuracy of each method.

RFT Calibration points	
Well 1	25 points
Well 2	75 points
Well 3	50 points

Well 1

The Input data used is given in Figure 37. Gamma ray, resistivity, sonic and bulk density data were available for this well. The gamma ray data were used to indicate the depths of the most clay-rich shales. These depths were applied in order to obtain the shale points on the resistivity and sonic logs. Shale points are the log indicators of shaly formations whose porosity values are used for pore pressure prediction based on the assumption of an undercompaction mechanism. As the next step, the normal compaction trend of resistivity and sonic log shale point is determined. This trend gives us the sonic and resistivity values which correspond to normal compaction. The deviation of the actual shale values from these trends will help to quantify the overpressure. Notice here that the normal trend line indicates where the pore pressure is expected to be hydrostatic according to the logging measurement in the shale. The amount of deviation helps to quantify pore pressure using, for example, the Eaton algorithm. Bulk density is used to calculate overburden stress, vertical stress. Overburden is used to predict pore pressure alone, as well as it is an input for mean total stress.

Eaton's sonic- and resistivity-based equations are used to predict pore pressure. There are four pore pressure predictions for each method: using overburden gradient, PP OBG, and pore pressure predictions using mean total stress estimates, PP M 1.2, PP M 1.3, PP M 1.4. Each pore-pressure prediction is given in Figure 33 and Figure 34. If we look in the result gradients track, on the right side of the plot, we can observe pore-pressure predictions, and the stresses on which these predictions are based. Black points are RFT values. The scatter, observed in pore pressure prediction lines are due to lithological and textural variations in the depth intervals identified as "shale". An age shift/fault is the reason for the trend line being broken. RFT trend values are used to as RFT pseudo values. RFT pseudo values are cross plotted against calculated pore pressure predictions. These cross plots for Well 1 are given in Figure 40 and Figure 41.To measure the amount of error for each stress state between pore pressure prediction, and RFT, the MSE value and MAE value between RFT values and pore pressure estimates are calculated.

The MSE and MAE analysis are both done for pore pressure predictions using sonic log data and resistivity log data. Results are given in Tables 4-8.

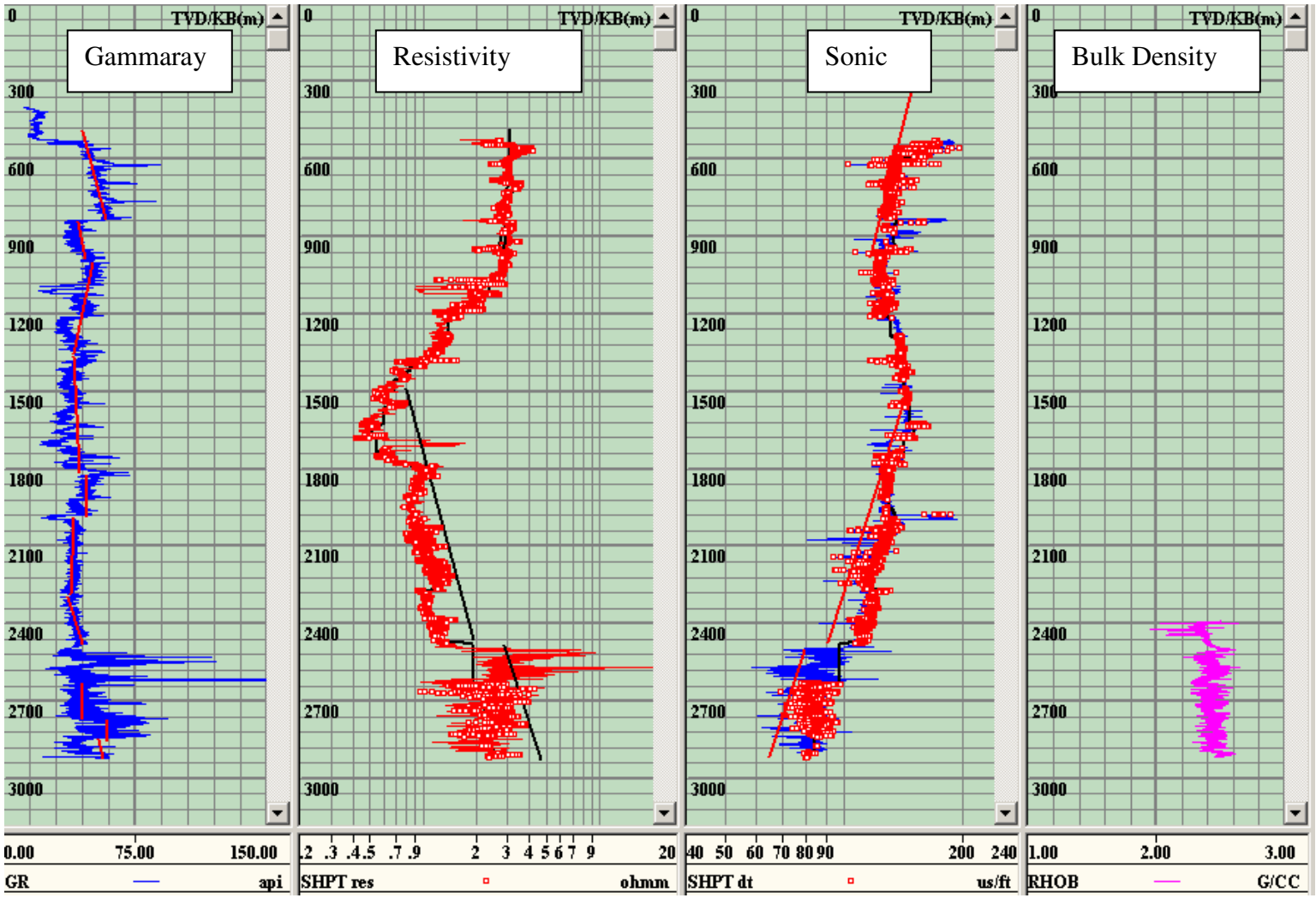

Figure 37 Input data for well 1, Gamma ray, resistivity, sonic and bulk density log data are plotted

For well 1 MSE analysis for sonic data suggest that pore pressure calculation using OBG has the smallest error and it is the suggested stress component for Eaton's sonic equation. MAE suggests this result as well. However MSE analysis for resistivity log data using pore pressure prediction indicates that M 1.3 pore pressure prediction has the smallest error. This result is also confirmed by MAE analysis. Figure 38 and Figure 39 show resistivity and sonic log data based pore pressure comparison for each method to RFT. Apparently resistivity log data gives better results for Snorre Field. The other two wells which are analyzed as well are given in Appendix B.

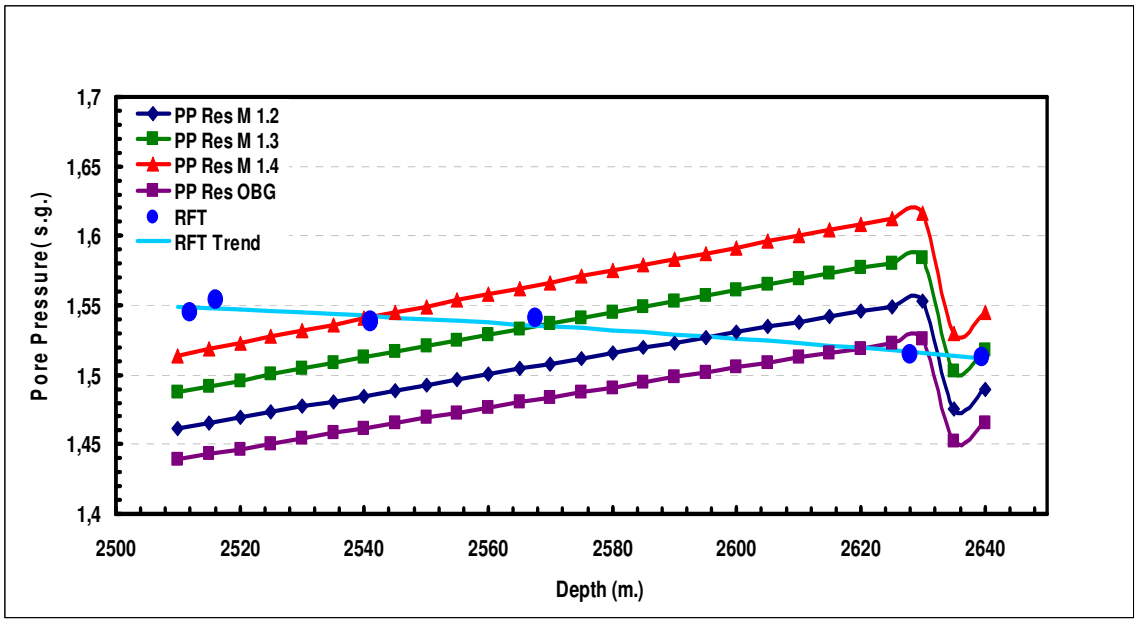

Figure 38 Resistivity log data based pore pressure comparison for each method to RFT.

Conclusions

Pore pressure predictions using mean total stress estimate and vertical stress are compared for the Snorre Field data. Shale porosity pore pressure prediction based Eaton Sonic and Resistivity equations are used. Pore pressure predictions and RFT values are cross plotted. MSE and MAE are performed. Resistivity log data based pore pressure prediction is suggested for the Snorre Field. MSE and MAE analysis give the same suggested stress estimate for each well. However sonic log data based pore pressure predictions do not confirm the same results in MSE and MAE error analysis.

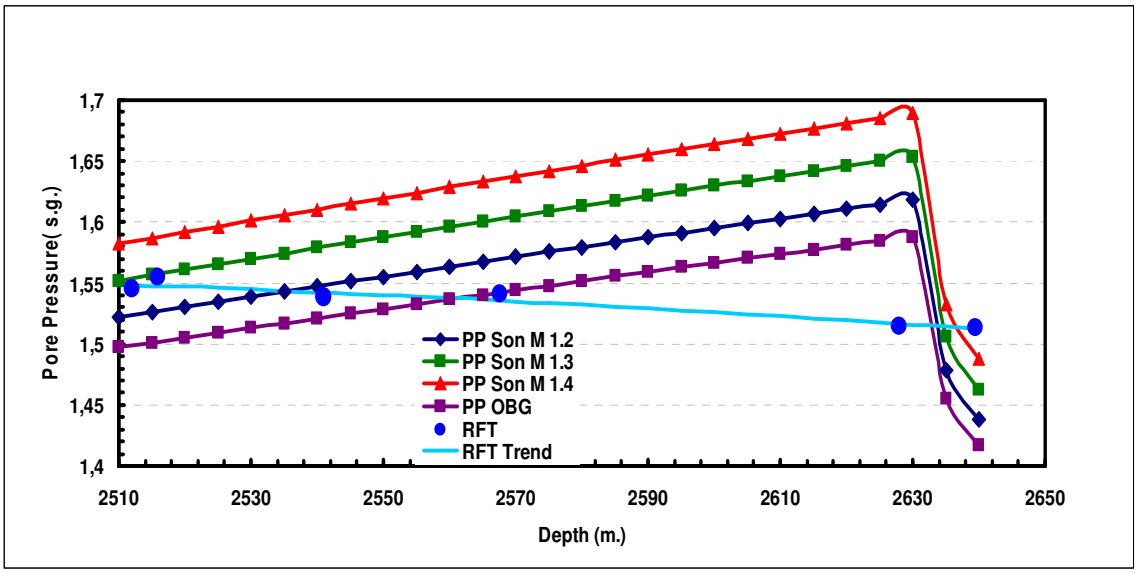

Figure 39 Sonic log data based pore pressure comparison for each method to RFT.

Analyses suggest that for each well, different pore pressure estimates give minimum error when compared to RFT values. For Well 2, vertical stress pore pressure calculation (PP OBG) using resistivity data give less error.

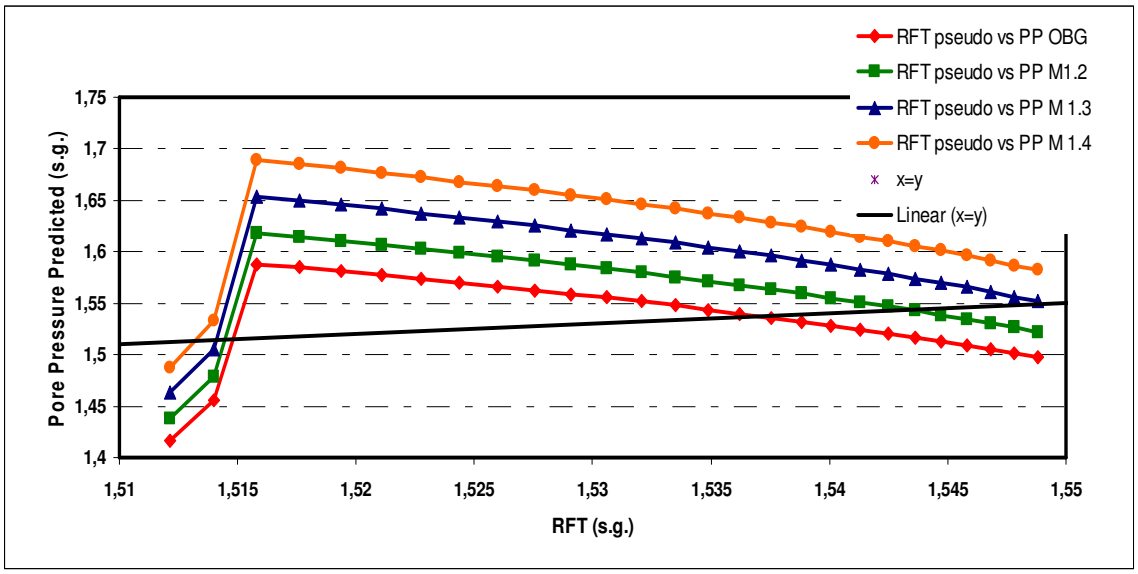

Figure 40 Sonic pseudo RFT vs. pore pressure predicted analysis.

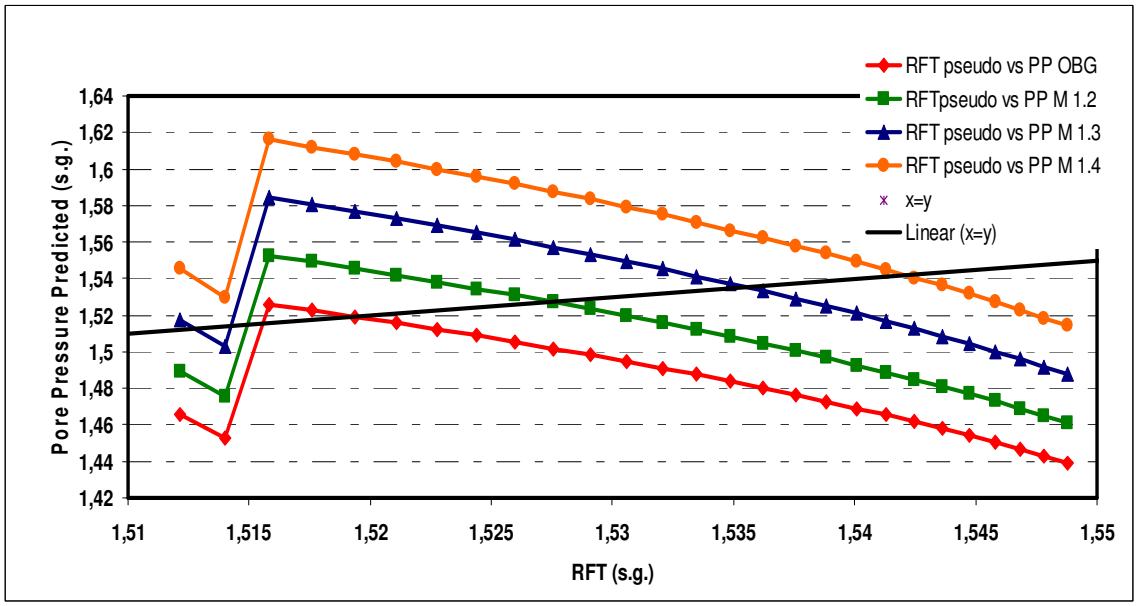

Figure 41 Resistivity pseudo RFT vs. pore pressure predicted analysis.

However for Well 1 and 3 Mean total stress estimate pore pressure (PP M) calculations give less error. Using the same horizontal stress ratio through out the field, below 1500m might not be a correct assumption. Observing different suggested stress pore pressure estimates can result due to this assumption. Nevertheless, mean total stress based pore pressure prediction seems to work for some part of the area. Mean total stress estimate pore pressure estimation is the suggested pore pressure calculation method for the Snorre Field.

CHAPTER VI

SUMMARY, CONCLUSION AND SUGGESTIONS FOR FUTURE WORK

Summary

In this work I have tried to emphasize the importance of 3D compaction for pore pressure analysis. the previous research performed focused on giving an explanation for overpressure in the lithosphere assuming 1D compaction, without accounting for the effect of horizontal stresses. Terzaghi's experiment to demonstrate effective stress and pore-pressure took overburden as the main stress-inducing agent. However, when we look at the stress tensor we see eight other components besides the vertical normal stress. The other eight components of the stress tensor, which represent the stress state at a point in the subsurface, were neglected in the 1D compaction theory assumed for pore pressure estimation. There are, however, some research examples like Goulty[12], Schutjens et al.[22], which bring up the fact that compaction is actually 3D and this must be taken into account when pore-pressure determination techniques are applied.

There are many mechanisms generating pore pressure. Well logs tend to be sensitive to undercompaction since the porosity change in this mechanism can be related to the state of compaction. Overburden is taken into account to quantify the pore pressure according to 1D compaction. Unloading, i.e. reduction in effective stress, due to fluid expansion after compaction, defined by Bowers[36], can be quantified by Bowers technique as well. There are other techniques to define and may be able to quantify overpressure generated

by other than undercompaction and unloading. It is important to state here that there may be more than one mechanism generating the overpressure for a given area. For the purpose of quantifying the pore-pressure use of more than one method might be necessary.

Geologically tectonically relaxed environments like the Gulf of Mexico were a great starting point for research on overpressure. Since it is tectonically relaxed, minimum and maximum horizontal stresses were not significant when the wells drilled were near the shore. Useful empirical equations were developed using the data from these wells.

Porosity is reduced during compaction due to the compressive stresses applied on the formation. With increasing depth, porosity decreases. Porosity is a rock parameter which influences well logs such as resistivity and sonic properties. All the previous pore-pressure prediction methods considered only overburden stress as the compressive stress responsible for porosity reduction over geologic time.

Unlike the usual petrophysical formation evaluation techniques, overpressure determination techniques tend to be based on observed general trends, rather than explicit deterministic equations. They require an interpretation of shale points throughout the well, assuming it is the most compactable formation and that its compaction characteristics remain fixed throughout the well. The deeper formations will

be expected to be more compacted, i.e. shale porosity is expected to decrease with depth and increasing effective stress.

It is known that shale, which is generally assumed to be impermeable, is actually permeable to some degree, which may result in another questionable assumption being made, namely that the permeable formations adjacent to the shale will have the same pore pressure as that interpreted in the shale. Some researchers questioned this assumption after the centroid concept was introduced. The centroid concept assumes that at the "centroid depth" the pore pressure in a permeable formation will be the same as the adjacent shale that bounds it. However, at depths shallower than the centroid, the pore pressure will be higher than the adjacent shale, and at depths deeper than the centroid, the shale pore pressure will exceed the pore pressure in the permeable formation. Sonic or resistivity logs can show the porosity change with compaction in shales, but will not be useful when shale pore pressures are not in equilibrium with the sands.

Terzaghi's definition for effective stress with a porosity-effective stress relationship gave the practitioners what they needed to detect and estimate overpressure. Shale porosity affected by compaction disequilibrium (undercompaction) was indicated by a deviation from a normal compaction trend. Pore fluid trapped by a good low permeability seal was actually helping the grains to resist the compactional stress to which it was exposed.

Researchers like Hottmann[25] and Pennbaker[27] related the observed porosity to measured pressures directly, as the state of the art in pore-pressure determination was just beginning to develop. Eaton[33] combined the use of trend lines obtained from porosity-sensitive logging measurements in shale with the Terzaghi effective stress concept and quantified pore pressure estimates from the deviations from a normal compaction trend. Holbrook[39] and others developed methods which did not explicitly use trend lines and which included the effect of lithology. Direct, horizontal, vertical or other all the methods used today employ some kind of relationship between effective stress and porosity.

The methods which were useful for the Gulf of Mexico did not work as well in some of the other parts of the world. Hottmann[41] pointed out the fact that where faults are observed, the methods were not effective. Many tried to match the porosity they observed to overpressure they observed but the efforts failed. A porosity-effective stress relationship obtained only from vertical stress was not sufficient to explain the porosity change and overpressure. The 1D compaction theory was not adequate to explain the overpressure in tectonically active areas where lateral (horizontal stresses) are bigger than normal.

In this thesis, compaction disequilibrium due to overburden and additional compressional stresses at a point subsurface was discussed. Because 1D theory was

inadequate to assess pore pressures due to undercompaction in the situations described above, this thesis was proposed to explore improvements that a 3D approach might provide. The importance of three principal stresses on compaction recognized by Traugott[8] and Goulty[12] explained the importance of mean stress on compaction.

According to Goulty[12], if the formation did not change under diagenesis, the elastic porosity change due to unloading can be recovered by increasing lateral stresses. This means that the present stress state of the area is helpful to explain the porosity today.
The yielding due to shear is ignored for this stage of application of the method. Where yielding happens, the rock material and state of shear is very important on the porosity change in the formation.

Harrold et al.[55] and Van Ruth et al.[45] actually used mean stress to quantify the overpressure. Harrold et al.[55] used the method for Southeast Asia. However, they gave very little regard to the stress distribution by only noting the presence of high lateral stresses not categorizing the area by strike-slip or reverse faulting environment. They used Van Eekelen equation for fracture gradient for the field and assumed that the horizontal stresses were equal. They claimed success in estimating the pore pressure by using the mean stress and recommended that it should be a general practice. They did not state the details of the pore-pressure technique they used.

It must be noted that the stress distribution for a given area is extremely important. Anderson's faulting theory clearly states that there are three stress regimes and orientation of maximum principal stress is different for each case. Where normal faulting is observed the maximum principal stress is the overburden and is vertical and, the two horizontal stresses will be less in the magnitude. Furthermore, when you add three normal stresses and divide the sum by three, you will obtain mean stress smaller than overburden alone. If mean stress obtained from a normal faulting area is used to calculate pore pressure the result may be an underestimate of pore pressure. But where the vertical stress is either the intermediate or minimum principal stress for the area, as strike slip and reverse faulting environments respectively, the mean total stress based pore-pressure estimate is likely to be the more accurate pore-pressure estimate due to it is accounting for 3D compaction.

Van Ruth et al.[45] applied the mean total stress method for a site in Australia. They also used the assumption that the minimum and horizontal stresses are equal. They did not give much detail about the stress distribution of the area. Their point was the mean stress method can also be applied to old sediments rather than young ones. Goulty[12] put a 3km depth restriction on the method. However, this suggestion and the applicability of the method for use in old sediments are topics open for additional research.

In this study, the Snorre Field data were used to demonstrate the mean total stress, pore-pressure prediction method. The anisotropic stress state of the field is the reason why this field was chosen. It was shown by geological studies, LOT studies and borehole observations that the field is in a strike slip to reverse faulting stress state. There was no unloading observed, so Snorre field was a good candidate for analysis of overpressure by 3D compaction disequilibrium. The mean total stress estimate method was applied to 3 wells from this region.

Pore pressure predictions using mean total stress estimate and vertical stress are compared for the Snorre Field data. Shale porosity pore pressure prediction based Eaton Sonic and Resistivity equations are used. Pore pressure predictions and RFT values are cross plotted. MSE and MAE analysis are performed. Resistivity log data based pore pressure prediction is suggested for the Snorre Field. MSE and MAE error analysis give the same suggested stress estimate for each well. However sonic log data based pore pressure predictions do not confirm the same results in MSE and MAE analysis.

Conclusions

- The stress distribution for a given target area is very important.
- Where the stress tensor is known for a given area, pore-pressure prediction methods can be implemented more accurately.
- If the stress state of a given area is either a strike-slip or reverse faulting regime as defined by Anderson, special attention should be given to how pore-pressure predictions will be made.
- The shale porosity distribution of the area can be used by mean total stress method to estimate pore pressure. It is important to eliminate the other mechanisms during analysis since mean stress method is also another kind of compaction-based effective stress method, which is only sensitive to porosity distribution of the area.
- Any porosity-vertical effective stress based method can be used by replacing overburden stress with mean stress in that method.
- If the mean stress method is used for normal faulting regimes pore pressure can be underestimated, and dominate compaction since vertical stress is the maximum principal stress for that area.
- Where lateral stresses are significant, as in strike-slip or reverse faulting environments, vertical effective stress methods will likely underestimate the pore pressure. The mean total stress method is a proposed pore-pressure estimation method for these kinds of environments.

- Analyses suggest that for each well, different pore pressure estimates give minimum error when compared to RFT values. For Well 2, vertical stress pore pressure calculation (PP OBG) using resistivity data give less error. However for Well 1 and 3 Mean total stress estimate pore pressure (PP M) calculations give less error.
- The mean total stress method is recommended for the Snorre Field and any other field with a similar strike-slip to reverse faulting stress state as found in the Snorre Field.

Suggestions for Future Work

- In this thesis, σ_3 is presented by a function changing with depth. This is an assumption to make computation easier. In reality, σ_3 relative to the other stresses has a lithology dependency. A constant σ_3 function is not an accurate model. The method can be revised by using an actual lithology dependent σ_3 trend.
- The assumption of one of principal stresses being parallel to vertical stress direction may not be true. The full stress tensor should be used to obtain the direction and magnitude of principal stresses.

- Yielding of the rock under shear is not covered in this thesis as well. The amount of yielding and its effect on porosity generation or dilatation should be considered. The mean stress method will not be able to predict the pore pressure due to yielding under shear. Pore pressure due to yielding under shear is an open research area. A method to determine pore pressure due to yielding under shear, which uses well logs, has not been found yet.

NOMENCLATURE

a	tartuosity constant
A	Curve fit parameter for Bower's equation.
α	effective stress constant.
α	vertical stress gradient, psi/ft
α	Biot constant
α_{nc}	Biot coefficient during normal compaction
B	Curve fit parameter for Bower's equation.
BQ_v	Clay cation exchange capacity per pore volume
β	constant.
C	Curve fit parameter for Bower's equation.
C_t	rock conductivity, 1/ohm
C_w	conductivity of the water, 1/ohm
ς	the slope
γ	Gamma Ray readings, API
D	Curve fit parameter for Bower's equation.
$\Delta_{t\ matrix}$	Sonic log matrix travel time, μsec/ft
$\Delta_{t\ fluid}$	Sonic log fluid travel time, μsec/ft
e	solidity, %
F	Formation resistivity factor
g	acceleration gravity constant,
G	geometrical factor

G_p	Abnormal pore pressure gradient psi/ft
I	Compression index
K	constant for Drou et al, equation.
k_{nc}	matrix bulk modulus,
k_s	bulk modulus of the solid grains
LOT	Leak off Test, s.g.
m	porosity exponent
m	slope of the curve
μ	elastic rebound parameter
OB	overburden gradient at the mud line psi/ft
P	pore pressure. psi, ppg, s.g.
P_N	normally pressured pore pressure, psi, ppg, s.g
P_{lo}	leak off pressure, Pa, Mpa, psi s.g.
ϕ	Porosity, %.
ϕ_r	residual porosity,%
r	void ratio, unitless
R	resistivity reading, ohmm
R_w	shale water resistivity, ohmm
R_{sh}	shale resistivity, ohm
ρ	density, g/cc, s.g.
S_1	Maximum principal stress Pa, Mpa, psi., s.g.
S_2	Intermediate principal stress Pa, Mpa, psi, s.g.

S_3	Minimum principal stress Pa, Mpa, psi, s.g.
S_v	vertical stress, overburden stress Pa, Mpa, psi, s.g.
S_H	Maximum horizontal stress, Pa, Mpa, psi, s.g.
S_h	Minimum horizontal stress, Pa, Mpa, psi, s.g.
σ_e	effective stress, Pa, Mpa, psi, s.g.
σ_N	normally pressured zone effective stress, Pa, Mpa, psi, s.g.
σ_{act}	Actual effective stress, Pa, Mpa, psi, s.g.
σ_{max}	Maximum effective stress, Pa, Mpa, psi, s.g.
T_o	tensile strength of the rock, Pa, Mpa, psi, s.g.
T	Temperature, ^oF
U	unloading parameter
V	velocity, ft/s
V_{max}	maximum velocity, ft/s.
V_{shale}	Shale volume, %
V_s	volume of solid material
V	Volume
Z	Depth, m., ft.
Z_A	Abnormal pressure Depth. m., ft.
Z_N	Normal Pressure Depth, m., ft.

REFERENCES

1. Aadnoy, B.S.: "Effects of Reservoir Depletion on Borehole Stability," *J. Pet.Sci.Eng*. (1991) **6**, 57.

2. Watson, D., Brittenham, T., and Moore, P.L.: *Advanced Well Control*, Textbook Series, SPE, Richardson, Texas (2003).

3. Mouchet, J.P. and Mitchell, A.: *Abnormal Pressures While Drilling*, Manuels Techniques 2, Elf Aquitaine, Bouseens, France (1989).

4. Bowers, G.L.: "Detecting High Pressure," *The Leading Edge* (February 2002) **21**, No. 2, 174.

5. Armstrong, P., Nutt, L., and Minton, R.: "Drilling Optimization Using Drill-Bit Seismic in the Deepwater Gulf of Mexico," paper SPE 59222 presented at the 2000 SPE/IADC Drilling Conference, New Orleans, 23-25 February.

6. Yassir, N. and Addis, M.A.: "Relationships Between Pore Pressure and Stress in Different Tectonic Settings," *Pressure Regimes in Sedimentary Basins and Their Prediction:* A.R. Huffman, and G.L. Bowers (eds.), AAPG Memoir (2002) **76**, 79-88.

7. Draou, A. and Osisanya, S.O.: "New Methods for Estimating of Formation Pressures and Fracture Gradients From Well Logs," paper SPE 63263 presented at the 2000 SPE Annual Technical Conference and Exhibition, Dallas, 1-4 October.

8. Traugott, M.: "Pore Pressure and Fracture Pressure Determination in Deep Water," *Deep Water Technology Supplement to World Oil* (August 1997).

9. Bowers, G.: “State of Art in Pore Pressure Estimation,” Report No.1, DEA Project 119, Knowledge Systems Inc.,Stafford, Houston, Texas (1999).

10. Zoback, M.L.: “Stress Field Constraints on Intraplate Seismicity in Eastern North America,” *J. of Geophysical Research* (1992) **97**, B8, 11.

11. Anderson, E.M.: *The Dynamics of Faulting and Dyke Formation With Applications to Britain*, Oliver and Boyd, Edinburgh (1951).

12. Goulty, N.R.: “Relationships Between Porosity and Effective Stress in Shales,” *First Break* (12 December 1998) **16**, 413.

13. Desroches, J. *et al.*: “Combination of Microhydraulic Fracturing and Wellbore Images Provides Measurement of the Full Stress Tensor: A Case Study,” paper presented at the 2005 SPWLA Annual Logging Symposium, New Orleans, Louisiana, 26-29 June.

14. Boonen, P. *et al.*: “ Rock Mechanics and Wellbore Stability Analysis While Drilling Using LWD Sonic, Density and Caliper Measurements,” paper SPE/ISRM 78208-MS presented at the 2002 SPE/ISRM Rock Mechanics Conference, Irving, Texas, 20-23 October.

15. Zoback, M.D. *et al.*: “Determination of Stress Orientation and Magnitude in Deep Wells,” *International J. of Rock Mechanics & Mining Sciences* (2003) **40,** 1049.

16. Sinha, B. *et al.*: “Near-Wellbore Alteration and Formation Stress Parameters Using Borehole Sonic Data,” paper SPE 95841-MS presented at the 2005 SPE Annual Technical Conference, Dallas, Texas, 9-12 October.

17. Grollimund, B., Zoback, M.D., and Wiprut, D.: "Stress Orientation, Pore Pressure and Least Principal Stress in the Norwegian Sector of the North Sea," http://pangea.stanford. edu/~balz/ papers/pgeoscience.pdf, 7 June 2006.

18. Swarbrick, R.E. and Osborne, M.J.: "Mechanisms That Generate Abnormal Pressures: An Overview," *Abnormal Pressures in Hydrocarbon Environments*, Law, B.E., Ulmishek, G.F., Slavin, V.I. (eds.), AAPG Memoir (1998) **70**, 13-34.

19. Terzaghi, K., Peck, R.B.: *Soil Mechanics in Engineering Practice*, John Wiley & Sons Inc, New York (1948).

20. "Compaction in normal and overpressured situations," Oilfield Glossary, http://www.glossary.oilfield.slb.com/DisplayImage.cfm?ID=150, 7 June 2006.

21. Swarbrick, R.E., Osborne, M.J., and Yardley, G.S.: "Comparison of Overpressure Magnitude Resulting From the Main Generating Mechanisms," *Pressure Regimes in Sedimentary Basins and Their Prediction*, A.R. Huffman, and G.L. Bowers (eds.), AAPG Memoir (2002) **76**, 1-12.

22. Schutjens, P.M.T.M. *et al*.: "Compaction-Induced Porosity/Permeability Reduction in Sandstone Reservoirs: Data and Model for Elasticity-Dominated Deformation," *SPE Reservoir Evaluation & Engineering* (June 2004) **7**, No. 3, 202.

23. Moore, J.C. and Tobin, H.: "Estimated Fluid Pressures of the Barbados Accretionary Prism and Adjacent Sediments," in *Proc.,* Ocean Drilling Program Results (1997), **156**. 229-238.

24. Athy, L.F.: "Density, Porosity, and Compaction of Sedimentary Rocks," *AAPG Bull.* (January 1930) **14**, 1.

25. Hottmann, C.E. and Johnson, R.K.: "Estimation of Formation Pressures From Log-Derived Shale Properties," *JPT* (June 1965) 717.

26. Wallace, W.E.: "Abnormal Surface Pressure Measurements From Conductivity or Resistivity Logs," *Oil & Gas J*. (1965) **63**, 102.

27. Pennebaker, E.S.: "An Engineering Interpretation of Seismic Data," paper SPE 2165 presented at the 1968 SPE Annual Meeting, Houston, 29 September-2 October.

28. Ham, H.H.: "A Method of Estimating Formation Pressures From Gulf Coast Well Logs," *Trans*., Gulf Coast Association of Geological Societies (1966). **16**,185.

29. Foster, J.B. and Whalen, H.E.: "Estimation of Formation Pressures From Electrical Surveys-Offshore Louisiana," paper SPE 1200 presented at the1965 SPE Annual Fall Meeting, Denver, Colorado 6-8 October.

30. Ransom, R.C.: "A Method for Calculation Pore Pressures From Well Logs," *SPWLA J.* (1986) **27**, No. 2, a5.

31. Bryant, T.M.: "A Dual Shale Pore Pressure Detection Technique," paper SPE/ IADC 18714 presented at the 1989 SPE/ IADC Drilling Conference, New Orleans, Louisiana 28 February- 3 March.

32. Alixant, J.L. and Desbrandes, R.: "Explicit Pore-Pressure Evaluation Concept and Application," *SPE Drilling Engineering* (September 1991) 182.

33. Eaton, B. A.: "The Effect of Overburden Stress on Geopressure Prediction From Well Logs," *JPT* (August1972) 29.

34. Fertl, W.H. and Chilingarian, G.V.: "Detection and Evaluation of Geopressured Subsurface Formations Based on Dielectric (Electromagnetic Wave Propagation) Measurements," *Energy Sources* (1988) **10**, 195.

35. Weakley, R.R.: "Plotting Sonic Logs To Determine Formation Pore Pressures and Creating Overlays To Do So Worldwide," paper IADC/SPE 19995 presented at the1990 IADC/SPE Drilling Conference, Houston, 27 February-2 March.

36. Bowers, G.L.: "Pore Pressure Estimation From Velocity Data: Accounting for Overpressure Mechanisms Besides Undercompaction," paper SPE 27488 presented at the 1994 IADC/SPE Drilling Conference, Dallas, 15-18 February.

37. Bowers, G.L.: "Determining an Appropriate Pore –Pressure Estimation Strategy," paper OTC 13042 presented at the 2001 Offshore Technology Conference, Houston, 30 April- 3 May 2001.

38. Ward, C.D., Coghill, K., and Broussard, M.D.: "The Application of Petrophysical Data to Improve Pore and Fracture Pressure Determination in North Sea Central Graben HPHT Wells," paper SPE 28297 presented at the 1994 SPE Annual Technical Conference and Exhibition, New Orleans, Louisiana 26-28 September.

39. Holbrook, P.W. and Hauck, M.L.: "A Petrophysical-Mechanical Math Model for Real-Time Well Site Pore Pressure/Fracture Gradient Prediction," paper SPE16666 presented at the 1987 SPE Annual Technical Conference and Exhibition, Dallas, 27-30 September.

40. Holbrook, P.W., Maggiori, D.A., and Hensley, R.: "Real-Time Pore Pressure and Fracture- Pressure Determination in All Sedimentary Lithologies," paper SPE 26791

presented at the 1995 SPE Offshore European Conference, Aberdeen, Scotland 7-10 September.

41. Hottman, C.E., Smith, J. H., and Purcell, W.R.: "Relationship Among Earth Stresses, Pore Pressure, and Drilling Problems Offshore Gulf of Alaska," *JPT* (November 1979) 1477.

42. Hermanrud, C. *et al*.: "Shale Porosities From Well Logs on Haltenbanken (Offshore Mid-Norway) Show No Influence of Overpressuring," *Abnormal Pressures in Hydrocarbon Environments,* B.E. Law, G.F. Ulmishek, and V.I. Slavin (eds.), AAPG Memoir (1998) **70**, 65–85.

43. Swarbrick, R.E.: "Challenges of Porosity-Based Pore Pressure Prediction," *CSEG Recorder* (September 2002) 75.

44. Harrold, T.W.D., Swarbrick, R.E., and Goulty, N.R.: "Pore Pressure Estimation From Mudrock Porosities in Tertiary Basins, Southeast Asia," *AAPG Bull.* (July 1999) **83**, No. 7, 1057.

45. Van Ruth, P. *et al*.: "The Origin of Overpressure in 'Old ' Sedimentary Basins: An Example From the Cooper Basin, Australia," *Geofluids* (2003) **3**, 125.

46. Bloch, M. *et al*.: "Techniques for Determining In Situ Stress Direction and Magnitude," paper SPE 39075 presented at the 1997 SPE Latin American and Caribbean Petroleum Engineering Conference and Exhibition, Rio de Janeiro, Brazil, 30 August-3 September.

47. Detournay, E. and Carbonell, R.: "Fracture Mechanics Analysis of the Breakdown Process in Minifrac or Leak-Off Tests," paper SPE/ISRM 28076 presented at the1994

SPE/ISRM Rock Mechanics in Petroleum Engineering Conference, Delft, The Netherlands, 29-31August.

48. Postler, D. P.: "Pressure Intergity Test Interpretation," paper SPE/IADC 37589 presented at the 1997 SPE/IADC Drilling Conference, Amsterdam, 4-6 March.

49. Addis, M. A. *et al*.: "A Comparison of Leak-Off Test and Extended Leak-Off Test Data for Stress Estimation," paper SPE/ISRM 47235 presented at the1998 SPE/ISRM Eurock Conference, Trondheim, Norway, 8-10 July.

50. Raaen, A.M. and Brudy, M.: "Pump-In/Flowback Tests Reduce the Estimate of Horizontal In-Situ Stress Significantly," paper SPE 71367 presented at the 2001 SPE Annual Technical Conference and Exhibition, New Orleans, 30 September-3 October.

51. Reinecker, J., Tingay. M., and Muller, B.: "Borehole Breakout Analysis From Four-Arm Caliper Logs", World Stress Map Project, http://www-gpi.physik.uni-karlsruhe.de/wsm/ guidelines/BOanalysis_4armcaliper.pdf,7 June 2006.

52. Reinecker, J. et al.: "The release 2005 of the World Stress Map," http://www-wsm.physik.uni-karlsruhe.de/pub/introduction/introduction_frame.html, 7 June 2006.

53. WSM Database Details, http://www-wsm.physik.uni-karlsruhe.de/pub/stress_data/ stress_data_frame.html, 7 June 2006.

54. Stress Map of the World, http://www-wsm.physik.uni-karlsruhe.de/pub/stress_data /stress_data_frame.html, 7 June 2006.

55. Harrold, T.W.D., Swarbrick, R.E., and Goulty, N.R.: "Pore Pressure Estimation From Mudrock Porosities in Tertiary Basins, Southeast Asia," *AAPG Bull.* (July 1999) **83**, No. 7, 1057.

56. Aadnoy, B.S., Bratli, R.K., and Lindholm, C.D.: “In Situ Stress Modeling of the Snorre Field,” paper SPE/ISRM 28138 presented at the 1994 SPE/ISRM Rock Mechanics in Petroleum Engineering Conference, Delft, The Netherlands, 29-31 August.

57. Wiprut, D. and Zoback, M.: “High Horizontal Stresses in the Visund Field, Norwegian North Sea: Consequences for Borehole Stability and Sand Production,” paper SPE/ISRM 47244 presented at the 1998 SPE/ISRM Eurock Conference, Trondheim, Norway, 8-10 July.

58. Grollimund, B., Zoback, M.D., Arnesen, L.: “Flexurally Induced Stresses in the Northern North Sea: Preliminary Comparison of Observation and Theory,” paper SPE/ISRM 47243 presented at the 1998 SPE/ISRM Eurock Conference, Trondheim, Norway, 8-10 July.

APPENDIX A

DRILLWORKS PREDICT 11.03 (2005 SP3) VERIFICATION

LIST OF FIGURES

FIGURE Page

LIST OF TABLES

The name of the software used for this study is Drillworks Predict 11.03 (2005 SP3) by Knowledge Systems Inc. This appendix tries to verify the results and compare them by simple calculations preformed by Microsoft Excel.

Calculation Steps are as follows:

1. Overburden Gradient Calculation

Overburden gradient (OBG) is calculated from;

$$\sigma_v = \int_o^D \rho g dD \quad \text{..... (A-1)}$$

Where, ρ is density of the strata, g is acceleration gravity and D is the vertical depth of the target.

2- Pore Pressure Gradient Calculation

Eaton pore pressure equations for both resistivity and sonic log data are applied to predict pore pressure. These equations are:

For resistivity analysis;

$$\frac{P}{D} = \frac{OBG}{D} - \frac{(OBG - Hydrostatic\ Pore\ pressure)}{D} * \left(\frac{Observed\ \ Rsh}{Normal\ Rsh} \right)^{1.2} \quad \text{..... (A-2)}$$

For sonic data analysis;

$$\frac{P}{D} = \frac{OBG}{D} - \frac{(OBG - HydrostaticPore\,\mathrm{Pr}\,essure)}{D} * \left(\frac{Normal\ \Delta t_{sh}}{Observed \Delta t_{sh}} \right)^{3} \quad \text{..... (A-3)}$$

Sonic and resistivity data used for the analysis is given in Table A 1. Notice that this data is not real and not taken from any well. It has been created for verification purposes.

Table A 3 shows bulk density data created and used for verification purposes.

Comparison of calculated overburden gradient and computed overburden gradient by Drillworks Predict software is given in Figure A 1.

Trend lines which are used to compute pore pressure using Eaton resistivity equation and sonic equation are given in Figure A 2 and Figure A 3.

Pore pressure calculated from Eaton resistivity and sonic equations and computed values from Drillworks Predict software is given in Figure A-4 and Figure A-5.

Drillworks Predict software views are given in Figure A 6, Figure A 7 and Figure A 8.

Table A 1 Sonic data which are used for verification analysis

Sonic					
m	us/ft	m	us/ft	m	us/ft
500	167,33275	980	168,36249	1460	121,63804
510	166,68916	990	167,33275	1470	120,99445
520	166,04558	1000	166,68916	1480	120,35086
530	173,76863	1010	166,04558	1490	119,70728
540	167,97634	1020	173,76863	1500	119,06369
550	164,7584	1030	167,97634	1510	118,4201
560	168,36249	1040	164,7584	1520	117,77651
570	167,33275	1050	168,36249	1530	117,13293
580	166,68916	1060	167,33275	1540	116,48934
590	166,04558	1070	164,11481	1550	115,84575
600	173,76863	1080	163,47123	1560	121,63804
610	167,97634	1090	162,82764	1570	120,99445
620	164,7584	1100	162,82764	1580	120,35086
630	168,36249	1110	162,18405	1590	119,70728
640	167,33275	1120	161,54046	1600	119,06369
650	166,68916	1130	160,89688	1610	118,4201
660	166,04558	1140	160,25329	1620	117,77651
670	173,76863	1150	159,6097	1630	117,13293
680	167,97634	1160	158,96611	1640	116,48934
690	164,7584	1170	158,32253	1650	115,84575
700	168,36249	1180	158,64432	1660	121,63804
710	167,33275	1190	154,461	1670	120,99445
720	166,68916	1200	148,02513	1680	120,35086
730	166,04558	1210	141,58925	1690	119,70728
740	173,76863	1220	141,58925	1700	119,06369
750	167,97634	1230	138,37131	1710	118,4201
760	164,7584	1240	135,79696	1720	117,77651
770	168,36249	1250	135,15338	1730	117,13293
780	167,33275	1260	134,50979	1740	116,48934
790	166,68916	1270	131,93544	1750	115,84575
800	166,04558	1280	128,7175	1760	121,63804
810	173,76863	1290	130,00468	1770	120,99445
820	167,97634	1300	125,49956	1780	120,35086
830	164,7584	1310	124,85598	1790	119,70728
840	168,36249	1320	124,21239	1800	119,06369
850	167,33275	1330	123,5688	1810	118,4201
860	166,68916	1340	122,92521	1820	117,77651
870	166,04558	1350	122,28163	1830	117,13293
880	173,76863	1360	121,63804	1840	116,48934
890	167,97634	1370	120,99445	1850	115,84575
900	164,7584	1380	120,35086	1860	121,63804
910	168,36249	1390	119,70728	1870	120,99445
920	167,33275	1400	119,06369	1880	120,35086
930	166,68916	1410	118,4201	1890	119,70728
940	166,04558	1420	117,77651	1900	119,06369
950	173,76863	1430	117,13293	1910	118,4201
960	167,97634	1440	116,48934	1920	117,77651
970	164,7584	1450	115,84575	1930	117,13293

Sonic					
m	us/ft	m	us/ft	m	us/ft
1940	116,48934	2420	106	2900	54,443498
1950	115,84575	2430	103	2910	54,098919
1960	115,20216	2440	93	2920	53,75434
1970	114,55858	2450	83	2930	53,065181
1980	113,91499	2460	79	2940	53,409761
1990	113,2714	2470	74	2950	52,720602
2000	113,59319	2480	64	2960	52,376023
2010	113,20704	2490	62	2970	52,203734
2020	112,62781	2500	58,923026	2980	52,031444
2030	111,98423	2510	58,750737	2990	51,859155
2040	111,91987	2520	58,716279	3000	51,686865
2050	111,85551	2530	58,681821	3010	51,342286
2060	111,79115	2540	58,647363	3020	50,997707
2070	111,66243	2550	58,612905	3030	50,653128
2080	111,34064	2560	58,578447	3040	50,308549
2090	110,69705	2570	56,855552	3050	49,96397
2100	113,59319	2580	57,54471	3060	49,61939
2110	113,20704	2590	57,889289	3070	49,274811
2120	112,62781	2600	56,510972	3080	48,930232
2130	111,98423	2610	55,132656	3090	48,585653
2140	111,91987	2620	58,681821	3100	48,241074
2150	111,85551	2630	58,647363	3110	47,896495
2160	111,79115	2640	58,612905	3120	47,551916
2170	111,66243	2650	58,578447	3130	47,207337
2180	111,34064	2660	56,855552	3140	46,862758
2190	110,69705	2670	57,54471	3150	46,518179
2200	113,59319	2680	57,889289	3160	46,345889
2210	113,20704	2690	56,510972	3170	47,896495
2220	112,62781	2700	55,132656	3180	47,551916
2230	111,98423	2710	58,681821	3190	47,207337
2240	111,91987	2720	58,647363	3200	46,862758
2250	111,85551	2730	58,612905	3210	46,518179
2260	111,79115	2740	58,578447	3220	46,345889
2270	111,66243	2750	56,855552	3230	47,896495
2280	111,34064	2760	57,54471	3240	47,551916
2290	110,69705	2770	57,889289	3250	47,207337
2300	113,59319	2780	56,510972	3260	46,862758
2310	113,20704	2790	55,132656	3270	46,518179
2320	112,62781	2800	58,681821	3280	46,345889
2330	111,98423	2810	58,647363	3290	47,896495
2340	111,91987	2820	58,612905	3300	47,551916
2350	111,85551	2830	58,578447	3310	47,207337
2360	111,79115	2840	56,855552	3320	46,862758
2370	111,66243	2850	57,54471	3330	46,518179
2380	111,34064	2860	57,889289	3340	46,345889
2390	110,69705	2870	56,510972	3350	47,896495
2400	109	2880	55,132656	3360	47,551916
2410	108	2890	54,788077	3370	47,207337

Table A 2 Resistivity data which are used for verification analysis.

Resistivity					
m	ohmm	m	ohmm	m	ohmm
500	2,6	980	2,616	1460	1,89
510	2,59	990	2,6	1470	1,88
520	2,58	1000	2,59	1480	1,87
530	2,7	1010	2,58	1490	1,86
540	2,61	1020	2,7	1500	1,85
550	2,56	1030	2,61	1510	1,84
560	2,616	1040	2,56	1520	1,83
570	2,6	1050	2,616	1530	1,82
580	2,59	1060	2,6	1540	1,81
590	2,58	1070	2,55	1550	1,8
600	2,7	1080	2,54	1560	1,89
610	2,61	1090	2,53	1570	1,88
620	2,56	1100	2,53	1580	1,87
630	2,616	1110	2,52	1590	1,86
640	2,6	1120	2,51	1600	1,85
650	2,59	1130	2,5	1610	1,84
660	2,58	1140	2,49	1620	1,83
670	2,7	1150	2,48	1630	1,82
680	2,61	1160	2,47	1640	1,81
690	2,56	1170	2,46	1650	1,8
700	2,616	1180	2,465	1660	1,89
710	2,6	1190	2,4	1670	1,88
720	2,59	1200	2,3	1680	1,87
730	2,58	1210	2,2	1690	1,86
740	2,7	1220	2,2	1700	1,85
750	2,61	1230	2,15	1710	1,84
760	2,56	1240	2,11	1720	1,83
770	2,616	1250	2,1	1730	1,82
780	2,6	1260	2,09	1740	1,81
790	2,59	1270	2,05	1750	1,8
800	2,58	1280	2	1760	1,89
810	2,7	1290	2,02	1770	1,88
820	2,61	1300	1,95	1780	1,87
830	2,56	1310	1,94	1790	1,86
840	2,616	1320	1,93	1800	1,85
850	2,6	1330	1,92	1810	1,84
860	2,59	1340	1,91	1820	1,83
870	2,58	1350	1,9	1830	1,82
880	2,7	1360	1,89	1840	1,81
890	2,61	1370	1,88	1850	1,8
900	2,56	1380	1,87	1860	1,89
910	2,616	1390	1,86	1870	1,88
920	2,6	1400	1,85	1880	1,87
930	2,59	1410	1,84	1890	1,86
940	2,58	1420	1,83	1900	1,85
950	2,7	1430	1,82	1910	1,84
960	2,61	1440	1,81	1920	1,83
970	2,56	1450	1,8	1930	1,82

Resistivity					
m	ohmm	m	ohmm	m	ohmm
1940	1,81	2420	1,75	2900	1,58
1950	1,8	2430	1,74	2910	1,57
1960	1,79	2440	1,739	2920	1,56
1970	1,78	2450	1,738	2930	1,54
1980	1,77	2460	1,737	2940	1,55
1990	1,76	2470	1,735	2950	1,53
2000	1,765	2480	1,73	2960	1,52
2010	1,759	2490	1,72	2970	1,515
2020	1,75	2500	1,71	2980	1,51
2030	1,74	2510	1,705	2990	1,505
2040	1,739	2520	1,704	3000	1,5
2050	1,738	2530	1,703	3010	1,49
2060	1,737	2540	1,702	3020	1,48
2070	1,735	2550	1,701	3030	1,47
2080	1,73	2560	1,7	3040	1,46
2090	1,72	2570	1,65	3050	1,45
2100	1,765	2580	1,67	3060	1,44
2110	1,759	2590	1,68	3070	1,43
2120	1,75	2600	1,64	3080	1,42
2130	1,74	2610	1,6	3090	1,41
2140	1,739	2620	1,703	3100	1,4
2150	1,738	2630	1,702	3110	1,39
2160	1,737	2640	1,701	3120	1,38
2170	1,735	2650	1,7	3130	1,37
2180	1,73	2660	1,65	3140	1,36
2190	1,72	2670	1,67	3150	1,35
2200	1,765	2680	1,68	3160	1,345
2210	1,759	2690	1,64	3170	1,39
2220	1,75	2700	1,6	3180	1,38
2230	1,74	2710	1,703	3190	1,37
2240	1,739	2720	1,702	3200	1,36
2250	1,738	2730	1,701	3210	1,35
2260	1,737	2740	1,7	3220	1,345
2270	1,735	2750	1,65	3230	1,39
2280	1,73	2760	1,67	3240	1,38
2290	1,72	2770	1,68	3250	1,37
2300	1,765	2780	1,64	3260	1,36
2310	1,759	2790	1,6	3270	1,35
2320	1,75	2800	1,703	3280	1,345
2330	1,74	2810	1,702	3290	1,39
2340	1,739	2820	1,701	3300	1,38
2350	1,738	2830	1,7	3310	1,37
2360	1,737	2840	1,65	3320	1,36
2370	1,735	2850	1,67	3330	1,35
2380	1,73	2860	1,68	3340	1,345
2390	1,72	2870	1,64	3350	1,39
2400	1,765	2880	1,6	3360	1,38
2410	1,759	2890	1,59	3370	1,37

Resistivity			
m	ohmm	m	ohmm
3380	1,36	3860	0,58
3390	1,35	3870	0,57
3400	1,345	3880	0,56
3410	1,34	3890	0,55
3420	1,335	3900	0,54
3430	1,33	3910	0,53
3440	1,329	3920	0,53
3450	1,325	3930	0,52
3460	1,31	3940	0,519
3470	1,3	3950	0,53
3480	1,29	3960	0,54
3490	1,2	3970	0,55
3500	1,1	3980	0,56
3510	1	3990	0,57
3520	0,95	4000	0,58
3530	0,92	4010	0,59
3540	0,9	4020	0,6
3550	0,85	4030	0,6
3560	0,83	4040	0,61
3570	0,85		
3580	0,82		
3590	0,8		
3600	0,75		
3610	0,7		
3620	0,69		
3630	0,685		
3640	0,682		
3650	0,68		
3660	0,67		
3670	0,66		
3680	0,65		
3690	0,64		
3700	0,643		
3710	0,68		
3720	0,67		
3730	0,66		
3740	0,65		
3750	0,64		
3760	0,643		
3770	0,68		
3780	0,67		
3790	0,66		
3800	0,65		
3810	0,64		
3820	0,643		
3830	0,64		
3840	0,6		
3850	0,59		

Table A 3 Bulk density data.

Bulk Density					
m	g/cc	m	g/cc	m	g/cc
0	1,05	480	1,3445758	960	1,7061776
10	1,05	490	1,3528142	970	1,7129759
20	1,05	500	1,3610225	980	1,7197443
30	1,05	510	1,3692009	990	1,7264827
40	1,05	520	1,3773493	1000	1,733191
50	1,05	530	1,3854676	1010	1,7398694
60	1,05	540	1,393556	1020	1,7465178
70	1,05	550	1,4016144	1030	1,7531361
80	1,05	560	1,4096428	1040	1,7597245
90	1,05	570	1,4176411	1050	1,7662829
100	1,05	580	1,4256095	1060	1,7728113
110	1,05	590	1,4335479	1070	1,7793096
120	1,05	600	1,4414562	1080	1,785778
130	1,05	610	1,4493346	1090	1,7922164
140	1,05	620	1,457183	1100	1,7986247
150	1,05	630	1,4650013	1110	1,8050031
160	1,05	640	1,4727897	1120	1,8113515
170	1,05	650	1,4805481	1130	1,8176698
180	1,05	660	1,4882765	1140	1,8239582
190	1,05	670	1,4959748	1150	1,8302166
200	1,05	680	1,5036432	1160	1,836445
210	1,05	690	1,5112816	1170	1,8426433
220	1,05	700	1,5188899	1180	1,8488117
230	1,05	710	1,5264683	1190	1,8549501
240	1,05	720	1,5340167	1200	1,8610584
250	1,05	730	1,541535	1210	1,8671368
260	1,05	740	1,5490234	1220	1,8731852
270	1,05	750	1,5564818	1230	1,8792035
280	1,05	760	1,5639102	1240	1,8851919
290	1,05	770	1,5713085	1250	1,8911503
300	1,05	780	1,5786769	1260	1,8970787
310	1,1999335	790	1,5860153	1270	1,902977
320	1,2086819	800	1,5933236	1280	1,9088454
330	1,2174002	810	1,600602	1290	1,9146838
340	1,2260886	820	1,6078504	1300	1,9204921
350	1,234747	830	1,6150687	1310	1,9262705
360	1,2433754	840	1,6222571	1320	1,9320189
370	1,2519737	850	1,6294155	1330	1,9377372
380	1,2605421	860	1,6365439	1340	1,9434256
390	1,2690805	870	1,6436422	1350	1,949084
400	1,2775888	880	1,6507106	1360	1,9547124
410	1,2860672	890	1,657749	1370	1,9603107
420	1,2945156	900	1,6647573	1380	1,9658791
430	1,3029339	910	1,6717357	1390	1,9714175
440	1,3113223	920	1,6786841	1400	1,9769258
450	1,3196807	930	1,6856024	1410	1,9824042
460	1,3280091	940	1,6924908	1420	1,9878526
470	1,3363074	950	1,6993492	1430	1,9932709

Bulk Density					
m	g/cc	m	g/cc	m	g/cc
1440	1,9986593	1920	2,2220211	2400	2,3762628
1450	2,0040177	1930	2,2259394	2410	2,3787412
1460	2,0093461	1940	2,2298278	2420	2,3811896
1470	2,0146444	1950	2,2336862	2430	2,3836079
1480	2,0199128	1960	2,2375146	2440	2,3859963
1490	2,0251512	1970	2,2413129	2450	2,3883547
1500	2,0303595	1980	2,2450813	2460	2,3906831
1510	2,0355379	1990	2,2488197	2470	2,3929814
1520	2,0406863	2000	2,252528	2480	2,3952498
1530	2,0458046	2010	2,2562064	2490	2,3974882
1540	2,050893	2020	2,2598548	2500	2,3996965
1550	2,0559514	2030	2,2634731	2510	2,4018749
1560	2,0609798	2040	2,2670615	2520	2,4040233
1570	2,0659781	2050	2,2706199	2530	2,4061416
1580	2,0709465	2060	2,2741483	2540	2,40823
1590	2,0758849	2070	2,2776466	2550	2,4102884
1600	2,0807932	2080	2,281115	2560	2,4123168
1610	2,0856716	2090	2,2845534	2570	2,4143151
1620	2,09052	2100	2,2879617	2580	2,4162835
1630	2,0953383	2110	2,2913401	2590	2,4182219
1640	2,1001267	2120	2,2946885	2600	2,4201302
1650	2,1048851	2130	2,2980068	2610	2,4220086
1660	2,1096135	2140	2,3012952	2620	2,423857
1670	2,1143118	2150	2,3045536	2630	2,4256753
1680	2,1189802	2160	2,307782	2640	2,4274637
1690	2,1236186	2170	2,3109803	2650	2,4292221
1700	2,1282269	2180	2,3141487	2660	2,4309505
1710	2,1328053	2190	2,3172871	2670	2,4326488
1720	2,1373537	2200	2,3203954	2680	2,4343172
1730	2,141872	2210	2,3234738	2690	2,4359556
1740	2,1463604	2220	2,3265222	2700	2,4375639
1750	2,1508188	2230	2,3295405	2710	2,4391423
1760	2,1552472	2240	2,3325289	2720	2,4406907
1770	2,1596455	2250	2,3354873	2730	2,442209
1780	2,1640139	2260	2,3384157	2740	2,4436974
1790	2,1683523	2270	2,341314	2750	2,4451558
1800	2,1726606	2280	2,3441824	2760	2,4465842
1810	2,176939	2290	2,3470208	2770	2,4479825
1820	2,1811874	2300	2,3498291	2780	2,4493509
1830	2,1854057	2310	2,3526075	2790	2,4506893
1840	2,1895941	2320	2,3553559	2800	2,4519976
1850	2,1937525	2330	2,3580742	2810	2,453276
1860	2,1978809	2340	2,3607626	2820	2,4545244
1870	2,2019792	2350	2,363421	2830	2,4557427
1880	2,2060476	2360	2,3660494	2840	2,4569311
1890	2,210086	2370	2,3686477	2850	2,4580895
1900	2,2140943	2380	2,3712161	2860	2,4592179
1910	2,2180727	2390	2,3737545	2870	2,4603162

Bulk Density					
m	g/cc	m	g/cc	m	g/cc
2880	2,4613846	3360	2,4773864	3840	2,4242681
2890	2,462423	3370	2,4769847	3850	2,4224265
2900	2,4634313	3380	2,4765531	3860	2,4205549
2910	2,4644097	3390	2,4760915	3870	2,4186532
2920	2,4653581	3400	2,4755998	3880	2,4167216
2930	2,4662764	3410	2,4750782	3890	2,41476
2940	2,4671648	3420	2,4745266	3900	2,4127683
2950	2,4680232	3430	2,4739449	3910	2,4107467
2960	2,4688516	3440	2,4733333	3920	2,4086951
2970	2,4696499	3450	2,4726917	3930	2,4066134
2980	2,4704183	3460	2,4720201	3940	2,4045018
2990	2,4711567	3470	2,4713184	3950	2,4023602
3000	2,471865	3480	2,4705868	3960	2,4001886
3010	2,4725434	3490	2,4698252	3970	2,3979869
3020	2,4731918	3500	2,4690335	3980	2,3957553
3030	2,4738101	3510	2,4682119	3990	2,3934937
3040	2,4743985	3520	2,4673603	4000	2,391202
3050	2,4749569	3530	2,4664786	4010	2,3888804
3060	2,4754853	3540	2,465567	4020	2,3865288
3070	2,4759836	3550	2,4646254	4030	2,3841471
3080	2,476452	3560	2,4636538	4040	2,3817355
3090	2,4768904	3570	2,4626521		
3100	2,4772987	3580	2,4616205		
3110	2,4776771	3590	2,4605589		
3120	2,4780255	3600	2,4594672		
3130	2,4783438	3610	2,4583456		
3140	2,4786322	3620	2,457194		
3150	2,4788906	3630	2,4560123		
3160	2,479119	3640	2,4548007		
3170	2,4793173	3650	2,4535591		
3180	2,4794857	3660	2,4522875		
3190	2,4796241	3670	2,4509858		
3200	2,4797324	3680	2,4496542		
3210	2,4798108	3690	2,4482926		
3220	2,4798592	3700	2,4469009		
3230	2,4798775	3710	2,4454793		
3240	2,4798659	3720	2,4440277		
3250	2,4798243	3730	2,442546		
3260	2,4797527	3740	2,4410344		
3270	2,479651	3750	2,4394928		
3280	2,4795194	3760	2,4379212		
3290	2,4793578	3770	2,4363195		
3300	2,4791661	3780	2,4346879		
3310	2,4789445	3790	2,4330263		
3320	2,4786929	3800	2,4313346		
3330	2,4784112	3810	2,429613		
3340	2,4780996	3820	2,4278614		
3350	2,477758	3830	2,4260797		

Table A 4 Gamma ray log data

Gamma ray					
m	API	m	API	m	API
0	50	480	68	960	56,2
10	51	490	69	970	56,1
20	52	500	70	980	56
30	53	510	69,9	990	55,9
40	54	520	69,5	1000	55,8
50	55	530	69,4	1010	55,7
60	56	540	69,3	1020	55,6
70	57	550	69,2	1030	55,5
80	56	560	69,1	1040	55,4
90	55	570	69	1050	55,45
100	54	580	68,9	1060	55,4
110	53	590	68,8	1070	55
120	52	600	68,7	1080	54,9
130	51	610	68,6	1090	54,8
140	50	620	68,5	1100	54,7
150	51	630	68,4	1110	56,5
160	52	640	68,3	1120	56,4
170	53	650	68	1130	56,3
180	54	660	67,9	1140	56,2
190	55	670	67,8	1150	56,1
200	56	680	67,6	1160	56
210	57	690	67,5	1170	55,9
220	58	700	67,4	1180	55,8
230	59	710	67,3	1190	55
240	55	720	67,2	1200	54
250	56	730	67,2	1210	54
260	57	740	67,1	1220	53
270	58	750	67	1230	53,5
280	59	760	66,9	1240	52
290	55	770	69,8	1250	51
300	56	780	68,7	1260	50
310	57	790	68	1270	49
320	58	800	67	1280	48
330	59	810	66	1290	47
340	55	820	65	1300	46
350	56	830	65	1310	45
360	57	840	64	1320	44
370	58	850	63	1330	43
380	59	860	62	1340	42
390	60	870	63	1350	41
400	61	880	60	1360	40
410	62	890	59	1370	39
420	63	900	59	1380	38
430	63	910	58	1390	37
440	64	920	57	1400	36
450	65	930	56,5	1410	35
460	66	940	56,4	1420	34,9
470	67	950	56,3	1430	34,8

Gamma ray					
m	API	m	API	m	API
1440	34,7	1920	31,9	2400	24,2
1450	34,6	1930	31,7	2410	24,2
1460	34,5	1940	31,6	2420	24,1
1470	34,3	1950	31,4	2430	24
1480	34,2	1960	31,2	2440	23,9
1490	34,25	1970	30,9	2450	23,8
1500	34,1	1980	30,7	2460	23,7
1510	33,9	1990	30,6	2470	23,6
1520	33,8	2000	30,5	2480	23,6
1530	33,7	2010	30,9	2490	23,5
1540	33,6	2020	30,7	2500	23,4
1550	33,5	2030	30,6	2510	24,9
1560	33,4	2040	30,5	2520	24,8
1570	33,3	2050	30,4	2530	24,7
1580	33,2	2060	30,3	2540	24,6
1590	33,1	2070	29,9	2550	24,5
1600	33	2080	29,7	2560	24,4
1610	33,05	2090	29,5	2570	24,3
1620	34,25	2100	29,4	2580	24,2
1630	34,1	2110	29,2	2590	24,2
1640	33,9	2120	29,1	2600	24,1
1650	33,8	2130	29	2610	24
1660	33,7	2140	28,7	2620	23,9
1670	33,6	2150	28,6	2630	23,8
1680	33,5	2160	27,9	2640	23,7
1690	33,4	2170	27,8	2650	23,6
1700	33,3	2180	27,4	2660	23,6
1710	33,2	2190	27,2	2670	23,5
1720	33,1	2200	27,1	2680	23,4
1730	33	2210	27	2690	24,9
1740	33,05	2220	26,9	2700	24,8
1750	34,25	2230	26,7	2710	24,7
1760	34,1	2240	26,6	2720	24,6
1770	33,9	2250	26,4	2730	24,5
1780	33,8	2260	26,3	2740	24,4
1790	33,7	2270	26,1	2750	24,3
1800	33,6	2280	26	2760	24,2
1810	33,5	2290	25,5	2770	24,2
1820	33,4	2300	25,2	2780	24,1
1830	33,3	2310	25,1	2790	24
1840	33,2	2320	25	2800	23,9
1850	33,1	2330	24,9	2810	23,8
1860	33	2340	24,8	2820	23,7
1870	33,05	2350	24,7	2830	23,6
1880	32,9	2360	24,6	2840	23,6
1890	32,5	2370	24,5	2850	23,5
1900	32,4	2380	24,4	2860	23,4
1910	32,1	2390	24,3	2870	24,9

Gamma ray					
m	API	m	API	m	API
2880	24,8	3360	22,5	3840	13,6
2890	24,7	3370	22,4	3850	13,5
2900	24,6	3380	22,3	3860	13,4
2910	24,5	3390	22,2	3870	13,2
2920	24,4	3400	22,1	3880	13,1
2930	24,3	3410	22	3890	13
2940	24,2	3420	21,9	3900	12,9
2950	24,2	3430	21,8	3910	12,8
2960	24,1	3440	21,5	3920	12,7
2970	24	3450	19,9	3930	12,6
2980	23,9	3460	19,6	3940	12,5
2990	23,8	3470	19	3950	12,4
3000	23,7	3480	17,9	3960	12,3
3010	23,6	3490	16,4	3970	12,2
3020	23,6	3500	15,4	3980	12,1
3030	23,5	3510	15	3990	12
3040	23,4	3520	14,9	4000	11,9
3050	24,9	3530	14,8	4010	11,8
3060	24,8	3540	14,7	4020	11,7
3070	24,7	3550	14,6	4030	11,6
3080	24,6	3560	14,5	4040	11
3090	24,5	3570	14,4		
3100	24,4	3580	14,3		
3110	24,3	3590	14,2		
3120	24,2	3600	14,11		
3130	24,2	3610	13,9		
3140	24,1	3620	13,8		
3150	24	3630	13,7		
3160	23,9	3640	13,6		
3170	23,8	3650	13,5		
3180	23,7	3660	13,4		
3190	23,6	3670	13,2		
3200	23,6	3680	13,1		
3210	23,5	3690	13		
3220	23,4	3700	12,9		
3230	23	3710	12,8		
3240	22,9	3720	12,7		
3250	22,7	3730	12,6		
3260	22,5	3740	12,5		
3270	22,4	3750	12,4		
3280	22,3	3760	12,3		
3290	22,2	3770	12,2		
3300	22,1	3780	12,1		
3310	22	3790	12		
3320	21,9	3800	11,9		
3330	21,8	3810	11,8		
3340	21,5	3820	11,7		
3350	22,7	3830	11,6		

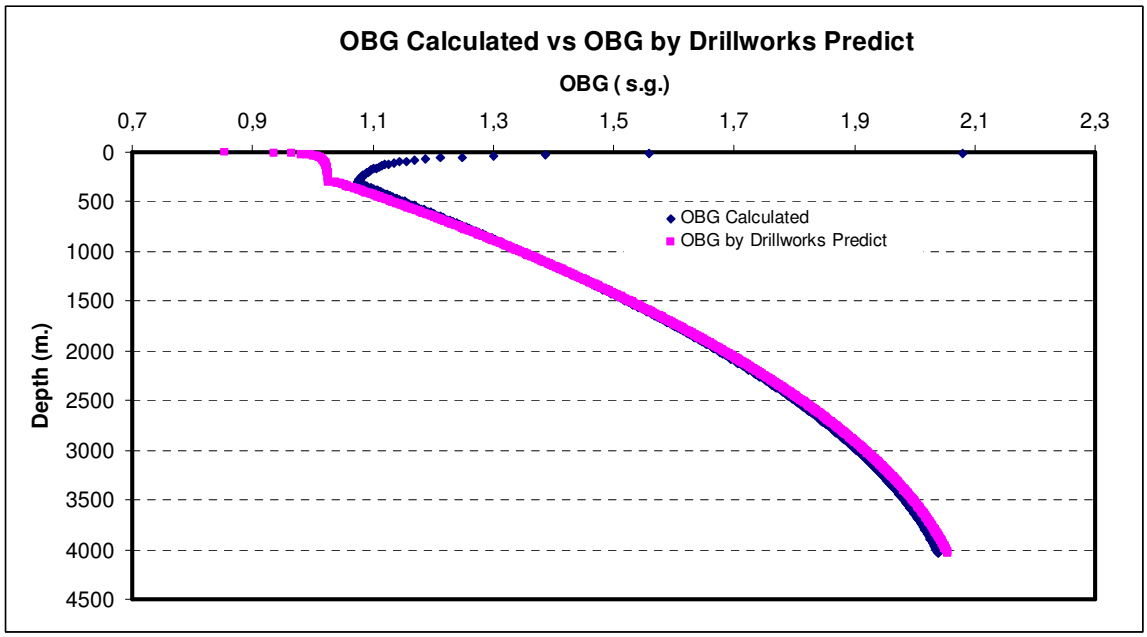

Figure A 1 OBG comparison between OBG calculated and OBG computed by Drillworks Predict software.

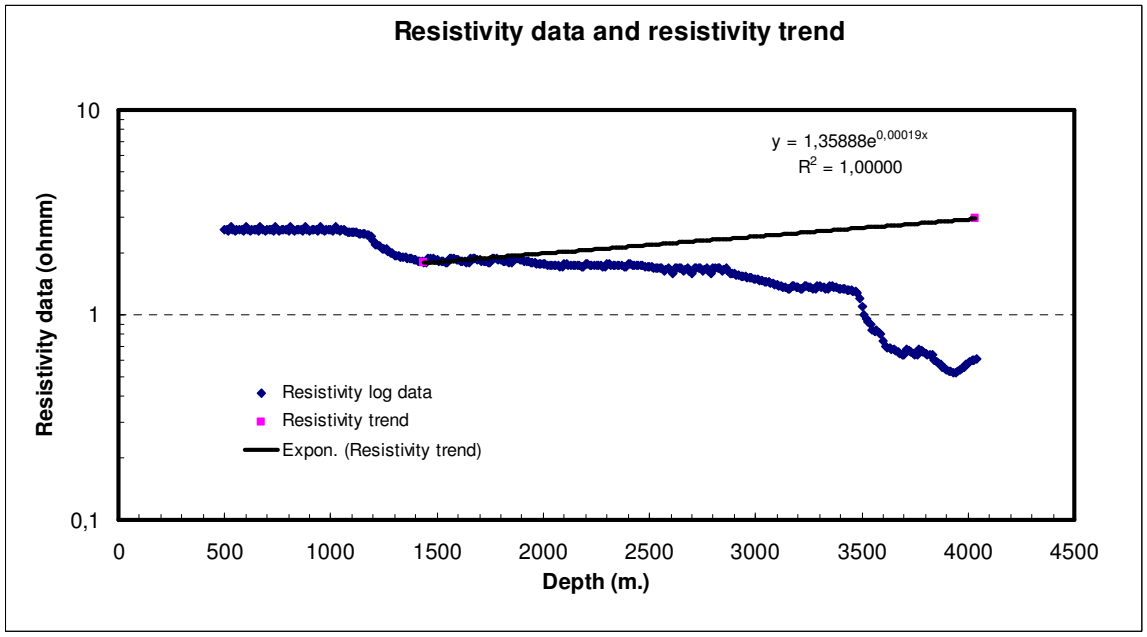

Figure A 2 Resistivity log data trend for Eaton resistivity equation.

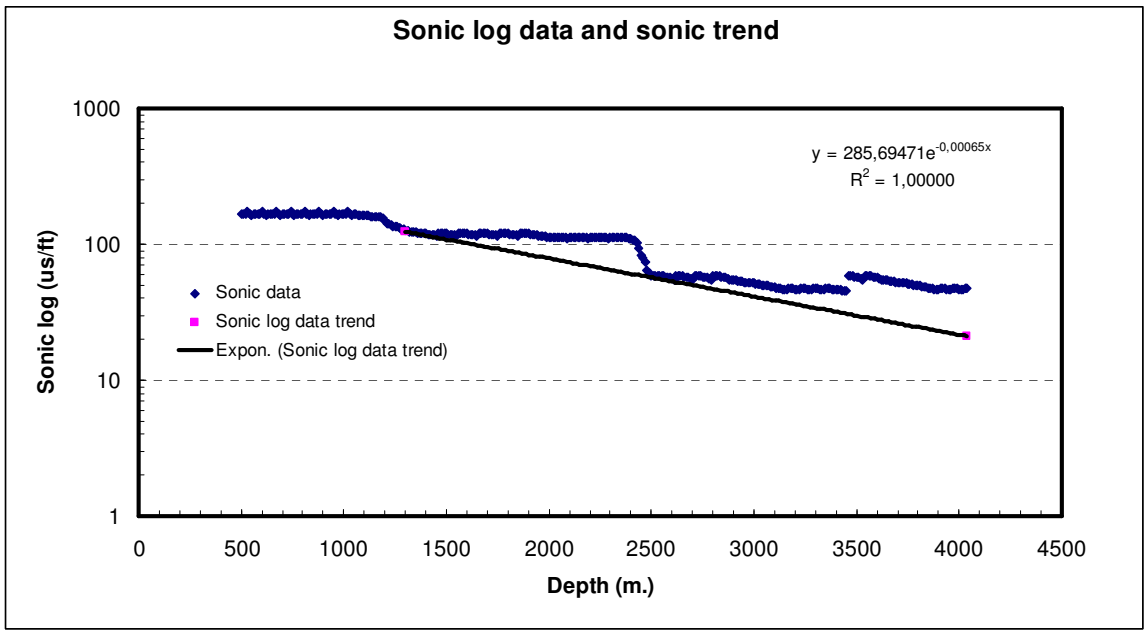

Figure A 3 Sonic log data trend for Eaton sonic equation.

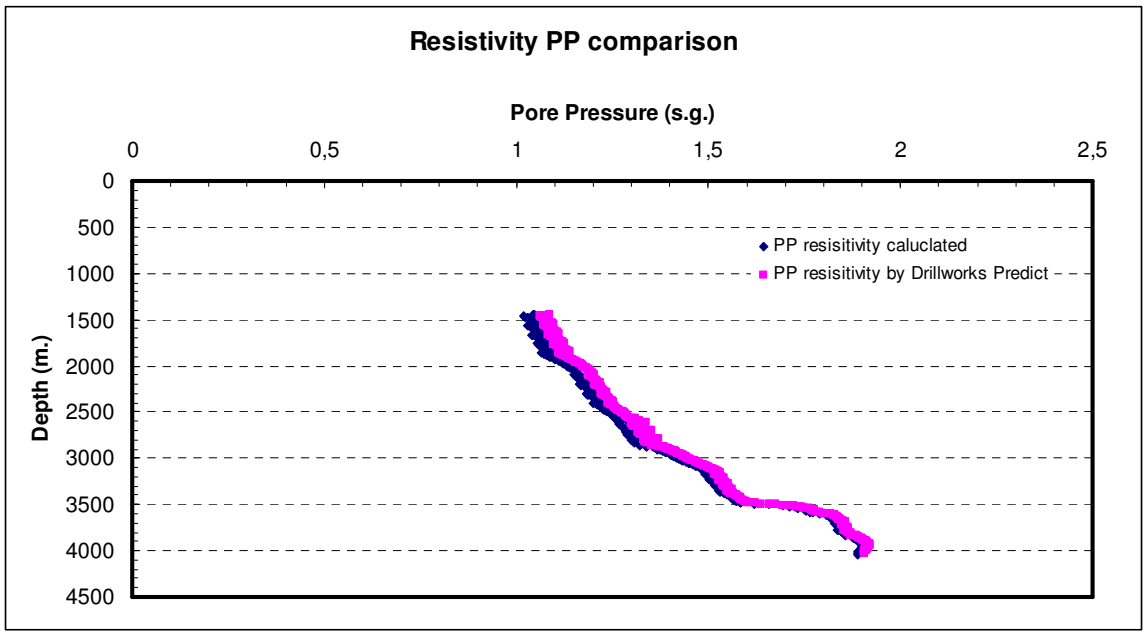

Figure A 4 Resistivity pore pressure differences between calculated by Excel and Drillworks Predict software using Eaton resistivity equation.

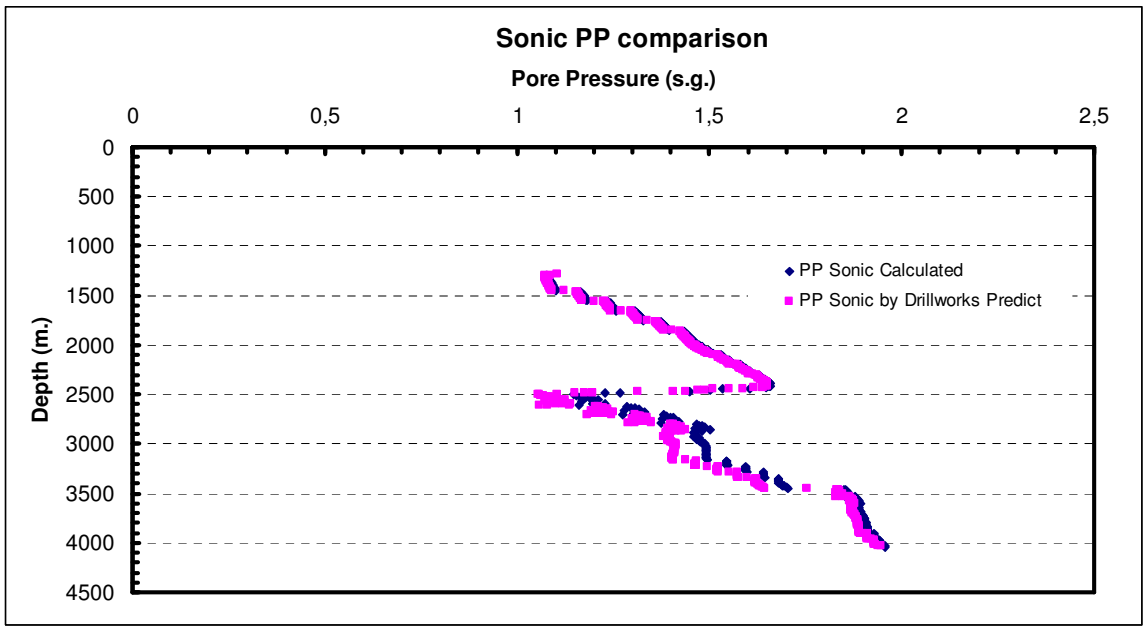

Figure A 5 Sonic pore pressure differences between calculated by Excel and Drillworks Predict software using Eaton sonic equation.

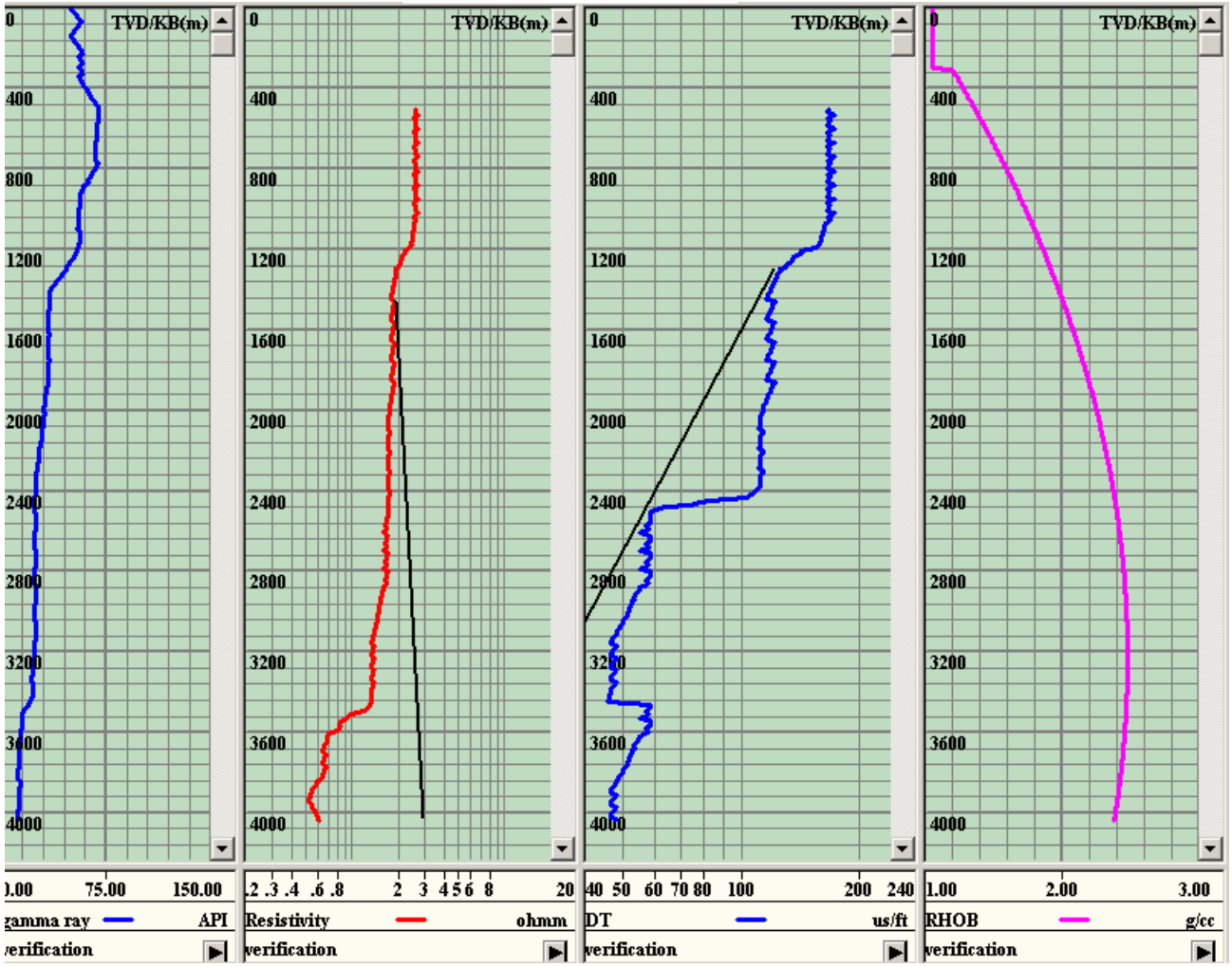

Figure A 6 Input data view from Drillworks Predict software for verification data.

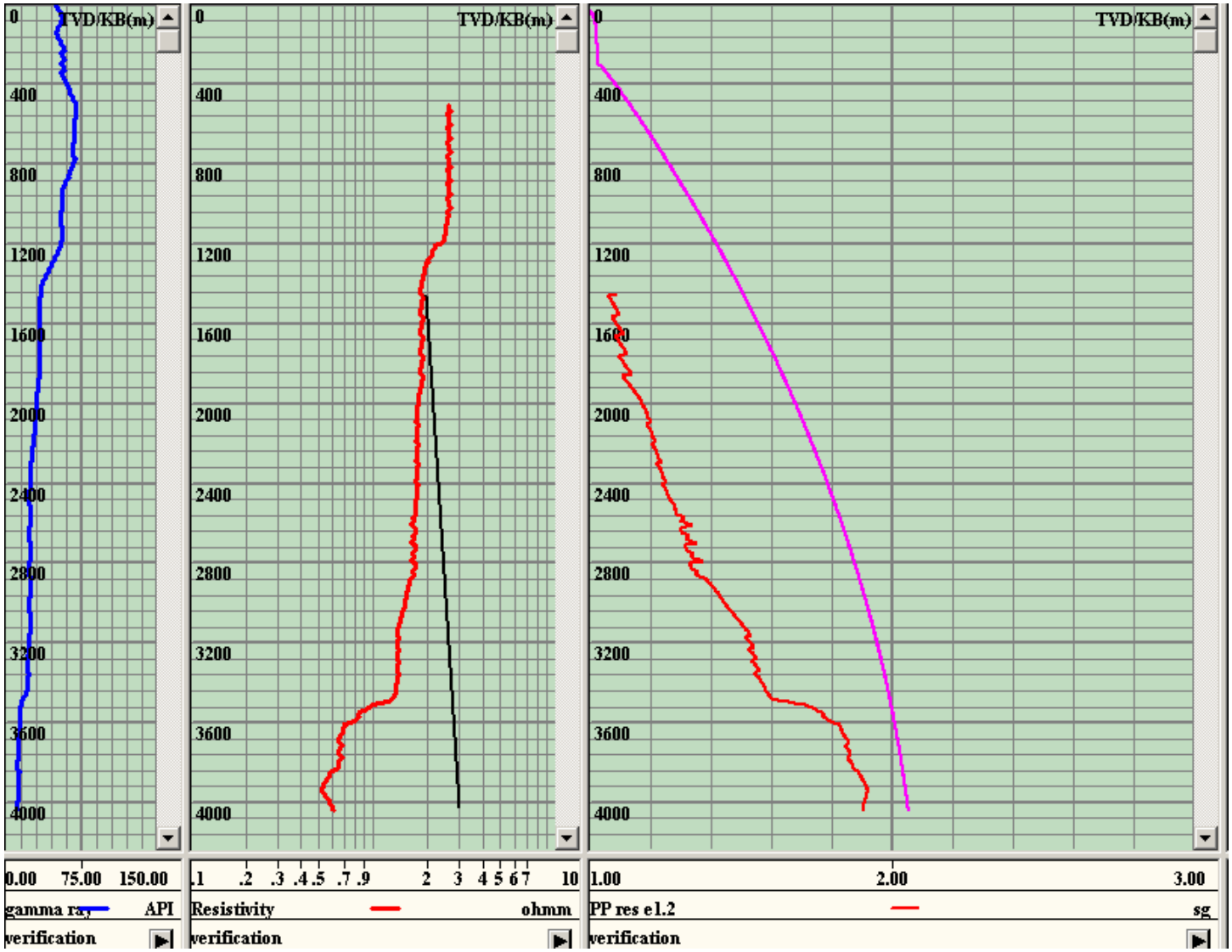

Figure A 7 Resistivity data used pore pressure prediction by Eaton's equation view from Drillworks Predict software.

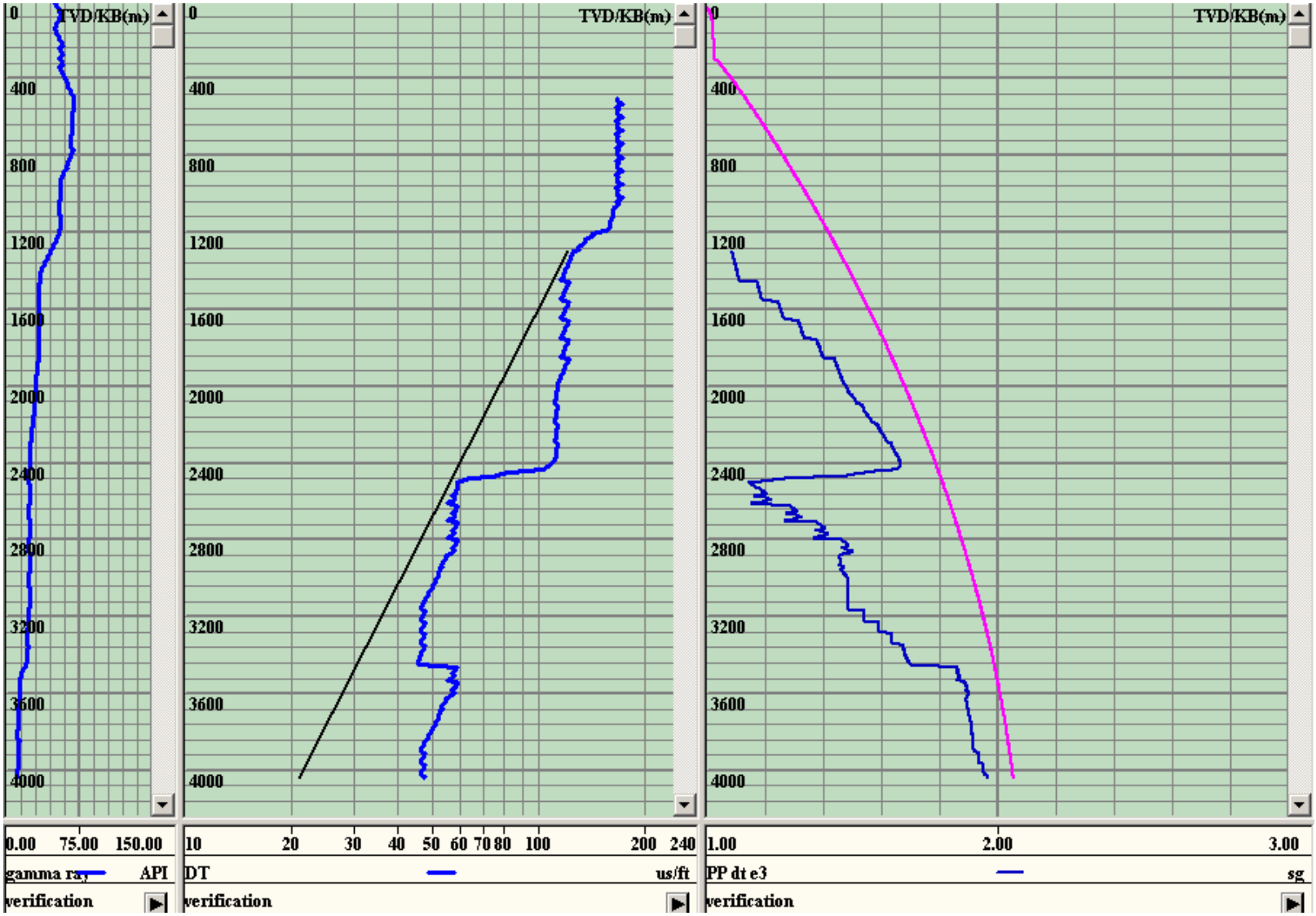

Figure A 8 Sonic data used pore pressure prediction by Eaton's eaution view from Drillworks Predict software.

APPENDIX B

RESULTS FOR WELL 2 AND WELL 3

LIST OF FIGURES

FIGURE Page

FIGURE Page

WELL 2

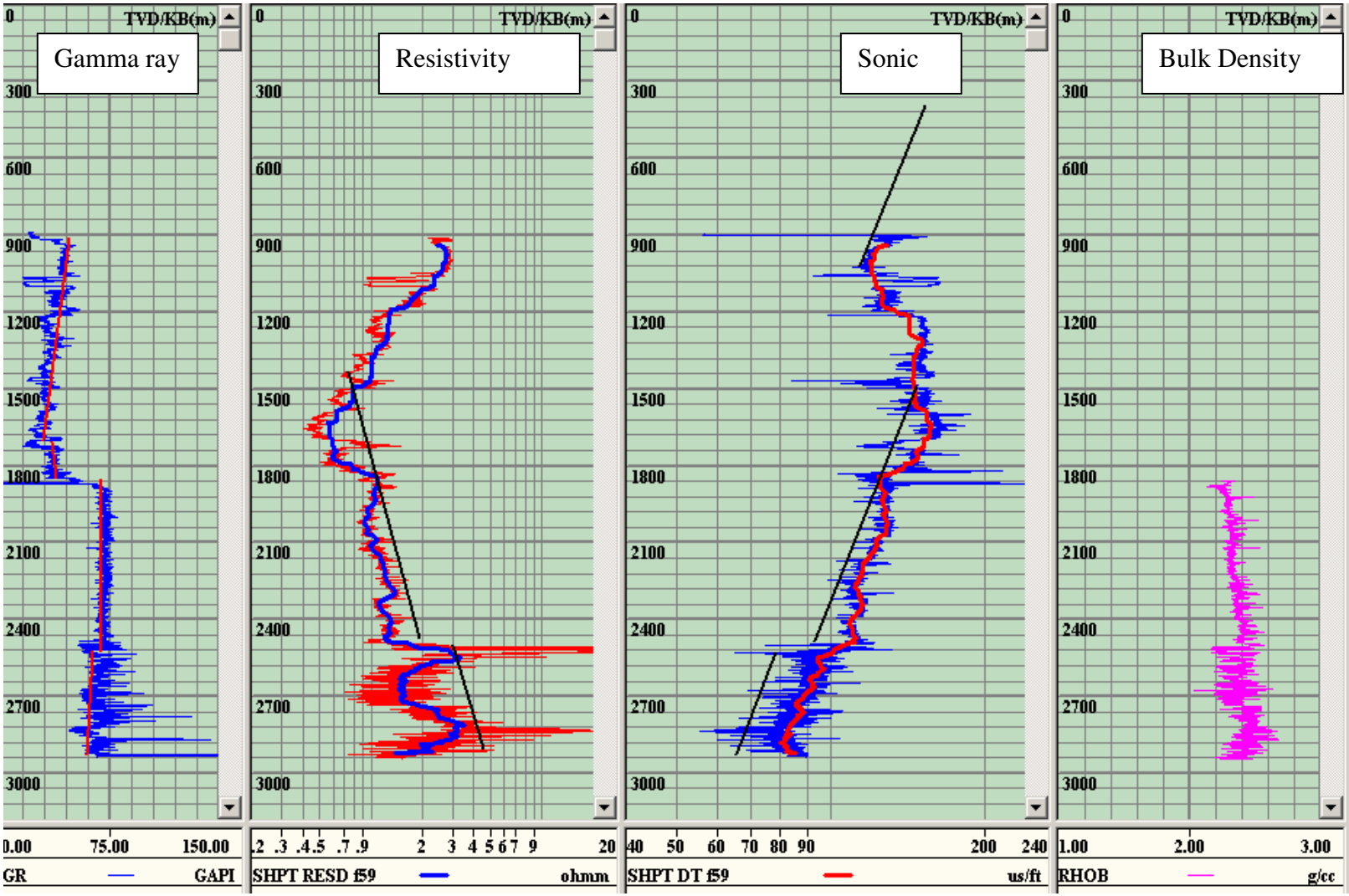

Figure B 1 Input data for well 2, Gamma ray, Resistivity, Sonic and Bulk Density log data is plotted.

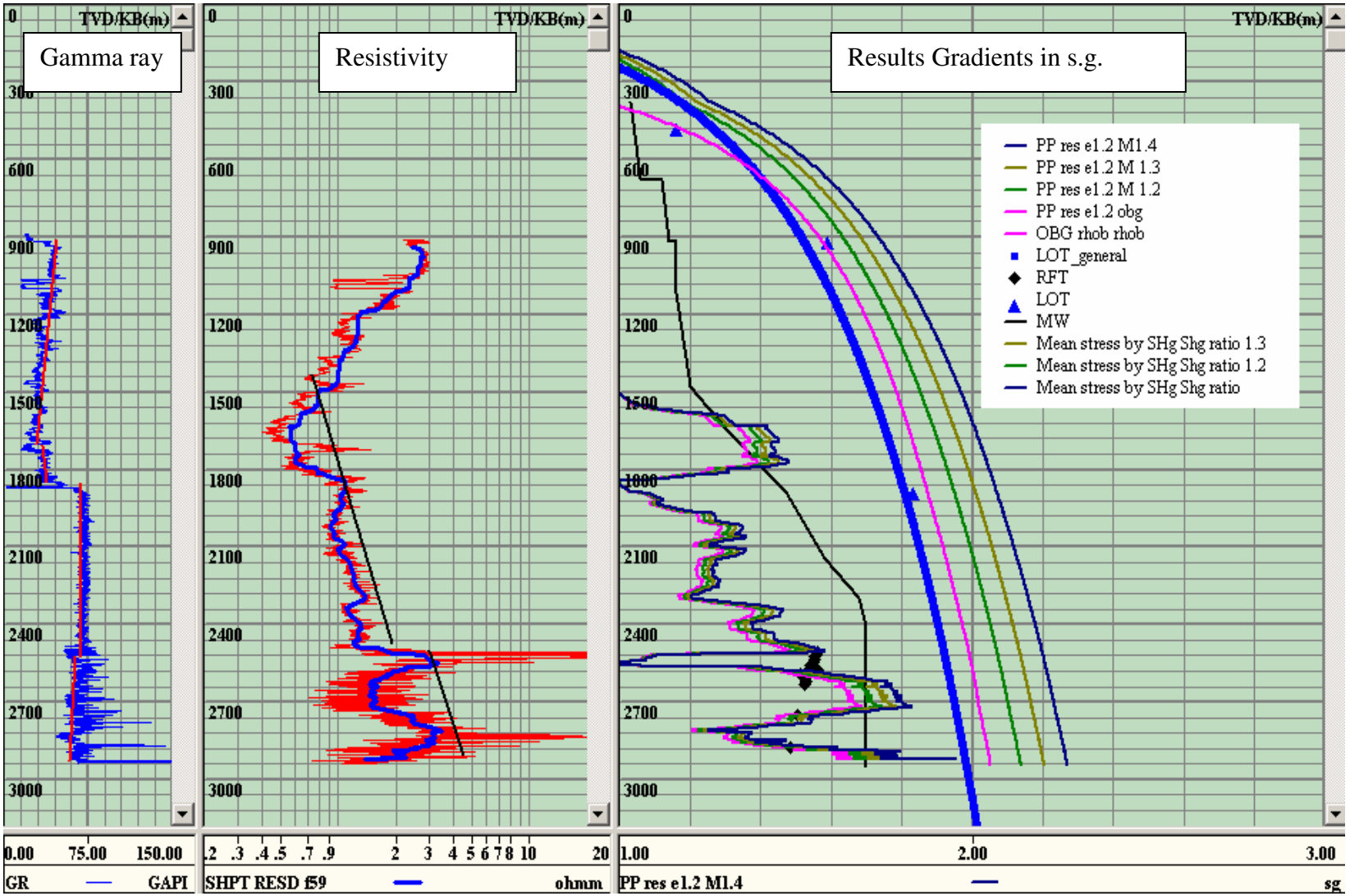

Figure B 2 Eaton Resistivity Method results for well 2, Results are plotted in result gradient part.

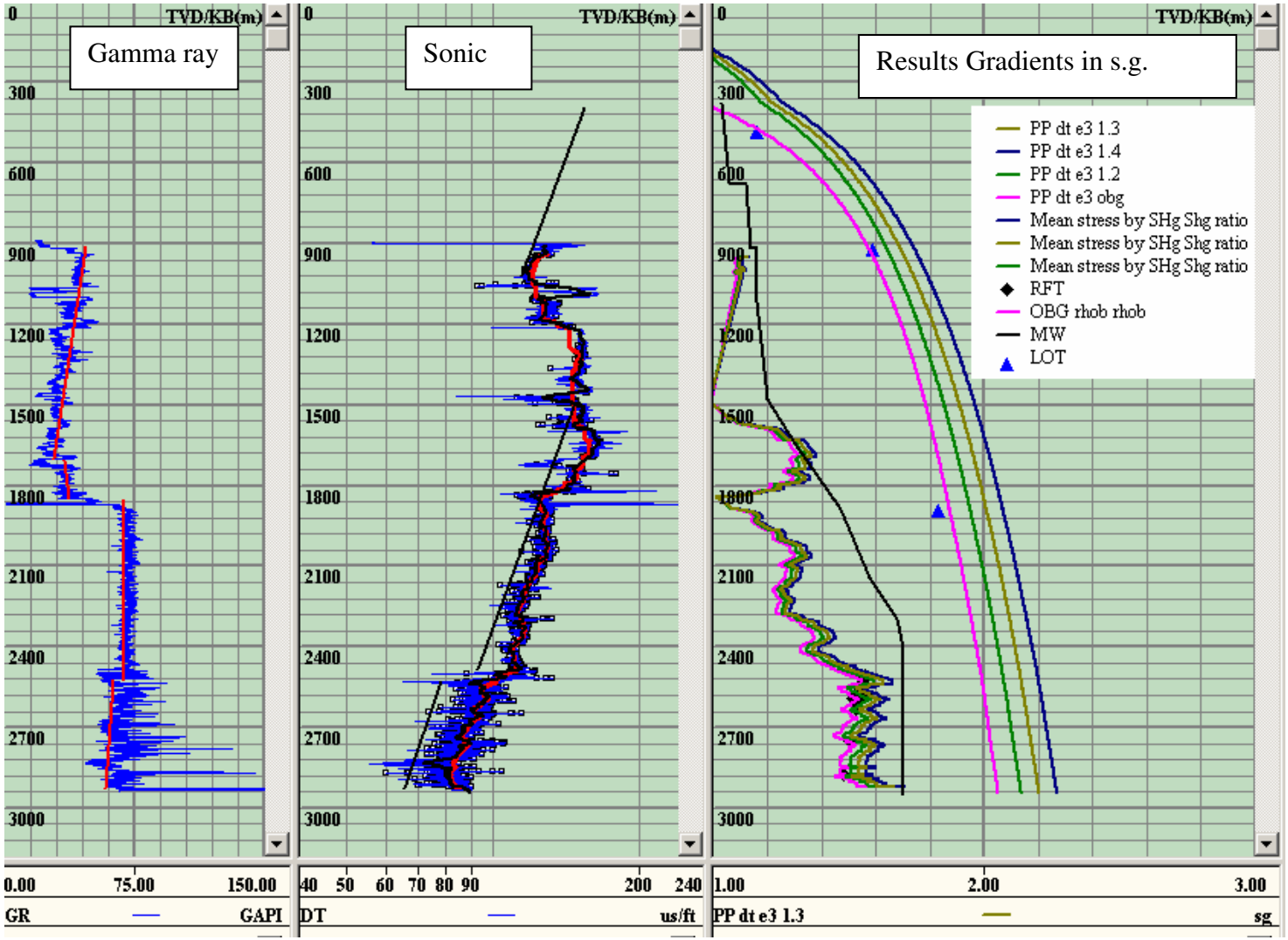

Figure B 3 Eaton Sonic Method results for well 2, Results are plotted in result gradient part.

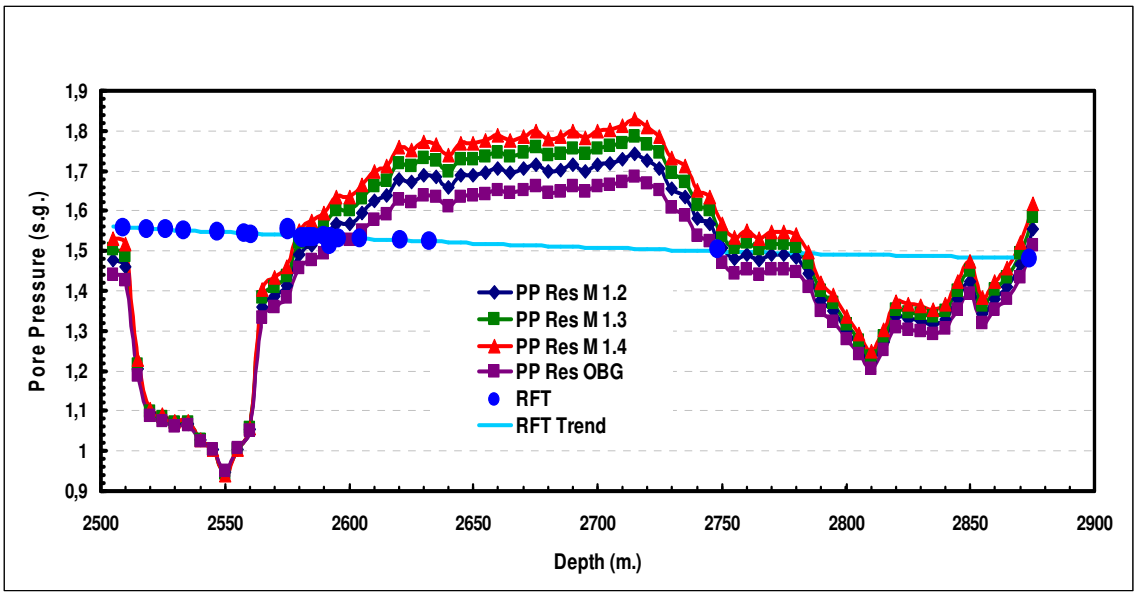

Figure B 4 Resistivity log data based pore pressure comparison for each method to RFT for well 2.

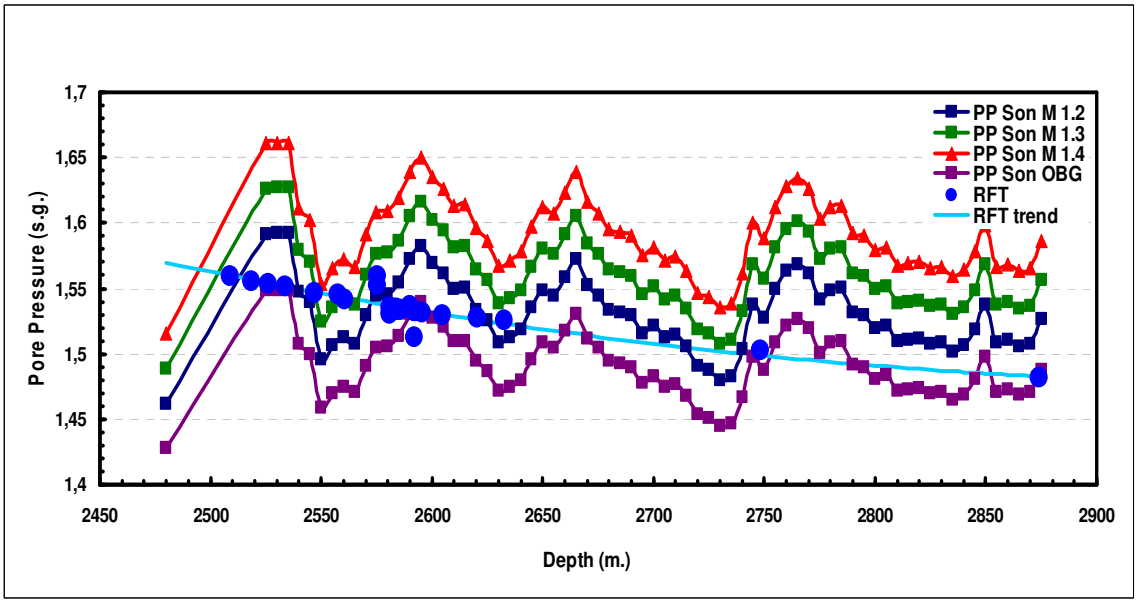

Figure B 5 Sonic log data based pore pressure comparison for each method to RFT for well 2

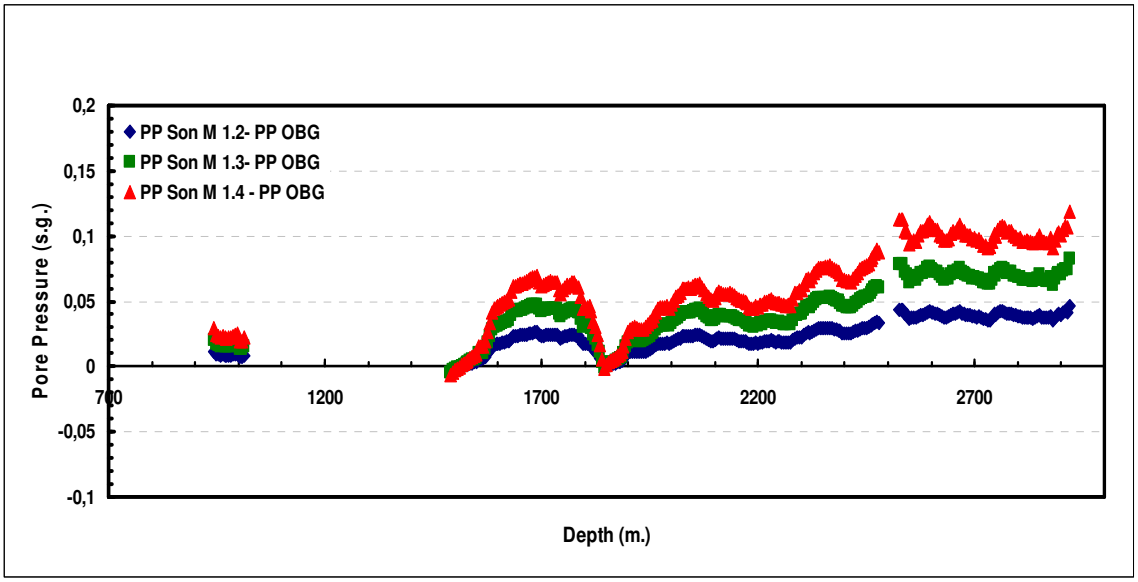

Figure B 6 Pore pressure difference between mean total stress used pore pressure prediction and overburden based pore pressure prediction using sonic log data for Well 2.

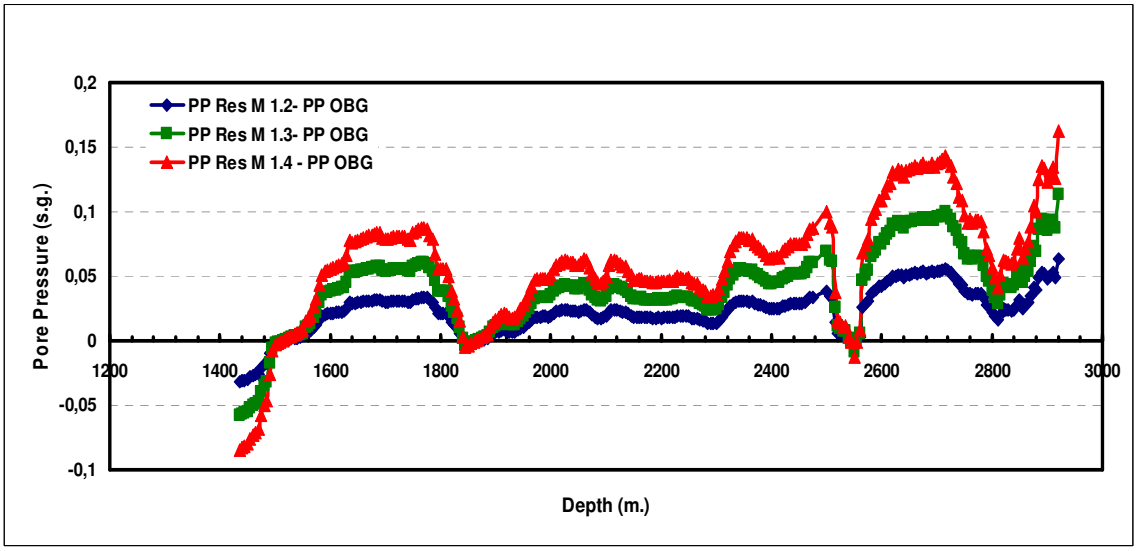

Figure B 7 Pore pressure difference between mean total stress used pore pressure prediction and overburden based pore pressure prediction using resistivity log data for Well 2.

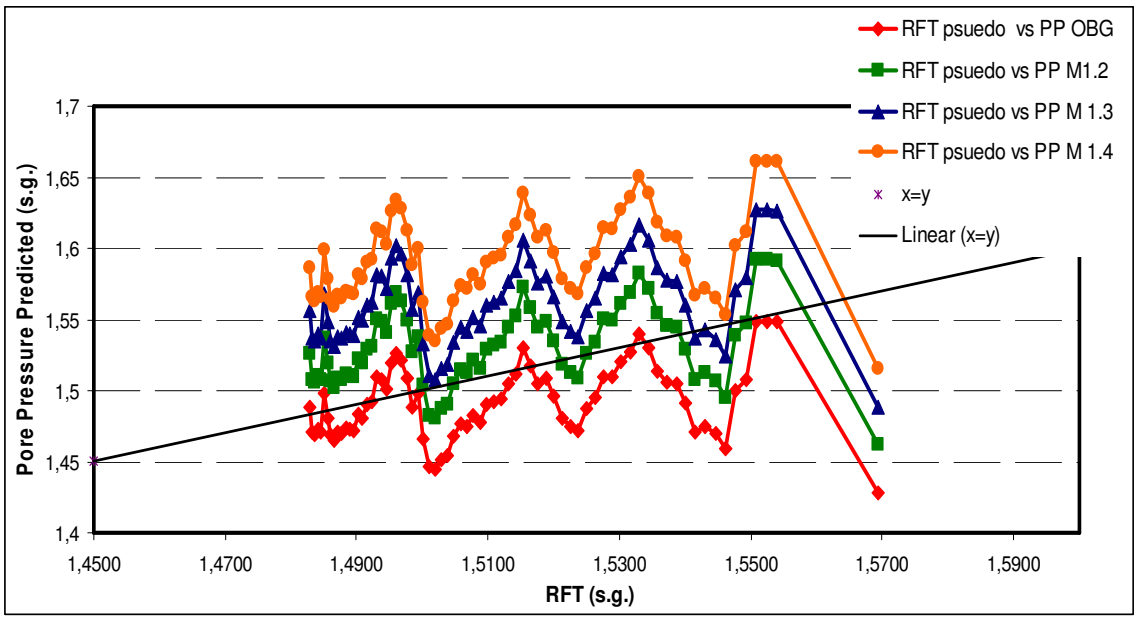

Figure B 8 Sonic Pseudo RFT vs. Pore Pressure Predicted Analysis for Well 2.

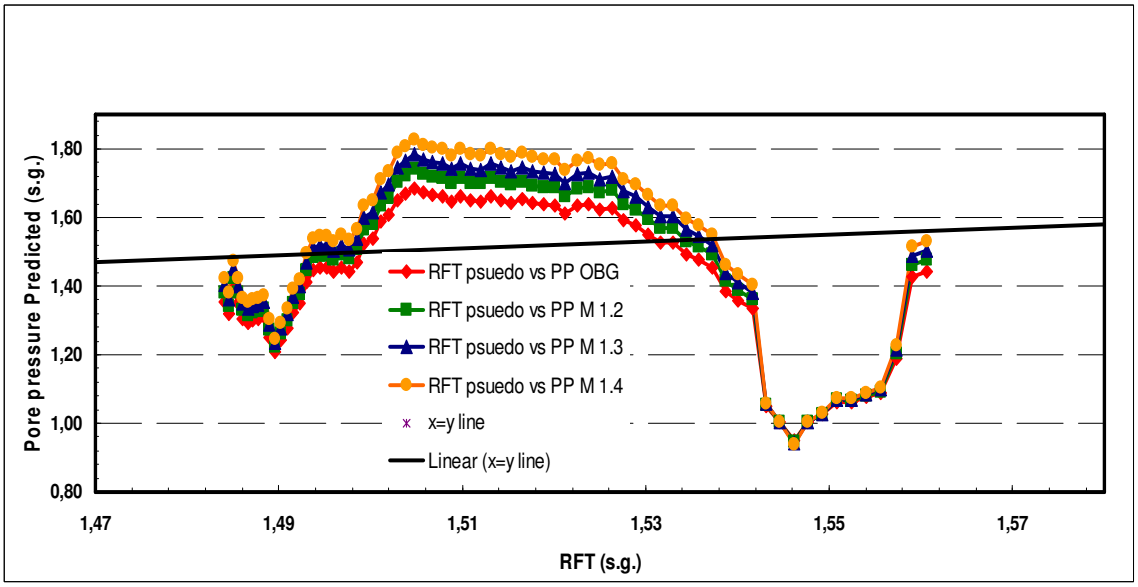

Figure B 9 Resistivity Pseudo RFT vs. Pore Pressure Predicted Analysis for Well 2.

WELL 3

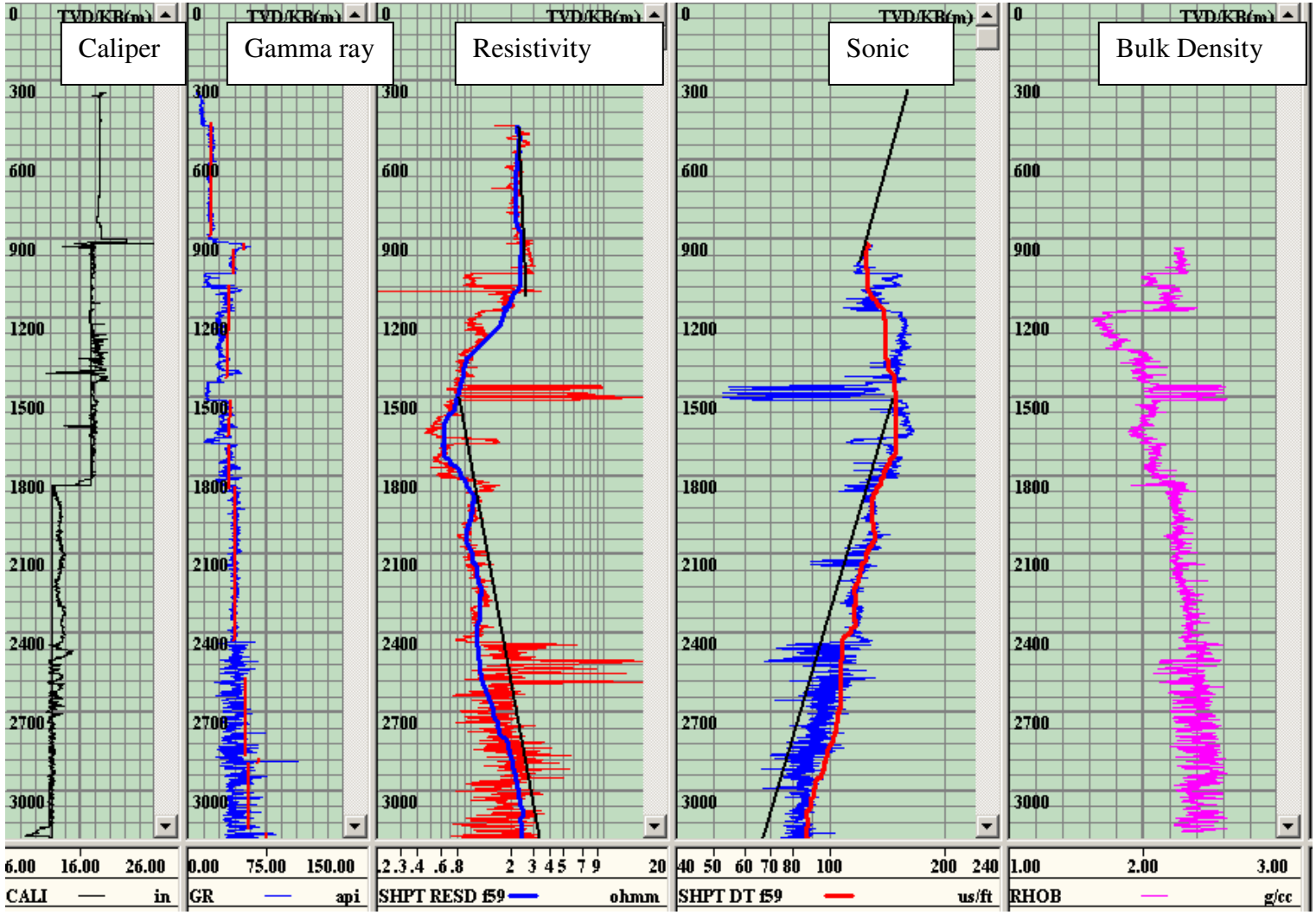

Figure B 10 Input data for well 3, Caliper, Gamma ray, Resistivity, Sonic and Bulk Density log data is plotted.

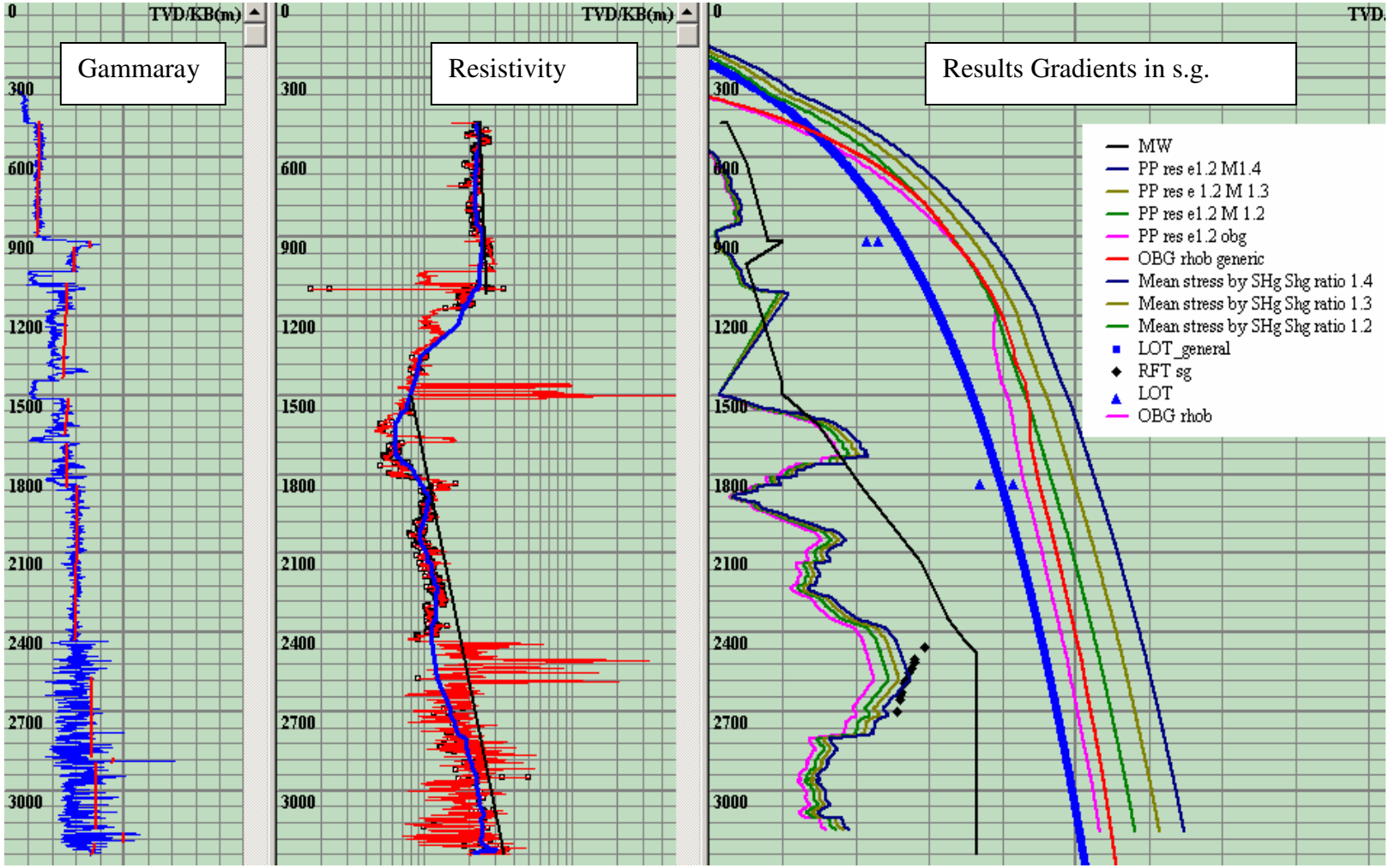

Figure B 11 Eaton Resistivity Method results for well 3, Results are plotted in result gradient part.

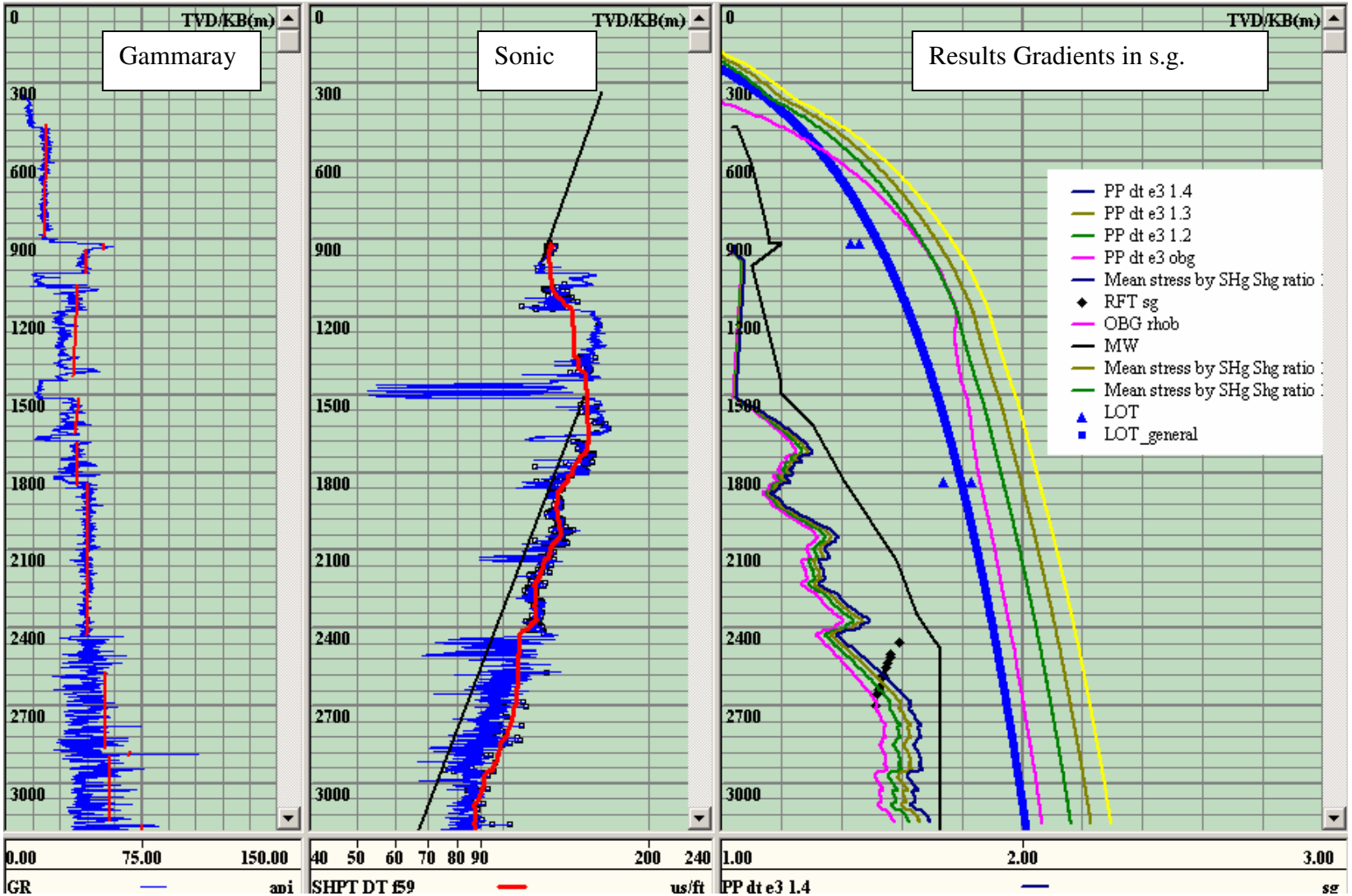

Figure B 12 Eaton Sonic Method results for well 3, Results are plotted in result gradient part.

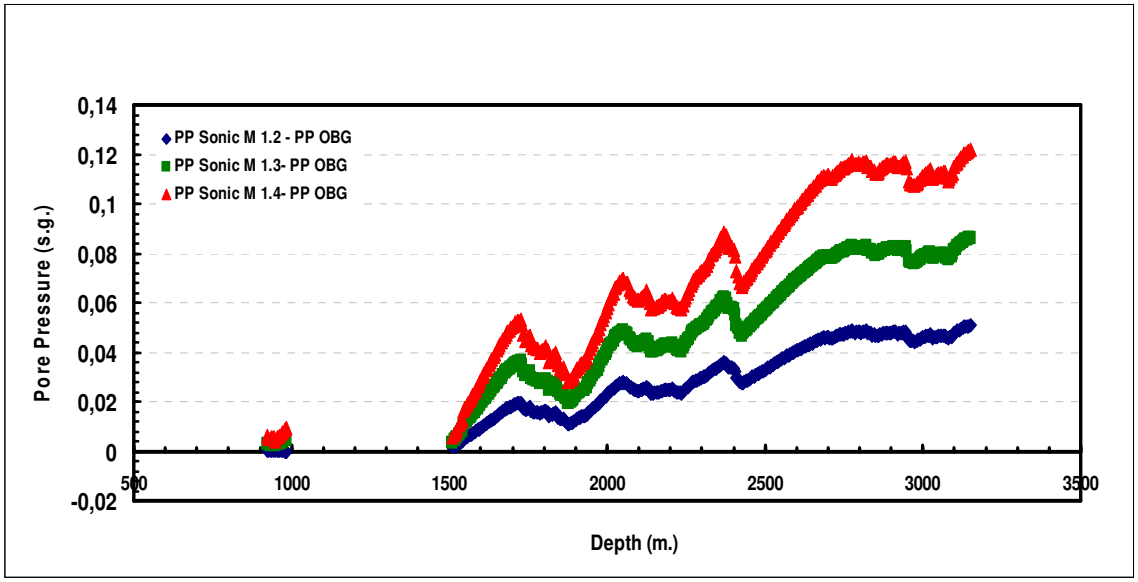

Figure B 13 Pore pressure difference between mean total stress used pore pressure prediction and overburden based pore pressure prediction using sonic log data for Well 3.

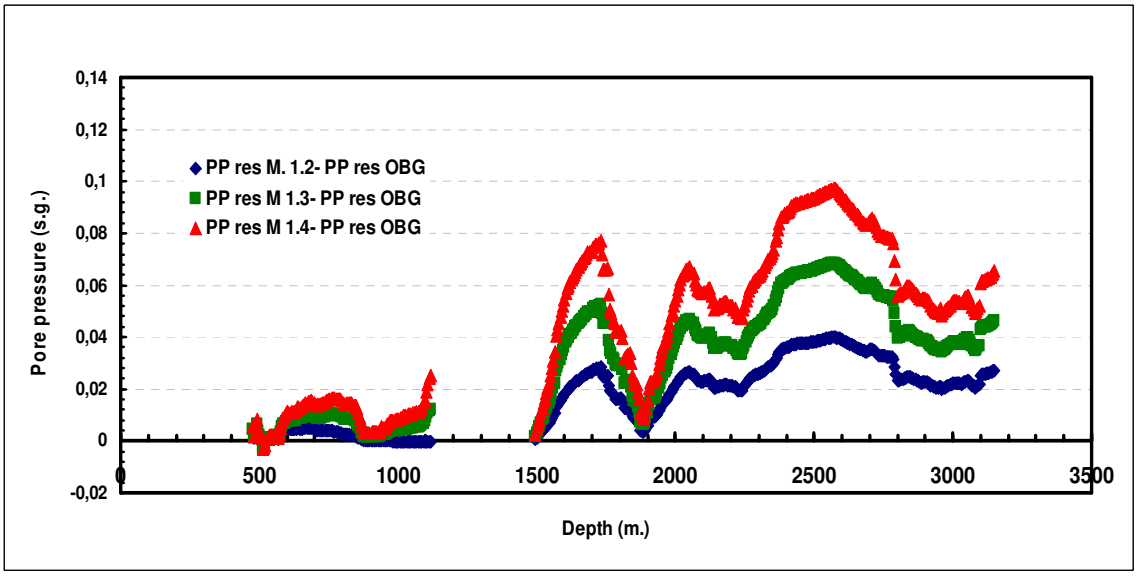

Figure B 14 Pore pressure difference between mean total stress used pore pressure prediction and overburden based pore pressure prediction using resistivity log data for Well 3.

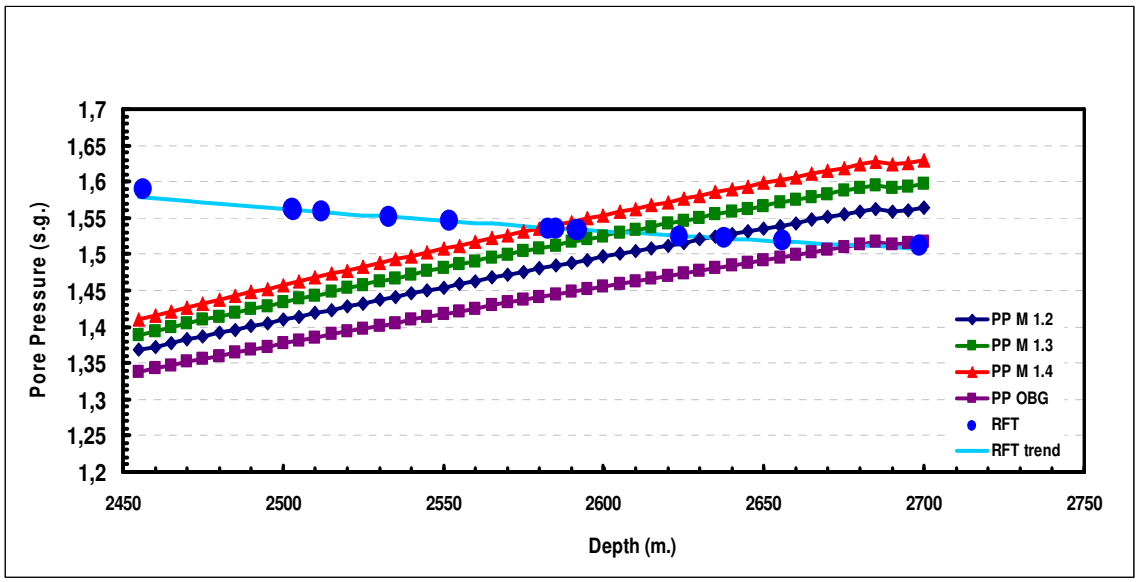

Figure B 15 Sonic log data based pore pressure comparison for each method to RFT for well 3.

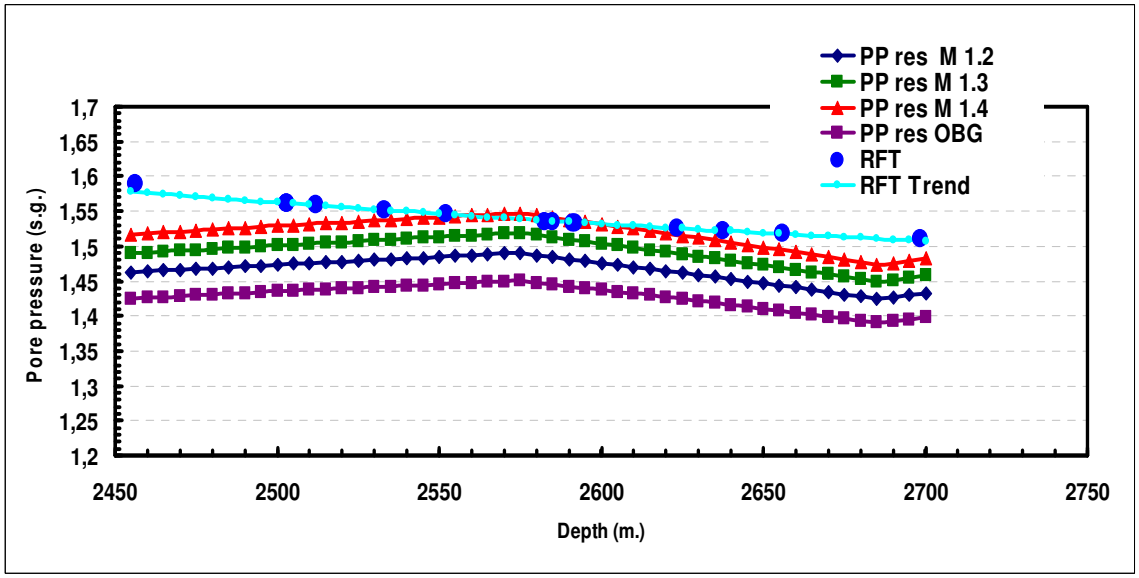

Figure B 16 Resistivity log data based pore pressure comparison for each method to RFT for well 3.

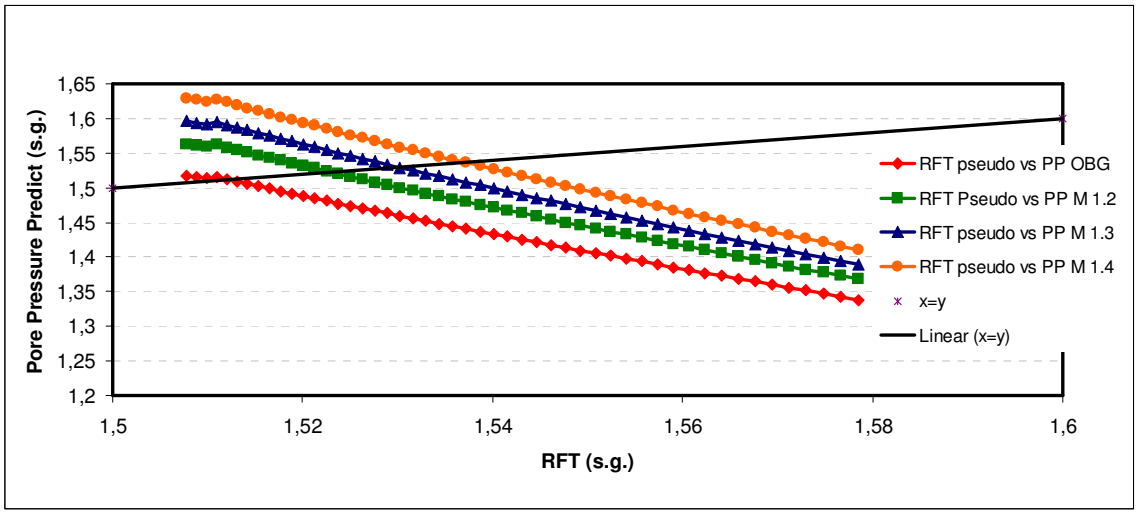

Figure B 17 Sonic Pseudo RFT vs. Pore Pressure Predicted Analysis .

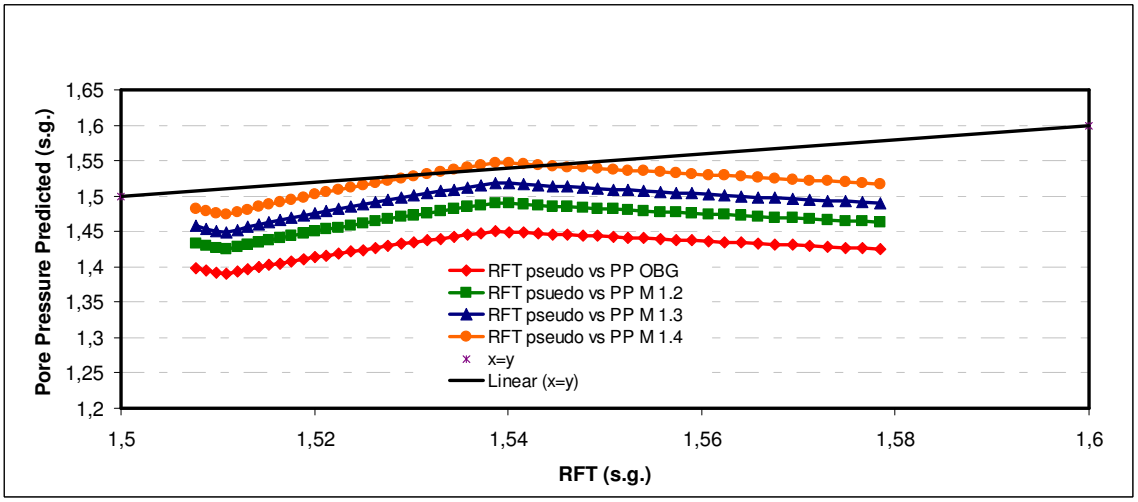

Figure B 18 Resistivity Pseudo RFT vs. Pore Pressure Predicted Analysis for well 3.

VITA

Name:	Aslihan Ozkale
Born:	August 1, 1980, Adana, Turkey
Address	Yesilyurt Mah. Necip Fazil Cad.
	Evim Apt. Kat:1, No.4
	Seyhan/ADANA
	TURKEY
Education	B.S., Middle East Technical University,Turkey
	Petroleum and Natural Gas Engineering (2002)
	M.S., Texas A&M University
	Petroleum Engineering (2006)